AN ABSTRACT OF THE DISSERTATION OF

Harman Ajiwibowo for the degree of Doctor of Philosophy in Civil Engineering presented on September 13, 2002.
Title: Fractal Solutions to The Long Wave Equations

Redacted for privacy

Abstract approved. _____
William G. McDougal

The fractal dimension of measured ocean wave profiles is found to be in the range of 1.5 – 1.8. This non-integer dimension indicates the fractal nature of the waves. Standard formulations to analyze waves are based on a differential approach. Since fractals are non-differentiable, this formulation fails for waves with fractal characteristics. Integral solutions for long waves that are valid for a non-differentiable fractal surfaces are developed. Field observations show a positive correlation between the fractal dimension and the degree of nonlinearity of the waves, wave steepness, and breaking waves. Solutions are developed for a variety of linear cases. As waves propagate shoreward and become more nonlinear, the fractal dimension increases. The linear solutions are unable to reproduce the change in fractal dimension evident in the ocean data. However, the linear solutions do demonstrate a finite speed of propagation.

The correlation of the fractal dimension with the nonlinearity of the waves suggests using a nonlinear wave equation. We first confirm the nonlinear behavior of the waves using the finite difference method with continuous function as the initial condition. Next, we solve the system using a Runge-Kutta method to integrate the characteristics of the nonlinear wave equation. For small times, the finite difference and Runge-Kutta solutions are similar. At longer times, however, the Runge-Kutta solution shows the leading edge of the wave extending beyond the base of the wave corresponding to over-steepening and breaking.

A simple long wave solution on multi-step bottom is developed in order to calculate the reflection coefficient for a sloping beach. Multiple reflections and transmissions are allowed at each step, and the resulting reflection coefficient is calculated. The reflection coefficient is also calculated for model with thousands of small steps where the waves are reflected and transmitted once over each step. The effect of depth-limited breaking waves is also considered.

FRACTAL SOLUTIONS TO THE LONG WAVE EQUATIONS

by

Harman Ajiwibowo

A DISSERTATION

submitted to

Oregon State University

in partial fulfillment of

the requirements for the

degree of

Doctor of Philosophy

Presented: September 13, 2002

Commencement : June 2003

Doctor of Philosophy dissertation of Harman Ajiwibowo presented on September 13, 2002

APPROVED:

Redacted for privacy

Major Professor, representing Civil Engineering

Redacted for privacy

Head of the Department of Civil, Construction and Environmental Engineering

Redacted for privacy

Dean of the Graduate School

I understand that my dissertation will become part of the permanent collection of Oregon State University libraries. My signature below authorizes release of my dissertation to any reader upon request.

Redacted for privacy

Harman Ajiwibowo, Author

ACKNOWLEDGMENTS

Alhamdulillah. I should like to thank foremost my advisor, Professor William G. McDougal, for the guidance and expertise he has supplied generously for the past few years in my training as an ocean engineer.

Professor Solomon Yim has been a constant source of enthuasiasm and inspiration, and also has been most generous with his time in helping sort out difficulties. My warmest thanks to him for his help and being my technical advisor. Most technical skills and techniques I have used in this present work have been gleaned from guidance by Professor Ronald Guenther. His teachings opened the door to the completion of this dissertation. I am most grateful to him for this and for giving so freely of his time. I should also thank Professor Robert Hudspeth who helped and supported me in the beginning of my doctoral program and gave me his time for my questions. My warmest thanks to Gunnar Gunderson for his generous help in editing my thesis.

It is appropriate to express my kindest regards to Valerie Rosenberg from Office of International Education for the financial support she has provided in 1999 and 2000 academic year under the International Student Scholarship. I have been most fortunate to be the recipient of this award, and I hope the present work will in some small way make me worthy of the honor.

Without a doubt, the greatest debt of my gratitude is due my parents, my wife, Peni, and son, Muhammad, and daughters, Amanda and Aisha, for their patience to endure the whole life trial during my doctoral program. And it is to them this work is dedicated.

TABLE OF CONTENTS

LIST OF FIGURES

LIST OF FIGURES (CONTINUED)

LIST OF FIGURES (CONTINUED)

Page

LIST OF FIGURES (CONTINUED)

Page

LIST OF FIGURES (CONTINUED)

LIST OF FIGURES (CONTINUED)

LIST OF FIGURES (CONTINUED)

FRACTAL SOLUTIONS TO THE LONG WAVE EQUATIONS

CHAPTER 1. INTRODUCTION

The word 'fractal' was coined by Mandelbrot (1975) from the Latin *fractus*, meaning broken. Fractal geometry is observed in many natural phenomena. In this work, we will concentrate on the fractal character of waves. Munzenmayer (1993) found that near breaking surface water waves exhibit fractal geometry. An important feature of these waves is that their surface is not continuous, and thus, non-differentiable.

Long waves, also called shallow water waves, are surface water waves that have a wavelength much greater than the water depth. Commonly used methods of solving the long wave equation are based on a differential approach. These methods fail when applied to waves with fractal geometry, since they are non-differentiable.

In this dissertation we develop a solution that is valid for fractal-shaped waves. The rough surface is treated using an integral-based solution. Fulks and Guenther (1972) used potential theory to develop an integral equation formulation of the problem. We simplify the problem by using the linear long wave equation. We consider four cases with a flat bottom: 1) without bottom friction and no reflective end wall, 2) without bottom friction with a reflective end wall, 3) with bottom friction without a reflective end wall, 4) with bottom friction with a reflective end wall. The 5^{th} case we consider is that of a sloping bottom, of infinite domain, without bottom friction.

Our analysis of field data taken from the Grays Harbor Wave Refraction Experiment, Washington, in 1999 shows that as waves propagate from intermediate water depth to shallow water depth, their fractal dimension changes. We are motivated by these findings to use nonlinear wave equation for the governing equation to the integral solution.

Chapter 2 considers the concept of fractal dimension and its measurement. Time series taken at Sandy Duck, North Carolina in 1992 are used to investigate the sensitivity of the fractal dimension calculation to the length of the data record. Results from fractal dimension calculations from several other data sets, reflecting measurements taken in varying wave conditions, are also discussed.

In Chapter 3, the long wave equations are derived from conservation of mass and momentum. The equations are depth-averaged, removing the vertical dependence of both equations and explicitly introducing the position of a free surface. Physical assumptions and non-dimensional scaling are used to simplify the equations. Integral equations which are able to treat the fractal nature of the wave forms are used. One method of determining the kernel to the integral equation, or Riemann function, is described. Several examples are presented to illustrate the use of the Riemann function.

In Chapter 4, hyperbolic potential theory is used to solve the boundary value problem for the linear long wave equation. We focus on the 5 cases previously mentioned. The appropriate Riemann function is determined, and the surface boundary condition is determined by assuming sinusoidal, Weierstrass function, or ocean waves, as appropriate. The fractal dimension is measured and analyzed for the ocean wave case.

In Chapter 5, we investigate the nonlinear formulation. We simplify the analysis by using smooth wave form as the initial condition. We then apply two methods of solution; the finite difference method and the Runge-Kutta numerical integration method. The Runge-Kutta method is more sophisticated in that it applies the method of characteristics, and we expect that it gives a more accurate solution. We compare the resulting solutions.

Chapter 6 focuses on reflected waves on a sloping bottom modeled by a multi-step bottom. The model is based on the principles of reflected and transmitted waves over an abrupt depth change (Dean, Dalrymple 1984). The reflection coefficient of the system is observed at the foot of the steps using the wave

envelope method. A depth-limited breaking criterion is also applied to observe the wave breaking effect on the reflection coefficient. This chapter also considers a linear profile and a curved profile based on Dean's beach profile equation.

CHAPTER 2. FRACTALS

To introduce the concept of fractals, we consider a curve existing in a space. We measure the length of the curve by joining a series of line segments, each of length δ, end to end along the curve. The number of segments needed to traverse the curve for a given segment length δ is called the measure M_δ. If we choose a smaller δ, then the measure M_δ increases. The concept of dimension is defined by the relationship between M_δ and δ as δ approaches zero:

$$M_\delta = \delta^{-s} \tag{2.1}$$

where s is defined to be the dimension of the curve. To illustrate this concept, let us consider Figure 2.1. For the straight line segment in Figure 2.1, evidently $M_\delta = \delta^{-1}$, and the dimension of the line in Figure 2.1 is 1.

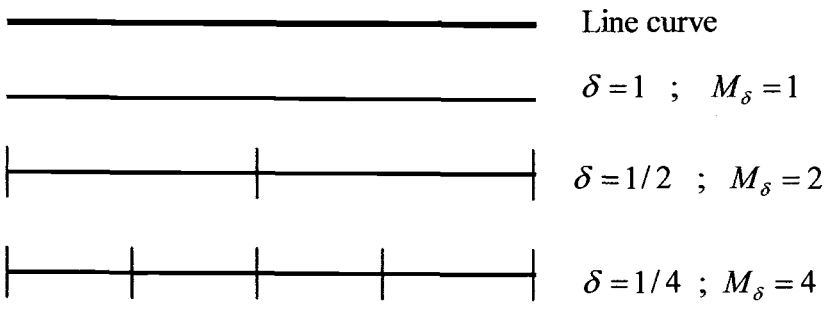

Figure 2.1 Line segments traversing a line curve

Next, we consider complex curve shown in Figure 2.2. For such a curve, $M_\delta = \delta^{-s}$, where $1 < s < 2$. When a curve's dimension is non-integer, the curve is called fractal and the dimension is called the fractal dimension.

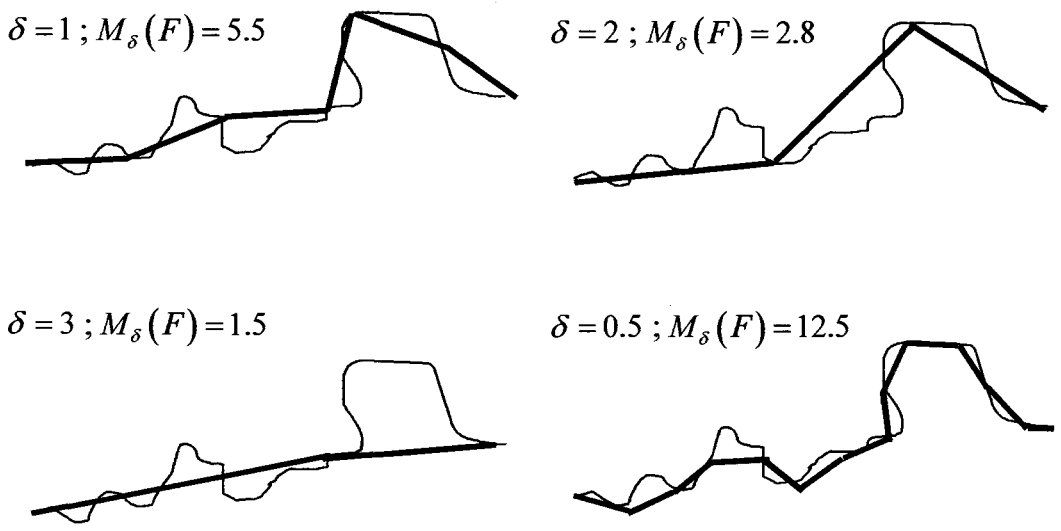

Figure 2.2 Measurement M_δ of a curve using various line segments δ

This concept can be generalized to higher dimensions. For instance, for a surface, we can construct a measure by covering the surface with squares of side δ. The number of squares is the measure M_δ, and the relation $M_\delta = \delta^{-s}$ still defines the dimension of the surface. A fractal surface would have $2 < s < 3$. A graphical way to describe dimension is to take the logarithm of (2.1) to obtain

$$\log M_\delta = -s \log \delta \tag{2.2}$$

We see that $-s$ is the slope of a plot of $\log M_\delta$ verse $\log \delta$.

2.1 FRACTAL DIMENSION

The most important method used to determine whether a set has a fractal structure is measuring its dimension. We describe two common measurement techniques; box counting and rescaled range analysis.

2.2.1 Box Counting Method

The box counting method is widely used. It can be used for hand computations and can also be easily programmed in a computer. The basic idea in box counting is to cover the fractal curve with a grid composed of boxes of side δ, and count the number of boxes that the curve possesses through, called N_δ. This procedure is repeated for smaller and smaller grid sizes. A linear regression of $\log N_\delta$ verse $\log \delta$ is made, where N_δ is the number of boxes for a given δ, and the slope of the regression line is the fractal dimension D_b. The relation among N_δ, δ and D_b may be expressed as

$$N_\delta = \frac{1}{\delta^{D_b}} \tag{2.3}$$

Equivalently,

$$D_b = -\frac{\log N_\delta}{\log \delta} \tag{2.4}$$

In theory, for each box size, the grid should be overlaid in such a way that the minimum number of boxes is occupied. The computer software, Benoit V1.2 Fractal Analysis (2000), implements the box counting dimension by determining the minimum number of boxes to cover the curves by rotating the grid. This method of box counting is suitable for examining a two-dimensional curve when the x and y coordinates have the same physical dimensions.

2.2.2 Rescaled Range Analysis

The requirement that x and y have the same physical dimension is a drawback of the box counting algorithm. Rescaled range analysis is appropriate for data not meeting this requirement. For example, the curve plotted in Figure 2.3 is a time series of free surface taken at Grays Harbor, WA in 1999. This is an example of a curve where the physical dimension in x and y are different. Hurst (1965) developed rescaled range analysis as a statistical method to analyze time series of natural phenomena. There are two parameters used in this analysis. The range R is the difference between the minimum and maximum of the cumulative sum $X(t,\tau)$. $X(t,\tau)$ represents the cumulative sum of measurement of some quantity ξ made at discrete time t over a total time τ. S denotes the standard deviation of the measurement ξ. We use the Benoit V1.2 Fractal Analysis software to calculate rescaled range analysis fractal dimension.

Hurst found an empirical relation satisfied by a large number of natural phenomena:

$$\frac{R}{S} = (c\ \tau)^H \tag{2.5}$$

where H is the Hurst exponent. The coefficient c is taken to be 0.5 by Hurst. R, S, ξ, and X are formally defined as

$$R(\tau) = \max X(t,\tau) - \min X(t,\tau) \tag{2.6}$$

and

$$S(\tau) = \sqrt{\left(\frac{1}{\tau}\sum_{t=1}^{\tau}\left\{\ \xi(t) - \langle\xi\rangle_\tau\right\}^2\right)} \tag{2.7}$$

where

$$\langle \xi \rangle_\tau = \frac{1}{\tau} \sum_{t=1}^{\tau} \xi(t) \tag{2.8}$$

and

$$X(t,\tau) = \sum_{u=1}^{t} \{ \xi(u) - \langle \xi \rangle_\tau \} \tag{2.9}$$

This method is appropriate for time series. The graphical representation uses time on the x axis, and the free surface elevation on the ordinate.

The Hurst exponent H has a value of about 0.72 for many natural phenomena. For ocean wave data, it is found to be between 0.12 – 0.5. The relationship between the Hurst exponent and the fractal dimension is simply (Vanouplines, 1995)

$$D = 2 - H \tag{2.10}$$

A Hurst exponent of $0.5 < H < 1$ corresponds to a time series with trending behavior. A Hurst exponent of $0 < H < 0.5$ indicates non-trending, oscillatory behavior. The oscillatory behavior has a rather high fractal dimension ($1.5 < D < 2$), corresponding to a highly variable time series with large standard deviation. Figure 2.3 shows ocean wave data measured at Grays Harbor, Washington, in 1999. The water depth was 25 meters. The fractal dimensions calculated using both rescaled range analysis and box counting are 1.756 and 1.926, respectively.

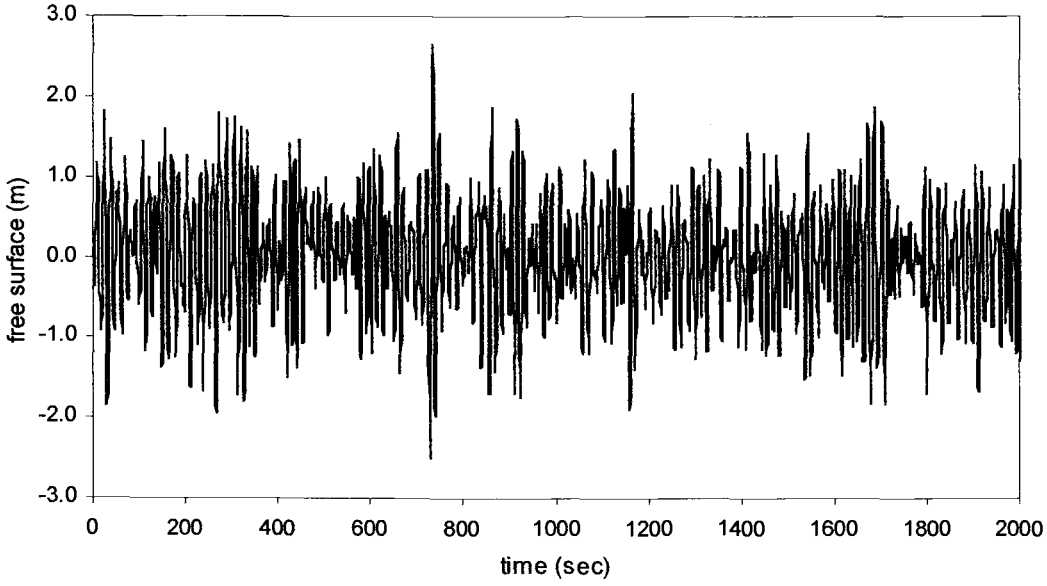

Figure 2.3 Free surface time series burst # 500, taken at Grays Harbor, WA in 1999. The data sampling is 2 Hz.

2.2 WEIERSTRASS FUNCTION

The Weierstrass function is an example of a continuous fractal curve that is non-differentiable. Suppose $\lambda > 1$ and $1 < \gamma < 2$, and consider

$$f(t) = \sum_{k=1}^{\infty} \lambda^{(\gamma-2)k} \sin(\lambda^k t) \tag{2.11}$$

Provided λ is large enough, the fractal dimension D of f is γ (Falconer, 1990). The time series $f(t)$ is composed of sinusoids with frequency λ^k, each of which is damped by the factor $\lambda^{(\gamma-2)k}$. The damping increases with increasing frequency, so that $\lambda^{(\gamma-2)k}$ can be viewed as a low-pass filter. Increasing γ decreases the degree of damping, and results in a signal with more high frequency content. Also, as k increases, damping term becomes more effective. Higher frequency terms are damped more.

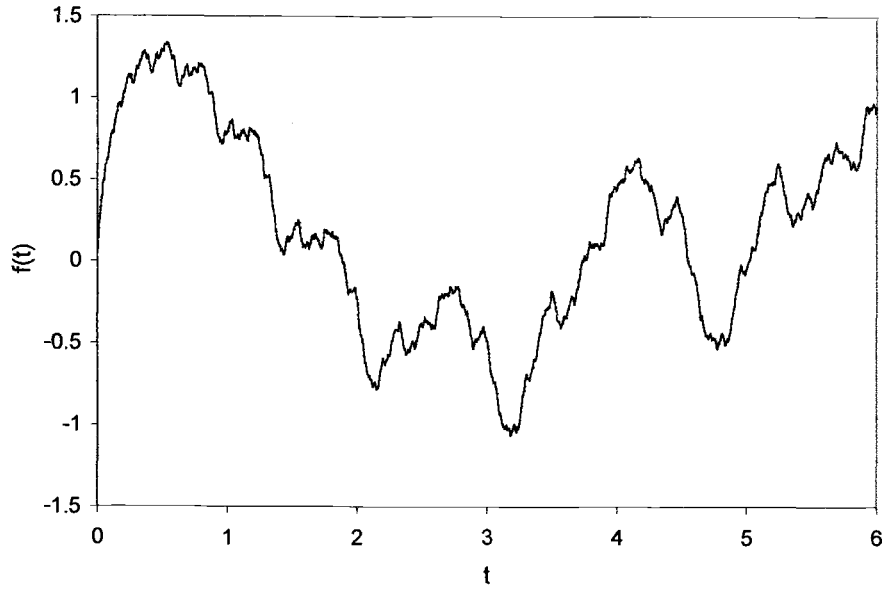

Figure 2.4a. The Weierstrass function $f(t)$ with λ=1.5 and $\gamma = 1.1$

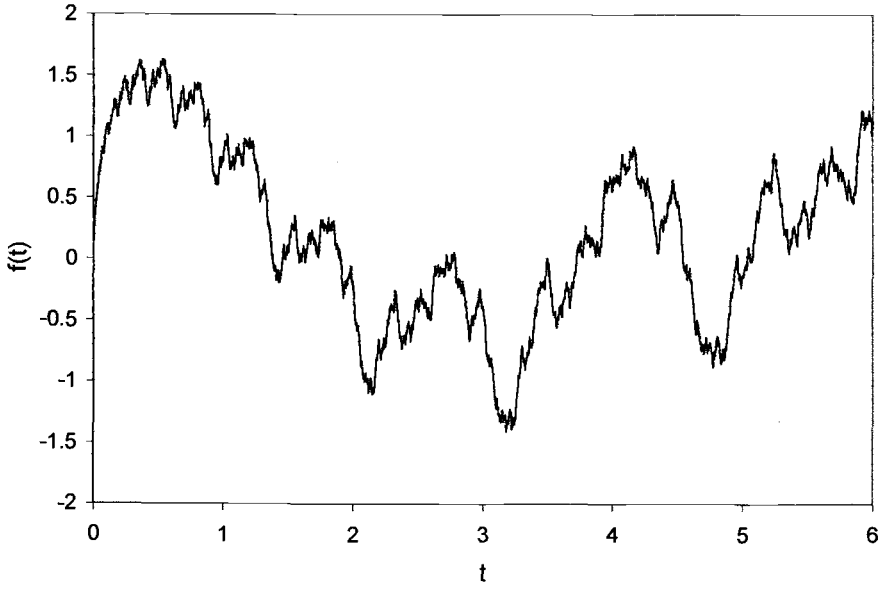

Figure 2.4b. The Weierstrass function *f(t)* with λ =1.5 and γ =1.3

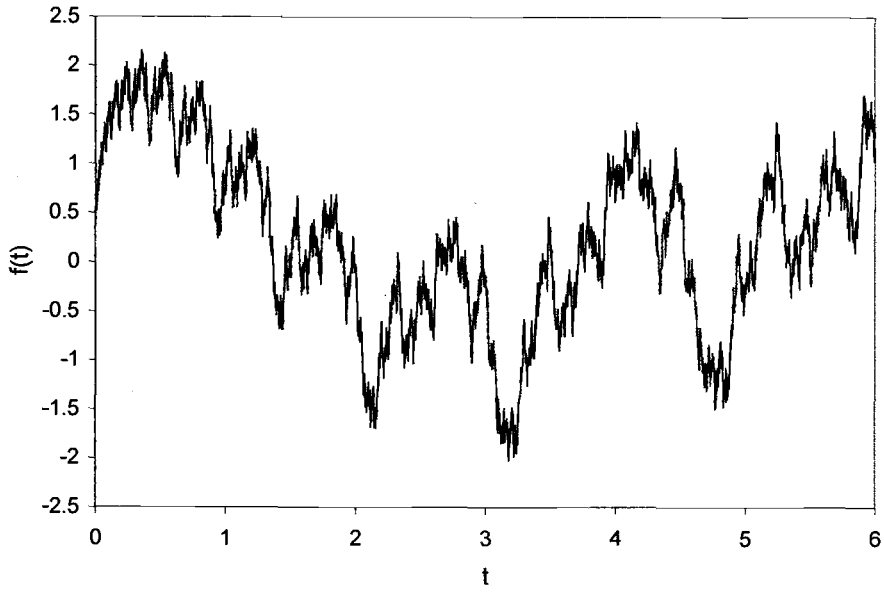

Figure 2.4c. The Weierstrass function $f(t)$ with λ =1.5 and γ = 1.5

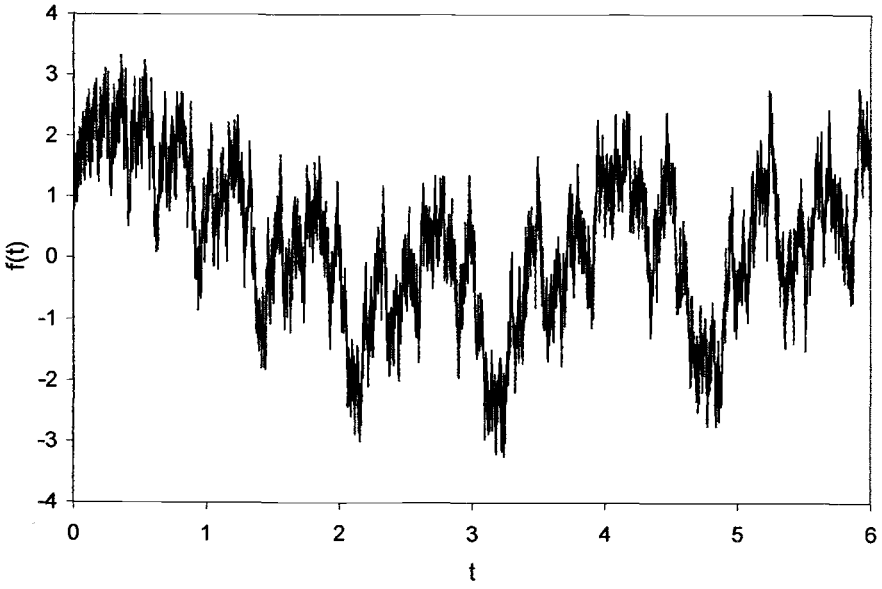

Figure 2.4d. The Weirstrass function $f(t)$ with λ =1.5 and γ =1.7

Figures 2.4a – 2.4d show that a larger γ results in more energy with high frequency.

2.3 GODA NONLINEARITY PARAMETER

Goda (1985) used skewness as a measure of the non-linearity of waves. The skewness $\sqrt{\beta_1}$ of a time series η_i is defined as

$$\sqrt{\beta_1} = \frac{1}{\eta_{rms}^{\ 3}} \ \frac{1}{N}\sum_{i=1}^{N}(\eta_i - \eta_{mean})^3 \tag{2.12}$$

where

$$\eta_{mean} = \frac{1}{N}\sum_{i=1}^{N}\eta_i \tag{2.13}$$

and

$$\eta_{rms} = \sqrt{\frac{1}{N}\sum_{i=1}^{N}\eta_i^{\ 2}} \tag{2.14}$$

Goda also proposed a parameter describing the extent of wave nonlinearity.

$$\Pi = \frac{H_s}{L}\coth^3 kh \tag{2.15}$$

Goda found that the skewness of the data increases as the degree of nonlinearity increases. The dispersion relation is written as

$$\omega^2 = g\ k \tanh kh \tag{2.16}$$

and

$$k = \frac{2\pi}{L} \tag{2.17}$$

H_s, h, ω and k are the significant wave height, water depth, wave frequency, and wave number, respectively. Significant wave height H_s is the average of the highest one-third of the wave.

2.4 OCEAN WAVE DATA

The method of rescaled range analysis is used to determine the fractal dimension of ocean wave data taken in Sandy Duck, North Carolina in 1997. The sampling rate was 2 Hz. To determine the sample size needed to obtain robust estimate of fractal dimension, a sensitivity test of fractal dimension to sample size was performed. The raw signal is shown in Figure 2.5. Figure 2.6 summarizes the sensitivity test.

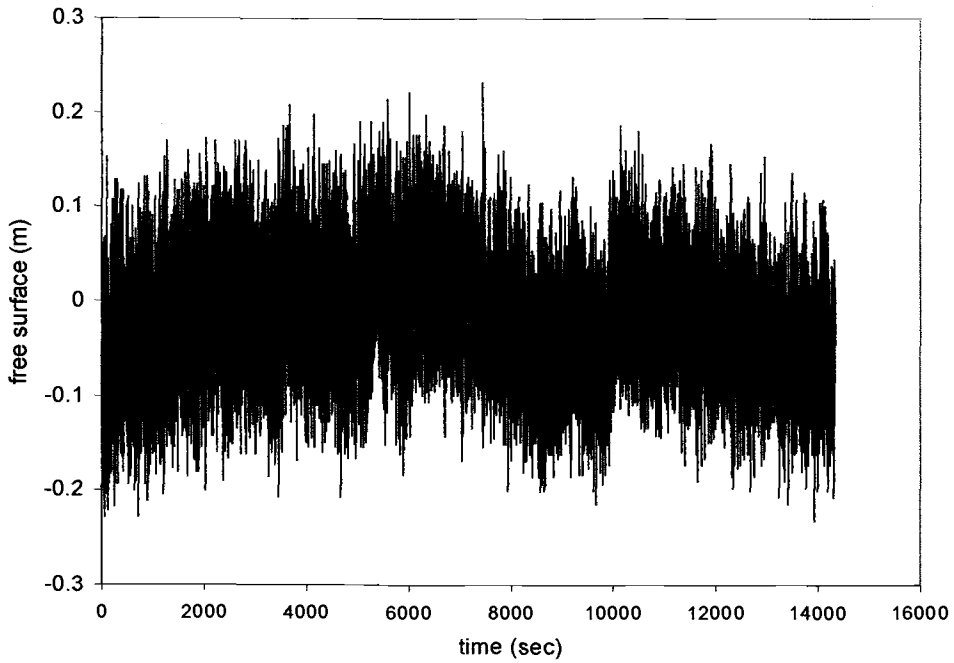

Figure 2.5. Ocean wave data, *dt* = 0.5 sec taken from Sandy Duck, North Carolina, 1997

From Figure 2.6, there is little improvement in the estimated dimension for record length above 5000 datapoints. We choose to use record lengths of 4000 data in our calculations.

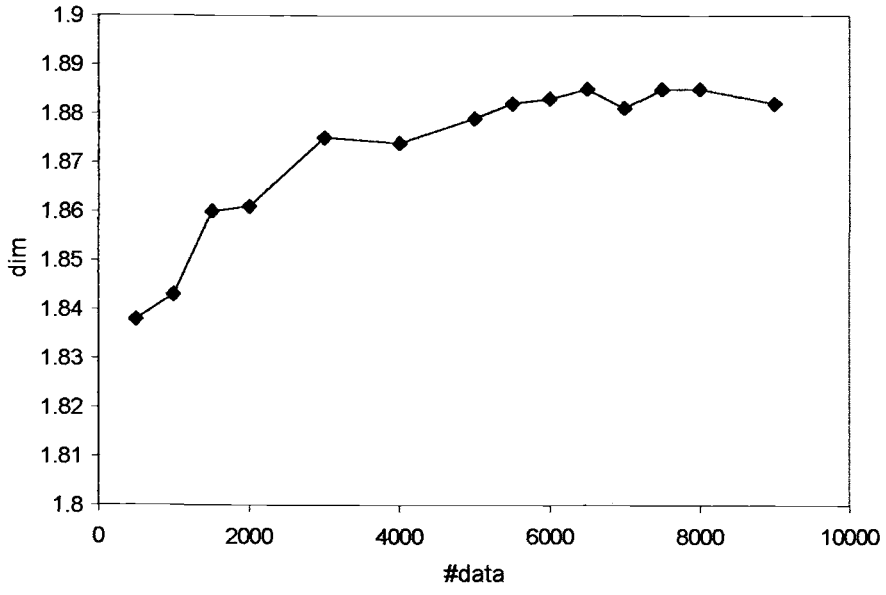

Figure 2.6. Average fractal dimension for different number of data blocks of ocean wave data.

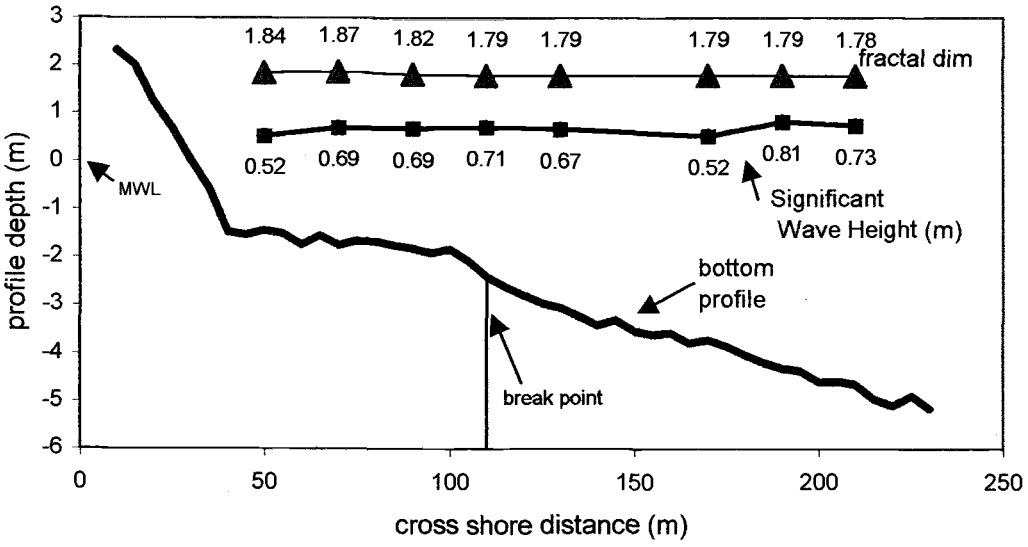

Figure 2.7. Cross-shore wave data across the surf zone, taken from the coast of Bulgaria in 1988 (Kutzetnov, 1988).

Figure 2.7 shows the results of a rescaled range analysis to measurements of wave height as a function of distance from the coast of Bulgaria in 1988 (Kuznetsov, 1988). Figure 2.7 shows the significant wave height and fractal dimensions of the ocean waves across the shore. The wave height increases right before the breaking point and then decreases as the waves breaks. Figure 2.7 also shows the changing of the fractal dimension of the wave surface verse cross-shore location. As the waves approach the coast, the fractal dimension increases. The fractal dimension is higher for the breaking waves. The average fractal dimension in the breaking zone is 1.84, and the average fractal dimension before breaking zone is 1.79, a 3% increase. Observations in the field show that the waves after breaking are visually rougher than the waves before breaking. The nonlinearity of the waves increases as the waves travel to shallower water. It is probable that the fractal dimension is directly related to the nonlinearity of the waves.

Next, we consider wave data from the Grays Harbor Wave Refraction Experiment (Gelfenbaum et.al., 2000). The data are divided into two groups of 20 records, one group consists of data taken at 25 meters water depth, the other at 12 meters water depth. The objective of the data analysis is to observe the relationship of fractal dimension with water depth and the degree of nonlinearity. Nonlinearity is estimated using both skewness and Goda's nonlinearity parameter. A plot of skewness verse nonlinearity parameter (Figure 2.8) shows the 12 meters data to have higher skewness and nonlinearity parameter values than the 25 meters data: the shallow waves are clearly more nonlinear.

Fractal dimension verse skewness is plotted in Figure 2.9. The fractal dimension increases as the skewness increases. Figure 2.10 shows that the fractal dimension also increases with increasing nonlinearity. These results indicate a strong positive correlation between fractal dimension and nonlinearity.

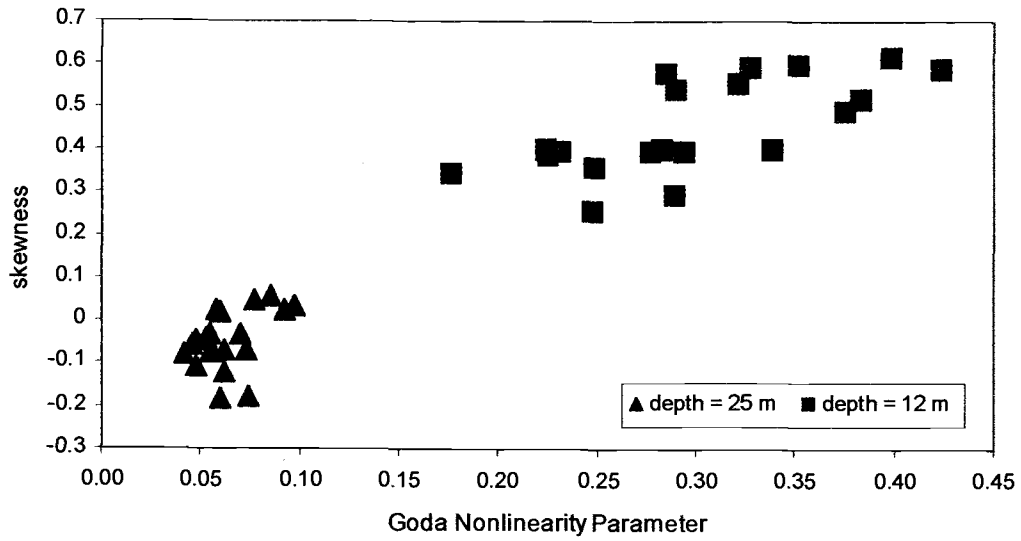

Figure 2.8. Skewness of surface elevation versus wave non-linearity parameter defined in (2.15). The data is taken from Grays Harbor, WA.

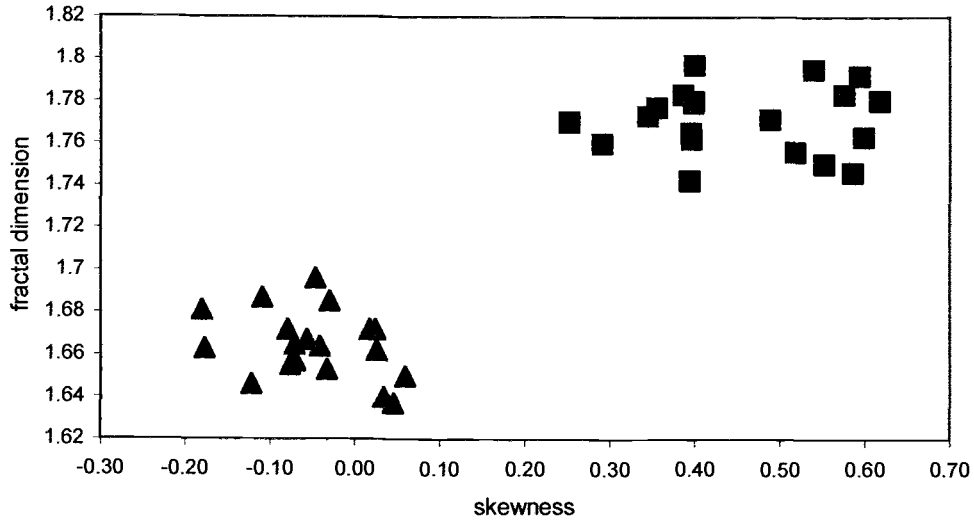

Figure 2.9. Fractal dimension of surface elevation versus the skewness of the statistical distribution.

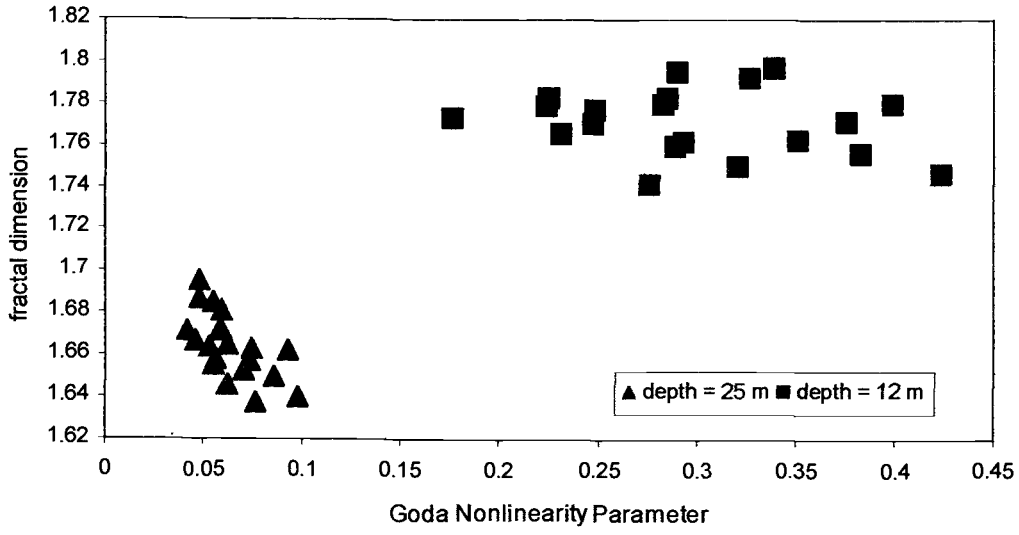

Figure 2.10. Fractal dimension of surface elevation versus the Goda nonlinearity parameter.

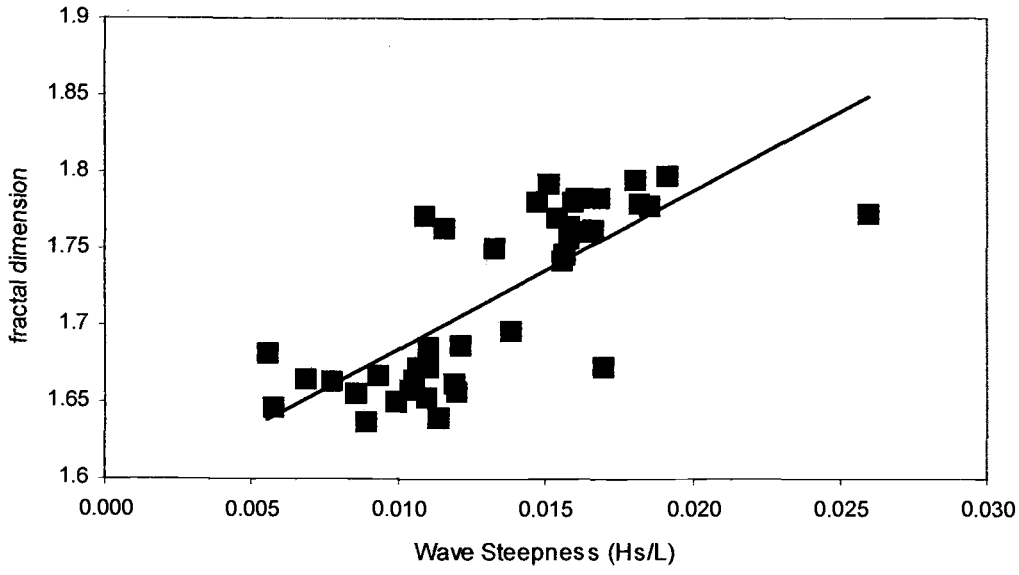

Figure 2.11 Fractal dimension as a function of wave steepness. The wave height is represented by significant wave height.

Another quantity of interest is the wave steepness, defined to be the ratio of the wave height to the wavelength. Figure 2.11 shows that fractal dimension also increases with increasing wave steepness. Thus, fractal dimension is expected to be larger during storm events, when wave steepness is high.

CHAPTER 3. WAVE EQUATION AND THE RIEMANN FUNCTION

The objective of this chapter is to derive the long wave equations using conservation of mass and momentum. These equations are scaled to identify the magnitude of each term so we can linearize the equations to obtain the linear long wave equation. We also apply the Riemann method to obtain the Riemann function of the linear long wave equations.

Fulks and Guenther (1972) present an integral solution to boundary value problems using hyperbolic potential theory. The Riemann function is the kernel of the integral solution. Solutions for the depth-averaged, one dimensional linear long wave equations are derived for the following cases: 1) without bottom friction and no reflective wall, 2) without bottom friction with a reflective wall, 3) with bottom friction without a reflective wall, 4) with bottom friction with a reflective wall. A 5th case considered is that of a sloping bottom without bottom friction.

3.1 CONSERVATION OF MASS

Consider the volume element depicted in Figure 3.1, with constant width w in y-direction, and area A in x-z plane. For an incompressible fluid, conservation of mass is equivalent to conservation of volume, which can be expressed as

$$\left\{\left\langle u_1\,(h_1+\eta_1)\right\rangle\right\} - \left\{\left\langle u_2\,(h_2+\eta_2)\right\rangle\right\} w = \frac{w\,\Delta A}{\Delta t} \qquad (3.1)$$

where u_1 and u_2 are depth-averaged velocities at $x = x_1$ and $x = x_2$, h is water depth, and η is free surface displacement. The subscripts 1 and 2 correspond to coordinates x_1 and x_2. $\left\langle u_1(h_1+\eta_1)\right\rangle$ and $\left\langle u_2(h_2+\eta_2)\right\rangle$ are time averages over time interval t, $t+\Delta t$. By using Figure 3.1 to obtain the formulation for area A, we can rewrite (3.1) as

$$\left\{\left\langle u_1\left(h_1+\eta_1\right)\right\rangle\right\} - \left\{\left\langle u_2\left(h_2+\eta_2\right)\right\rangle\right\} w = \frac{\left.\overline{h+\eta}\right|_{t+\Delta t} \Delta x - \left.\overline{h+\eta}\right|_{t} \Delta x}{\Delta t} w \quad (3.2)$$

where $\left.\overline{h+\eta}\right|_{t+\Delta t}$ is a spatial average over the volume element at time $t+\Delta t$. If we divide (3.2) through by $w\,\Delta x$, then we can rewrite (3.2) as

$$\frac{-\left[\left\langle u_2\left(h_2+\eta_2\right)\right\rangle - \left\langle u_1\left(h_1+\eta_1\right)\right\rangle\right]}{\Delta x} = \frac{\left.\overline{h+\eta}\right|_{t+\Delta t} - \left.\overline{h+\eta}\right|_{t}}{\Delta t} \quad (3.3)$$

In the limit $\Delta x,\ \Delta t \to 0$, (3.3) becomes

$$-\frac{\partial\left[u\left(h+\eta\right)\right]}{\partial x} = \frac{\partial\left(h+\eta\right)}{\partial t} \quad (3.4)$$

If we assume that the location of the bottom does not change with time, then we can write (3.4) as

$$\frac{\partial \eta}{\partial t} + \frac{\partial}{\partial x}\left[\left(h+\eta\right)u\right] = 0 \quad (3.5)$$

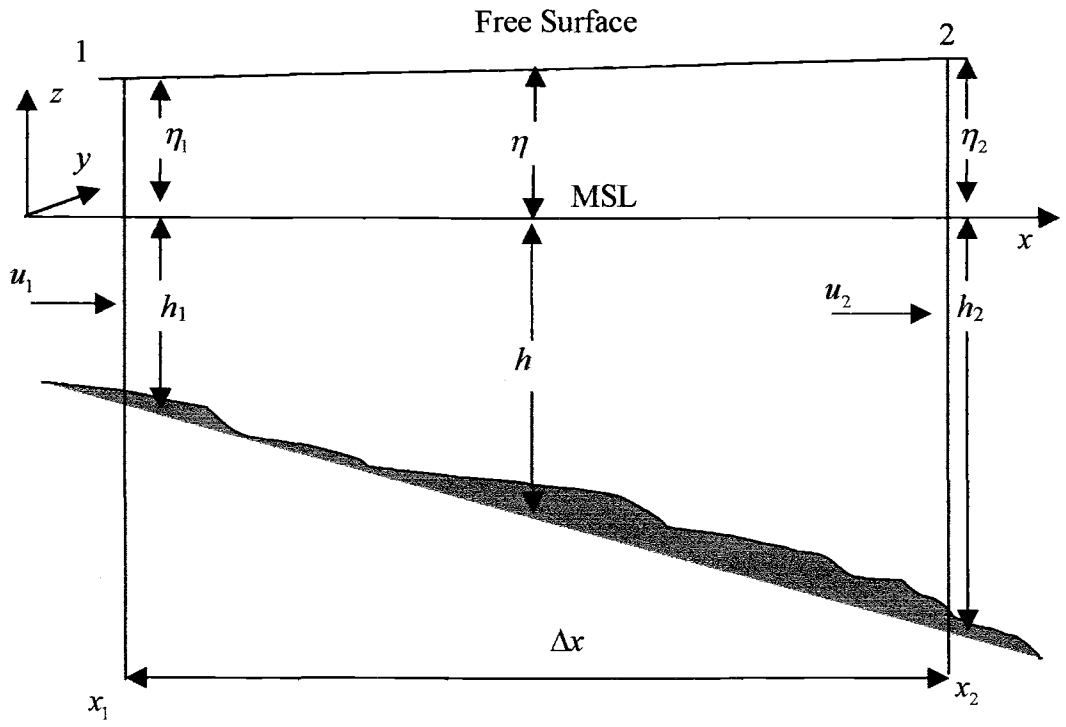

Figure 3.1 Small volume of ocean water with constant width. The average h and η are calculated near the middle of the domain.

3.2 CONSERVATION OF MOMENTUM

Consider the elemental volume in Figure 3.2. For constant width, the volume of water as sketched in Figure 3.1 can be represented by the area. The sum of the forces in the x-direction is

$$\sum F^x = m\, a^x \tag{3.6}$$

where m is the water mass and a^x is the acceleration in x-direction.

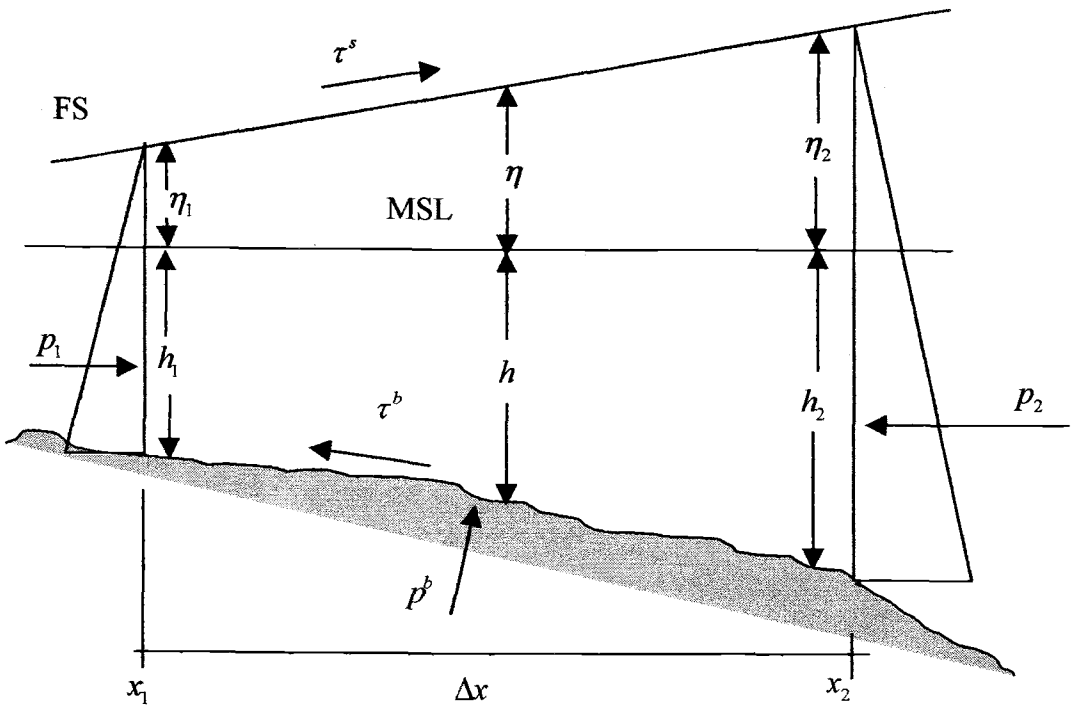

Figure 3.2. Force diagram for a volume element

In Figure 3.2, p_1 and p_2 are the pressures at locations x_1 and x_2, τ^s and τ^b are surface and bottom stresses and p^b is bottom pressure. By assuming the volume element to be of unit width, we can write (3.6) as

$$\frac{1}{2}\rho g\,(h_1+\eta_1)^2 - \frac{1}{2}\rho g\,(h_2+\eta_2)^2$$

$$+\tau^{sx}\,\Delta x\,\frac{1}{\left[1+(\partial\eta/\partial x)^2\right]^{1/2}} - \tau^{bx}\,\Delta x\,\frac{1}{\left[1+(\partial h/\partial x)^2\right]^{1/2}} \qquad (3.7)$$

$$+p^b\,\Delta x\,\frac{\partial h/\partial x}{\left[1+(\partial h/\partial x)^2\right]^{1/2}} = \rho A\frac{Du}{Dt}$$

where ρ is mass density of the water, g is gravity acceleration, and u is horizontal velocity. If we assume that the slope of the free surface, $\partial\eta/\partial x$, and the bottom slope, $\partial h/\partial x$, are small, then the squared terms in the denominator of (3.7) can be neglected. We can write (3.7) as

$$\begin{aligned} &\frac{1}{2}\rho g\left[(h_1+\eta_1)^2-(h_2+\eta_2)^2\right]+\left(\tau^{sx}-\tau^{bx}\right)\Delta x+p_b\,\Delta x\frac{\partial h}{\partial x} \\ &=\rho\,\frac{(h_1+\eta_1)+(h_2+\eta_2)}{2}\,\Delta x\,\left(\frac{\partial u}{\partial t}+u\frac{\partial u}{\partial x}\right) \end{aligned} \tag{3.8}$$

The average bottom pressure p_b is approximated as hydrostatic. We can write the pressure p^b as

$$p^b=\rho g\frac{(h_1+\eta_1)+(h_2+\eta_2)}{2} \tag{3.9}$$

The hydrostatic pressure p^b is substituted into (3.8). By expanding the first term on the left hand side of (3.8), we can modify (3.8) to

$$\begin{aligned} &\frac{1}{2}\rho g\left[(h_1+\eta_1)+(h_2+\eta_2)\right]\left[(h_1+\eta_1)-(h_2+\eta_2)\right]+\left(\tau^{sx}-\tau^{bx}\right)\Delta x \\ &+\frac{\rho g}{2}\left[(h_1+\eta_1)+(h_2+\eta_2)\right]\frac{\partial h}{\partial x}\,\Delta x= \\ &\rho\,\frac{(h_1+\eta_1)+(h_2+\eta_2)}{2}\,\Delta x\,\left(\frac{\partial u}{\partial t}+u\frac{\partial u}{\partial x}\right) \end{aligned} \tag{3.10}$$

In the limit $\Delta x \to 0$, (3.10) becomes

$$\left(\frac{\partial u}{\partial t}+u\frac{\partial u}{\partial x}\right)=-g\frac{\partial \eta}{\partial x}+\frac{\tau^{sx}-\tau^{bx}}{\rho\,(h+\eta)} \tag{3.11}$$

where $(h+\eta)$ is the average over the range $[x_1, x_2]$. If we multiply (3.11) by $(h+\eta)$, we can rewrite (3.11) as

$$\frac{\partial}{\partial t}\left[(h+\eta)u\right]+u\frac{\partial}{\partial x}\left[(h+\eta)u\right]=\ -g\ (h+\eta)\frac{\partial \eta}{\partial x}+\frac{\tau^{sx}-\tau^{bx}}{\rho} \tag{3.12}$$

The surface stress τ^{sx} is assumed to be zero. The bottom stress τ^{bx} can be written as (McDougal, 1983)

$$\tau^{bx}=\rho\ \frac{f^b}{8}\ |u|u \tag{3.13}$$

where f^b is a dimensionless friction coefficient, ρ is mass density of water, and u is depth-averaged horizontal velocity of the water. Because u is depth-averaged, $\tau^{bx}(u)$ is less than $\tau_{bx}(u(z))$. If we substitute τ^{bx} into (3.12), we can write the conservation of momentum as

$$\frac{\partial}{\partial t}\left[(h+\eta)u\right]+u\frac{\partial}{\partial x}\left[(h+\eta)u\right]=-g(h+\eta)\frac{\partial \eta}{\partial x}-\frac{f^b}{8}|u|u \tag{3.14}$$

3.3 SCALED WAVE EQUATIONS

To obtain dimensionless forms of (3.5) and (3.14), we introduce the following scaling factors;

$$
\begin{aligned}
x &= LX \\
t &= T_c T \\
h &= h_0 H \\
\eta(x,t) &= \eta_0 N(X,T) \\
u(x,t) &= \left(\frac{\eta_0}{h_0}\right) C_0 U(X,T)
\end{aligned}
\tag{3.15}
$$

where L, η_0, h_0, T_c, c_0 are dimensional scaling constants for the horizontal distance, free surface displacement, water depth, time, and velocity, respectively. The dimensionless equations corresponding to (3.5) and (3.14) are

$$
\frac{\partial N}{\partial T} + \frac{C_0 T_c}{L}\frac{\partial}{\partial X}\left[\left(H + \frac{\eta_0}{h_0}N\right)U\right] = 0, \tag{3.16}
$$

and

$$
\begin{aligned}
&\frac{\partial}{\partial T}\left[\left(H + \frac{\eta_0}{h_0}N\right)U\right] + \frac{\eta_0}{h_0}\frac{C_0 T_c}{L}U\frac{\partial}{\partial X}\left[\left(H + \frac{\eta_0}{h_0}N\right)U\right] = \\
&-\frac{g\, h_0 T_c}{L C_0}\left(H + \frac{\eta_0}{h_0}N\right)\frac{\partial N}{\partial X} - \frac{\eta_0}{h_0}\frac{C_0\, T_c}{h_0}\frac{f_b}{8}|U|U,
\end{aligned}
\tag{3.17}
$$

respectively. By defining $\varepsilon = \frac{\eta_0}{h_0}$, we can write

$$
\frac{\partial N}{\partial T} + \frac{C_0 T_c}{L}\frac{\partial}{\partial X}\left[(H + \varepsilon N)U\right] = 0 \tag{3.18}
$$

and

$$\frac{\partial}{\partial T}\left[(H+\varepsilon N)U\right]+\varepsilon\frac{C_0T_c}{L}U\frac{\partial}{\partial X}\left[(H+\varepsilon N)U\right]= \\ -\frac{g\,h_0T_c}{LC_0}(H+\varepsilon N)\frac{\partial N}{\partial X}-\varepsilon\frac{C_0\,T_c}{h_0}\frac{f_b}{8}|U|U \tag{3.19}$$

These equations are nonlinear, and become linear in the limit $\varepsilon \to 0$.

3.4 LINEAR SCALED WAVE EQUATIONS

First consider the linear case with $\varepsilon \to 0$. In this limit, the conservation of mass in (3.18) can be rewritten as

$$\frac{\partial N}{\partial T}+\frac{C_0T_c}{L}\frac{\partial}{\partial X}(UH)=0 \tag{3.20}$$

If we choose T_c and L, so that

$$\frac{C_0T_c}{L}=1, \tag{3.21}$$

then (3.20) becomes

$$\frac{\partial N}{\partial T}+\frac{\partial}{\partial X}(UH)=0 \tag{3.22}$$

For linear long wave theory, the wave celerity C_0 is given by

$$C_0=\sqrt{g\,h_0} \tag{3.23}$$

Equation (3.19) contains two terms of order ε, the convective acceleration and bottom stress terms. We form their ratio to obtain

$$\frac{\text{convective term}}{\text{bottom stress term}} = \frac{\frac{C_0 T_c}{L}}{\frac{C_0 T_c}{h_0}} = \frac{h_0}{L} \tag{3.24}$$

The long wave condition is

$$\frac{h_0}{L} < \frac{1}{20} \tag{3.25}$$

Thus, the long wave condition is equivalent to $\frac{\text{convective term}}{\text{bottom stress term}} < \frac{1}{20}$, and we may neglect the convective term to get

$$\frac{\partial}{\partial T}(UH) = -H\frac{\partial N}{\partial X} - \frac{\eta_0}{h_0}\frac{C_0 T_c}{h_0}\frac{f^b}{8}|U|U \tag{3.26}$$

By defining

$$F_b = \frac{\eta_0}{h_0}\left(\frac{L}{h_0}\right)\frac{C_0 T_c}{L} f^b, \tag{3.27}$$

we can write (3.26) as

$$\frac{\partial}{\partial T}(UH) = -H\frac{\partial N}{\partial X} - \frac{F^b}{8}|U|U \tag{3.28}$$

To linearize the bottom stress term, we use the Lorentz principle of equivalent work: the power loss over one wave period due to nonlinear drag is used to define an equivalent linear drag. The linear drag is defined as

$$T^{bx} = K\,\frac{F^b}{8}U \tag{3.29}$$

where K is the linearization coefficient. By letting

$$U = U^m(X)\,\cos(2\pi T) \tag{3.30}$$

where $U^m(X)$ is the spatially dependent amplitude of the velocity and using the Lorentz principle of equivalent work (McDougal, 1993), we find

$$K = \frac{8}{3\pi}U^m \tag{3.31}$$

Thus,

$$T^{bx} = \frac{F^b}{3\pi}U^m U \tag{3.32}$$

and (3.28) may be expressed as

$$\frac{\partial}{\partial T}(UH) = -H\frac{\partial N}{\partial X} - \frac{F^b}{3\pi}U^m U \tag{3.33}$$

We eliminate UH by cross-differentiating (3.22) and (3.33) to obtain

$$N_{TT} = H_X N_X + HN_{XX} + \frac{F^b}{3\pi}U^m U_X \tag{3.34}$$

From (3.22),

$$U_X = -\frac{1}{H}N_T - \frac{U}{H}H_X \tag{3.35}$$

Substitution of (3.35) into (3.34) gives

$$N_{TT} = HN_{XX} + H_X N_X - \frac{F^b}{3\pi}U^m\left(\frac{1}{H}N_T + \frac{U}{H}H_X\right) \tag{3.36}$$

By assuming a linear bottom slope

$$H_X = M \tag{3.37}$$

we obtain

$$N_{TT} = HN_{XX} + MN_X - \frac{F^b}{3\pi}U^m\left(\frac{1}{H}N_T + \frac{U}{H}M\right) \tag{3.38}$$

Equation (3.38) is the linear wave equation with bottom friction on a sloping bottom.

3.4.1 The Case of Flat Bottom with No Bottom Friction

We assume that $M = 0$ and $f^b = 0$. For all flat bottom cases, the scaled water depth is $H = 1$. With these assumptions (3.38) becomes

$$N_{TT} = N_{XX} \tag{3.39}$$

3.4.2 The Case of Flat Bottom with Bottom Friction

We assume $M = 0$, so that (3.38) becomes

$$N_{TT} = N_{XX} - \frac{F^b\ U^m}{3\pi} N_T \tag{3.40}$$

Let

$$N(X,T) = \exp(\delta T)\ W(X,T). \tag{3.41}$$

With

$$\delta = -\frac{b}{2}, \tag{3.42}$$

and

$$b = \frac{F^b\ U^m}{3\pi}, \tag{3.43}$$

(3.40) can be rewritten as

$$W_{TT} - \frac{b^2}{4} W = W_{XX} \tag{3.44}$$

3.4.3 The Case of Sloping Bottom without Bottom Friction

By setting $M \neq 0$ and $f_b = 0$, the wave equation (3.38) can be rewritten as

$$N_{TT} = HN_{XX} + MN_X \tag{3.45}$$

The bottom slope is assumed to be constant, so that

$$H = MX + 1 \tag{3.46}$$

where the value 1 on the right hand side is the scaled water depth at the beginning of the slope. By substituting (3.46) into (3.45), we obtain

$$N_{TT} = (MX + 1)N_{XX} + MN_X \tag{3.47}$$

The expression above is a partial differential equation with non-constant coefficients. We obtain the case of constant coefficients by assuming a small slope, so that

$$MX << 1, \tag{3.48}$$

and (3.47) becomes

$$N_{TT} = N_{XX} + MN_X \tag{3.49}$$

By letting

$$N(X,T) = \exp(\delta X)\ W(X,T) \tag{3.50}$$

and

$$\delta = -\frac{M}{2}, \tag{3.51}$$

we express (3.49) as

$$W_{TT} + \frac{M^2}{4}W = W_{XX} \tag{3.52}$$

3.5 THE RIEMANN FUNCTION

This section focuses on the Riemann method of determining a Riemann function. The Riemann function will become the kernel of the integral solution to

the boundary value problem of the linear wave equation. The general form of this equation is

$$N_{TT} + aN + eN_T + dN_X = N_{XX} + F^s(X,T) \tag{3.53}$$

in which the coefficients a, d, and e are greater than zero. The external forcing on the system is denoted by $F^s(X,T)$. The initial conditions are

$$N(X,0) = F(X) \tag{3.54}$$

and

$$N_T(X,0) = G(X) \tag{3.55}$$

Equation (3.53) is reduced to a canonical form by introducing the characteristic coordinates

$$\alpha = X + T \tag{3.56}$$

and

$$\beta = X - T \tag{3.57}$$

The two characteristic coordinates represent wave movement to the right and to the left. It follows that,

$$X = \frac{\alpha + \beta}{2} \tag{3.58}$$

and

$$T = \frac{\alpha - \beta}{2} \tag{3.59}$$

By applying the chain rule and collecting terms, we can transform (3.53) to

$$N_{\alpha\beta} = \frac{e+d}{4}N_{\alpha} + \frac{-e+d}{4}N_{\beta} + \frac{a}{4}N - \frac{1}{4}F^{s}\left(\frac{\alpha+\beta}{2}, \frac{\alpha-\beta}{2}\right) \tag{3.60}$$

If we introduce the change of variable

$$N(\alpha,\beta) = V(\alpha,\beta)\ \exp(\lambda\alpha + \mu\beta), \tag{3.61}$$

where

$$\lambda = \frac{-e+d}{4} \tag{3.62}$$

and

$$\mu = \frac{e+d}{4}, \tag{3.63}$$

then we can simplify (3.60) to

$$V_{\alpha\beta} = -\kappa V + G^{s}(\alpha,\beta) \tag{3.64}$$

where

$$G^{s}(\alpha,\beta) = -\frac{1}{4}\ \exp\left[-(\lambda\alpha+\mu\beta)\right] F^{s}\left(\frac{\alpha+\beta}{2}, \frac{\alpha-\beta}{2}\right) \tag{3.65}$$

and

$$\kappa = -\left(\frac{a}{4} + \lambda\mu\right) \tag{3.66}$$

If $T = 0$, then from (3.56) and (3.57), $X = \alpha = \beta$. By using (3.61), we can write the initial condition (3.54) as

$$V(\alpha,\alpha) = F(\alpha)\ \exp\left(-\frac{\alpha\, d}{2}\right) \tag{3.67}$$

Similarly, we can write N_T at $T = 0$ as

$$N_T(X,0) = N_\alpha(\alpha,\alpha) - N_\beta(\alpha,\alpha) \tag{3.68}$$

By using (3.61), we can write the initial conditions in (3.55) as

$$V_\alpha(\alpha,\alpha) - V_\beta(\alpha,\alpha) = \left[\frac{e}{2} F(\alpha) + G(\alpha)\right] \exp\left(-\frac{\alpha d}{2}\right) \tag{3.69}$$

After several substitutions, the initial conditions in (3.54) and (3.55) can be written as

$$V(\alpha,\alpha) = h^s(\alpha) = F(\alpha) \exp\left(-\frac{\alpha d}{2}\right) \tag{3.70}$$

$$V_\alpha(\alpha,\alpha) = \phi(\alpha) = \left[F(\alpha)\left(-\frac{d}{2}\right) + F_\alpha(\alpha)\right] \exp\left(-\frac{\alpha d}{2}\right) \tag{3.71}$$

$$V_\beta(\alpha,\alpha) = \psi(\alpha) = \left[F_\alpha(\alpha) - \left(\frac{e+d}{2}\right) F(\alpha) - G(\alpha)\right] \exp\left(-\frac{\alpha d}{2}\right) \tag{3.72}$$

To solve the differential equation in (3.64) with initial conditions given in (3.70), (3.71) and (3.72), the Riemann method is used (Guenther and Lee, 1996). The method solves $V(\alpha,\beta)$, using a function $R(\alpha,\beta;\xi,\eta)$ called the Riemann function. Let α,β be fixed and use ξ,η as the independent variables in the α,β plane. We multiply (3.64) by the function $R(\alpha,\beta;\xi,\eta)$, and integrate over the triangle $T(\alpha,\beta)$ (see Figure 3.3). We choose R so that integrals involving unknown values of v disappear.

$$\iint_{T(\alpha,\beta)} R\,G\,d\xi\,d\eta = \iint_{T(\alpha,\beta)} R\,(V_{\xi\eta} + \kappa V)\,d\xi\,d\eta$$

$$= \iint_{T(\alpha,\beta)} \left[\left(R\,V_{\xi}\right)_{\eta} - \left(R_{\eta}\,V\right)_{\xi} + \left(R_{\xi\eta} + \kappa R\right) V \right] d\xi\,d\eta \tag{3.73}$$

Because V is unknown in $T(\alpha,\beta)$, we can eliminate the last term by requiring

$$R_{\xi\eta} + \kappa R = 0 \qquad \alpha > \xi\,, \eta > \beta \tag{3.74}$$

The Integration on the exact derivative terms with the limits of integration shown in Figure 3.3 gives

$$\begin{aligned} \iint_{T(\alpha,\beta)} R\,G\,d\xi\,d\eta &= -R(\alpha,\beta;\xi,\eta)\;V(\alpha,\beta) + R(\alpha,\beta;\beta,\beta)\,h^{s}(\beta) \\ &+ \int_{\beta}^{\alpha} R(\alpha,\beta;\xi,\xi)\,\phi(\xi)\,d\xi + \int_{\beta}^{\alpha} R_{\xi}(\alpha,\beta;\xi,\beta)\,V(\xi,\beta)\,d\xi\,d\eta \\ &- \int_{\beta}^{\alpha} R_{\eta}(\alpha,\beta;\alpha,\eta)\,V(\alpha,\eta)\,d\eta + \int_{\beta}^{\alpha} R_{\eta}(\alpha,\beta;\eta,\eta)\,h^{s}(\eta)\,d\eta \end{aligned} \tag{3.75}$$

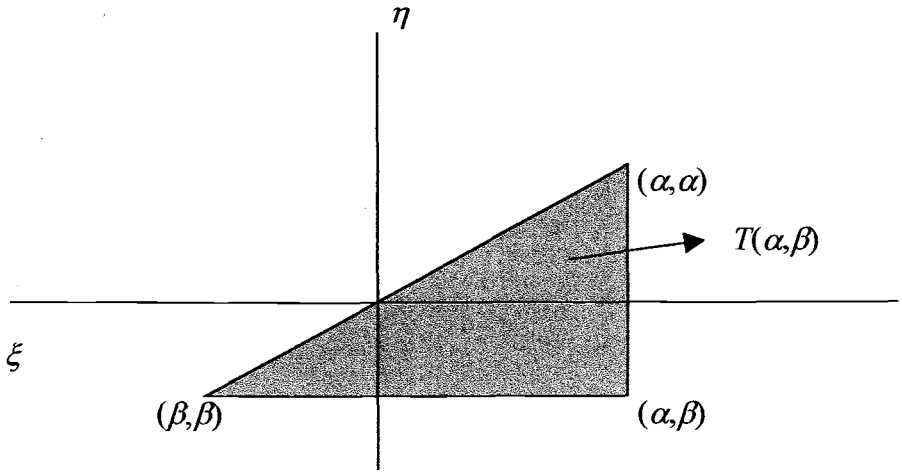

Figure 3.3 Limit of integration

Because $v(\xi,\beta)$ and $v(\alpha,\eta)$ are unknown, we can eliminate them by requiring

$$R_{\xi}(\alpha,\beta;\xi,\beta)=0 \tag{3.76}$$

and

$$R_{\eta}(\alpha,\beta;\alpha,\eta)=0 \tag{3.77}$$

Recall that

$$R(\alpha,\beta;\alpha,\beta)=1 \tag{3.78}$$

With the restrictions in (3.76) - (3.78), the solution to (3.64) can be written as

$$\begin{aligned} v(\alpha,\beta) &= R(\alpha,\beta;\beta,\beta)\ h(\beta)+\int_{\beta}^{\alpha} R(\alpha,\beta;\xi,\xi)\ \phi(\xi)\ d\xi \\ &+\int_{\beta}^{\alpha} R_{\eta}(\alpha,\beta;\eta,\eta)\ h^{s}(\eta)\ d\eta\ -\iint_{T(\alpha,\beta)} R(\alpha,\beta;\xi,\eta)\ G(\xi,\eta)\ d\xi\ d\eta \end{aligned} \tag{3.79}$$

The solution in (3.79) is valid provided that there is a function R such that

$$R_{\xi\eta}(\alpha,\beta;\xi,\eta)\ +\ \kappa\ R_{\xi\eta}(\alpha,\beta;\xi,\eta)\ =0 \qquad \alpha>\xi,\eta>\beta \tag{3.80}$$

with the restrictions

$$R_{\xi}(\alpha,\beta;\xi,\beta)=0 \qquad \alpha\ >\ \xi \tag{3.81}$$

$$R_{\eta}(\alpha,\beta;\alpha,\eta)\ =\ 0 \qquad \eta\ >\ \beta \tag{3.82}$$

and

$$R(\alpha,\beta;\alpha,\beta)=1 \tag{3.83}$$

We can solve (3.80) by letting $r=(\alpha-\xi)(\eta-\beta)$. We assume any smooth function $R=\rho(r)$, that satisfies (3.81), (3.82) and (3.83). The PDE in (3.80) can be modified as

$$-r\rho_{rr}(r) - \rho_r(r) + \kappa\,\rho(r) = 0 \tag{3.84}$$

By using the restriction $R(\alpha,\beta;\alpha,\beta)=1$ or $\rho(r=0)=1$, we can write the solution to (3.84) as

$$\rho(r) = I_o\left(2\sqrt{\kappa r}\right) \tag{3.85}$$

where $I_0(\ )$ is a modified Bessel function of the first type of order zero. By substituting $r=(\alpha-\xi)(\eta-\beta)$ into (3.85), we can get

$$R(\alpha,\beta;\xi,\eta) = I_o\left(2\sqrt{\kappa\,(\alpha-\xi)(\eta-\beta)}\right) \tag{3.86}$$

Equation (3.86) is the Riemann function of (3.64). If we substitute (3.86) into (3.79), we can get

$$\begin{aligned} V(\alpha,\beta) = {} & h^s(\beta) + \int_{\beta}^{\alpha} I_o\left(2\sqrt{\kappa(\alpha-\xi)\,(\xi-\beta)}\right)\phi(\xi)\,d\xi \\ & + \kappa\int_{\beta}^{\alpha} I_1\left(2\sqrt{\kappa(\alpha-\eta)\,(\eta-\beta)}\right)\frac{\alpha+\beta-2\eta}{\sqrt{\kappa(\alpha-\eta)\,(\eta-\beta)}}\,h^s(\eta)\,d\eta \\ & - \iint_{T(\alpha,\beta)} I_o\left(2\sqrt{\kappa(\alpha-\xi)\,(\eta-\beta)}\right)G(\xi,\eta)\,d\xi\,d\eta \end{aligned} \tag{3.87}$$

A more symmetrical solution can be developed which includes initial data $\psi(x,0)$. Consider the previous derivation starting at (3.73). The order of the independent variables ξ and η in (3.73) are interchanged by writing

$$R\,(v_{\xi\eta} + \kappa V) = (R\,V_{\eta})_{\xi} - (R_{\xi})_{\eta} + (R_{\xi\eta} + \kappa\,R)\,V \tag{3.88}$$

Equation (3.88) is integrated using the integral boundaries as shown in Figure 3.3 to find a form for $V(\alpha,\beta)$. After several steps, we can get

$$\begin{aligned} V(\alpha,\beta) = {} & R(\alpha,\beta;\ \alpha,\alpha)\ h_s(\alpha) - \int_{\beta}^{\alpha} R(\alpha,\beta;\eta,\eta)\ \ \psi(\eta)\,d\eta \\ & - \int_{\beta}^{\alpha} R_{\xi}(\alpha,\beta;\xi,\xi)\ \ h^s(\xi)\,d\xi \ - \iint_{T(\alpha,\beta)} R(\alpha,\beta;\xi,\eta)\ G(\xi,\eta)\,d\xi\,d\eta \end{aligned} \tag{3.89}$$

By substituting (3.86) into (3.89), and averaging (3.89) and (3.79), we can write the symmetrical $V(\alpha,\beta)$ as

$$\begin{aligned} V(\alpha,\beta) = {} & \frac{h(\alpha)+h(\beta)}{2} + \frac{1}{2}\int_{\beta}^{\alpha} I_o\left(2\sqrt{\kappa(\alpha-\xi)\,(\xi-\beta)}\right)\phi(\xi)\,d\xi \\ & - \frac{1}{2}\int_{\beta}^{\alpha} I_o\left(2\sqrt{\kappa(\alpha-\eta)\,(\eta-\beta)}\right)\psi(\eta)\,d\eta \\ & + \frac{1}{2}\,\kappa\int_{\beta}^{\alpha} I_1\left(2\sqrt{\kappa(\alpha-\eta)\,(\eta-\beta)}\right)\frac{\alpha+\beta-2\eta}{\sqrt{\kappa(\alpha-\eta)\,(\eta-\beta)}}\,h^s(\eta)\,d\eta \\ & - \frac{1}{2}\,\kappa\int_{\beta}^{\alpha} I_1\left(2\sqrt{\kappa(\alpha-\xi)\,(\xi-\beta)}\right)\frac{\alpha+\beta-2\eta}{\sqrt{\kappa(\alpha-\xi)\,(\xi-\beta)}}\,h^s(\xi)\,d\xi \\ & - \iint_{T(\alpha,\beta)} I_o\left(2\sqrt{\kappa(\alpha-\xi)\,(\eta-\beta)}\right)G(\xi,\eta)\,d\xi\,d\eta \end{aligned} \tag{3.90}$$

The 4^{th} and 5^{th} terms are equal, but are of opposite sign, thus, they cancel each other. We can rewrite (3.90) as

$$V(\alpha,\beta) = \frac{h^s(\alpha)+h^s(\beta)}{2} + \frac{1}{2}\int_{\beta}^{\alpha} I_o\left(2\sqrt{\kappa(\alpha-\xi)\,(\xi-\beta)}\right)\phi(\xi)\,d\xi$$
$$- \frac{1}{2}\int_{\beta}^{\alpha} I_o\left(2\sqrt{\kappa(\alpha-\eta)\,(\eta-\beta)}\right)\psi(\eta)\,d\eta \qquad (3.91)$$
$$- \iint_{T(\alpha,\beta)} I_o\left(2\sqrt{\kappa(\alpha-\xi)\,(\eta-\beta)}\right)G(\xi,\eta)\,d\xi\,d\eta$$

The 2^{nd} and 3^{rd} terms can be combined. We can rewrite (3.91) as

$$V(\alpha,\beta) = \frac{h^s(\alpha)+h^s(\beta)}{2}$$
$$+ \frac{1}{2}\int_{\beta}^{\alpha} I_o\left(2\sqrt{\kappa(\alpha-\tau)\,(\tau-\beta)}\right)\left(\phi(\tau)-\psi(\tau)\right)\,d\tau \qquad (3.92)$$
$$- \iint_{T(\alpha,\beta)} I_o\left(2\sqrt{\kappa(\alpha-\xi)\,(\eta-\beta)}\right)G(\xi,\eta)\,d\xi\,d\eta$$

$V(\alpha,\beta)$ is transformed back to $N(\alpha,\beta)$, and to $N(X,T)$ by using the following equations,

$$N(\alpha,\beta) = V(\alpha,\beta)\ \exp(\lambda\,\alpha + \mu\beta) \qquad (3.93)$$

and

$$N(X,T) = N\left(\frac{\alpha+\beta}{2}, \frac{\alpha-\beta}{2}\right) \qquad (3.94)$$

To demonstrate the use of the Riemann function, we use (3.92) for the case of a flat bottom without bottom friction. The governing equation is (3.39). The initial conditions are

$$N(X,0)=F(X) \tag{3.95}$$

and

$$N_T(X,0)=0 \tag{3.96}$$

$F(X)$ in (3.95) is taken to be a step function,

$$F(X)=\begin{cases}\dfrac{1}{h_0}+1 & -\dfrac{a^s}{L}\le X\le\dfrac{a^s}{L}\\[2ex] 1 & \text{otherwise}\end{cases} \tag{3.97}$$

where h_0 is a scaling constant for water depth, a^s is the limit of the spatial domain, and is set to be 0.5 m. By matching (3.39) to (3.53), the coefficients *a*, *e* and *d* can be obtained as zero. From (3.66), we can get $\kappa=0$. By using (3.86), the Riemann function can be written as

$$R(\alpha,\beta;\xi,\eta)=1 \tag{3.98}$$

We substitute (3.98) into (3.91) to get

$$\begin{aligned}V(\alpha,\beta) &= \frac{h^s(\alpha)+h^s(\beta)}{2}+\frac{1}{2}\int_{\beta}^{\alpha}\left(\phi(\tau)-\psi(\tau)\right)d\tau\\ &\quad -\iint_{T(\alpha,\beta)}G(\xi,\eta)\,d\xi\,d\eta\end{aligned} \tag{3.99}$$

Equations (3.93) and (3.94) are used to transform the solution $V(\alpha,\beta)$ back to $N(X,T)$. Figure 3.4 shows the solution of (3.99) with the initial displacement written in (3.97). The water depth h_0 is taken to be 1 meter. The solution is presented in dimensional form.

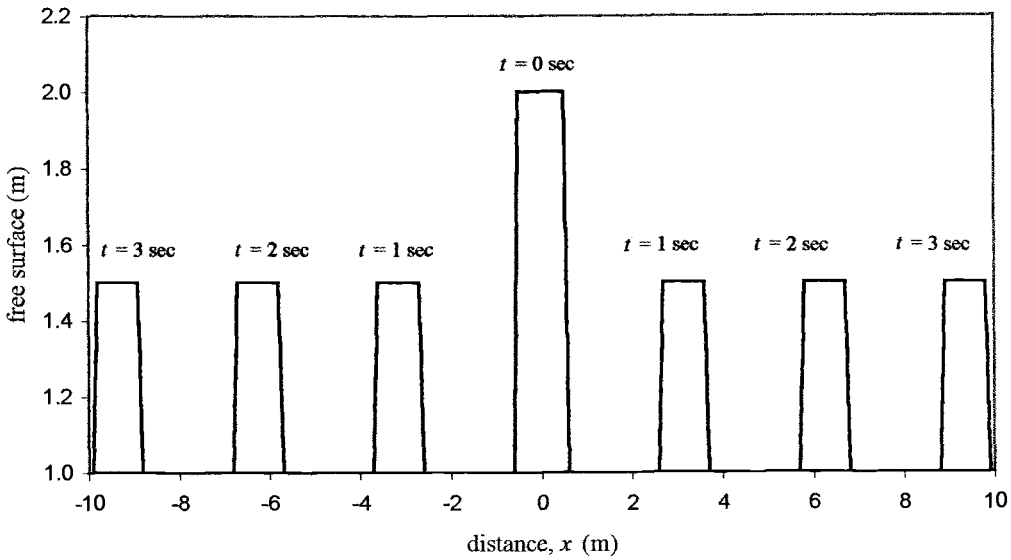

Figure 3.4 Propagation of a square wave on a flat bottom without friction

The total area under the curves in Figure (3.4) is found to be constant as time elapses. This indicates that the integral solution satisfies the conservation of mass. The waves start as one wave at $t=0$ sec and split into two identical waves exactly half the initial size and travel in opposite directions. The wave height at $t>0$ is constant. From the constant wave height and uniform water depth, it can be concluded that the total energy flux is constant. Thus, the integral solution satisfies the conservation of energy as well.

The next case is the problem of flat bottom with bottom friction. The governing equation follows (3.44). This case uses the same initial displacement

written in (3.97). Figure 3.5 shows the results in dimensional form. The bottom friction coefficient f^b is taken to be 0.1.

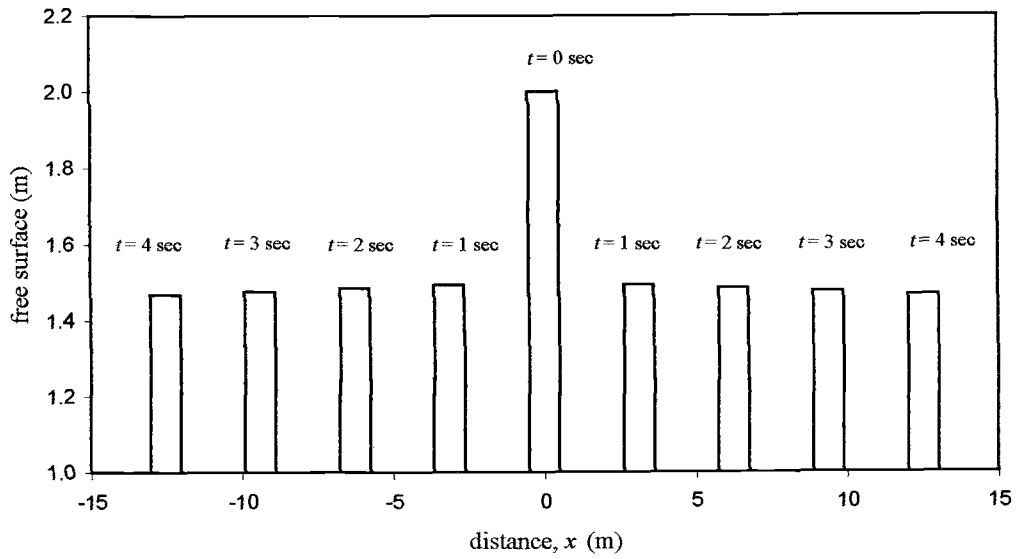

Figure 3.5 Propagation of a square wave on flat bottom with bottom friction $f^b = 0.1$.

From the above figure, the height of the step function decreases as the waves travel away from the initial condition.. The height decreases about 0.55% from $t = 0$ sec to $t = 1$ sec, 0.54% from $t = 1$ sec to $t = 2$ sec, and 0.53% from $t = 3$ sec to $t = 4$ sec. Since the energy is proportional to H^2, the energy loss is the squared of the wave height decrease.

We have shown that solving a linear PDE with constant coefficients can be reduced to determining a Riemann function for the problem. In the next chapter, more complex cases are considered.

CHAPTER 4. BOUNDARY VALUE PROBLEM WITH HYPERBOLIC POTENTIAL THEORY

Fulks and Guenther (1972) presented a method to solve boundary value problems using integral equations. In this chapter, the method is applied to the linear long wave equations derived in Chapter 3 to test the ability of the solution to represent fractal waves.

The discussion is divided into propagation of waves over a semi-infinite domain with a flat bottom with and without bottom friction, and over a finite domain with or without bottom friction with a reflective vertical wall. The case of sloping bottom without bottom friction is also discussed. Sinusoidal waves, Weierstrass function-generated waves, and measured ocean wave data are used as boundary conditions. Fractal dimensions are calculated for the wave data using rescaled range analysis.

The scaled linear wave equation can be written in general form as

$$N_{TT} + aN + eN_T + dN_X = N_{XX} \tag{4.1}$$

where a, d, e are the coefficients obtained from the scaling process as described in Section 3.4. The initial conditions are taken to be

$$N(X,0) = N_T(X,0) = 0 \tag{4.2}$$

The boundary condition at $X = B_1 = 0$ is

$$N(X = B_1, T) = F(T) \tag{4.3}$$

The boundary condition for the reflecting wall located at $X = A$ is written as

$$N_X\left(X = A, T\right) = 0 \tag{4.4}$$

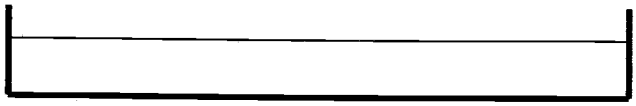

$X = 0$ $X = A$ or ∞

Sketch of boundaries

The Riemann function $R = R(\alpha, \beta; \xi, \eta)$ is applied at each boundary, where α, β are the characteristic coordinates, and ξ, η are the independent variables in the characteristic plane. Recall from (3.56) and (3.57) that the characteristic coordinates are defined as

$$\alpha = X + T \tag{4.5}$$

and

$$\beta = X - T \tag{4.6}$$

If we let s, τ be the independent variables in X, T plane, analogous to (4.5) and (4.6), then we can write the definitions of ξ and η as

$$\xi = s + \tau \tag{4.7}$$

and

$$\eta = s - \tau \tag{4.8}$$

By using the relationships in (4.5) to (4.8), we can write the Riemann function $R = R(\alpha,\beta;\xi,\eta)$ as $R = R(X,T;s,\tau)$. The fundamental solution κ of (4.1) is defined as

$$\kappa = \kappa(X,T;s,\tau) = \frac{1}{2}\begin{cases} R(X,T;s,\tau) & |X-s| \le T-\tau \\ 0 & \text{otherwise} \end{cases} \tag{4.9}$$

The factor $\frac{1}{2}$ is not critical. Its presence is explained by the form of the solution of the initial value problem by Riemann's method written in Section 3.5 (Fulks and Guenther, 1972).

For the Dirichlet-type boundary condition (4.3), the solution to (4.1) is defined as

$$N(X,T) = 2\int_{-\infty}^{\infty} \frac{\partial}{\partial s}\vartheta(X,T;s=B_1,\tau)\,\phi(\tau)\,d\tau \tag{4.10}$$

Equation (4.10) is called *double layer potential*. We substitute (4.9) into (4.10). Fulks and Guenther (1972) evaluate the derivative $\partial/\partial s$ in the region of $|X-s| \le T-\tau$ as

$$\begin{aligned} N(X,T) = &\int_0^{T_a} R_s(X,T;s=B_1,\tau)\,\phi(\tau)\,d\tau \\ &- R(X,T;s=B_1,T_a)\,\phi(T_a)\,\frac{\partial}{\partial X}T_a \end{aligned} \tag{4.11}$$

where the density $\phi(T) = 0$, for $T \le 0$. T_a is defined as

$$T_a = T - X + B_1 \tag{4.12}$$

If the boundary condition is a Neumann-type, written as

$$\frac{\partial}{\partial X} N(X = B_1, T) = G(T), \tag{4.13}$$

then the solution is written for $|X - s| \le T - \tau$ as

$$N(X,T) = 2 \int_{-\infty}^{\infty} \vartheta(X,T;s = B_1,\tau)\ \phi(\tau)\ d\tau \tag{4.14}$$

Equation (4.14) is called *single layer potential.* By substituting (4.9) into (4.14), we can rewrite (4.14) as

$$N(X,T) = \int_{0}^{T_a} R(X,T;s = B_1,\tau)\ \phi(\tau)\ d\tau \tag{4.15}$$

If the two boundary conditions exist as a combination of (4.3) and (4.4) at different locations, then the solution can be written as a combination of *double* and *single layer potentials* in the region of $|X - s| \le T - \tau$,

$$\begin{aligned} N(X,T) = & \int_{0}^{T_a} R_s(X,T;s = B_1,\tau)\ \phi(\tau)\ d\tau \\ & - R(X,T;s = B_1,T_a)\ \phi(T_a)\ \frac{\partial}{\partial X} T_a \\ & + \int_{0}^{S_a} R(X,T;s = A,\tau)\ \psi(\tau)\ d\tau \end{aligned} \tag{4.16}$$

where

$$S_a = T + X - A \tag{4.17}$$

The density $\psi(\tau)$ is zero for $\tau \leq 0$. To verify this solution, a simple sinusoidal function is applied as the boundary condition. The function can be written as

$$F(T) = \sin(2\pi T) \tag{4.18}$$

Next, we use the Weierstrass function written in (2.11) as a fractal boundary condition. The nondimensional form of the function is

$$F(T) = \sum_{k=1}^{\infty} \lambda^{(\gamma-2)k} \sin(\lambda^k T) \tag{4.19}$$

For the model, the parameters λ and γ are each taken to be 1.5.

The ocean wave data are taken from Sandy Duck, North Carolina, 1997 and Grays Harbor, Washington, 1999. The original data, unfortunately, are not in shallow water. In order to make the data consistent with the shallow water approximation, we process it in the following way. Working in the frequency domain, the energy spectrum is altered by multiplying it by a frequency dependent shoaling transfer function. The resulting spectrum is low pass filtered at 0.01 Hz to eliminate wind waves, and frequencies greater than a shallow water cutoff frequency. This truncated spectrum is then transformed to the time domain. The result is time series consistent with the shallow water approximations.

For the ocean data, the peak wave period is taken to be the nondimensional constant T_c. The nondimensional constant L is chosen so that (3.21) is fulfilled.

4.1 FLAT BOTTOM WITHOUT BOTTOM FRICTION ON SEMI-INFINITE DOMAIN

The objective of this section is to observe the change of fractal dimension as the waves propagate over a flat bottom without bottom friction, $F_b = 0$. Figure 4.1 shows a sketch of the domain.

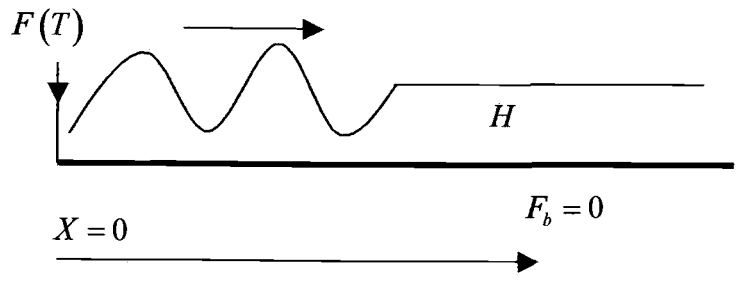

Figure 4.1 Wave propagation on a flat bottom without bottom friction.

The boundary value problem can be rewritten as

$$\begin{aligned} &N_{TT} = N_{XX} && X \geq 0,\ T \geq 0 \\ &N(X,0) = N_T(X,0) = 0 \\ &N(0,T) = F(T) \end{aligned} \qquad (4.20)$$

The boundary condition (4.20) is of Dirichlet-type. Thus, the solution of the boundary value problem is in the form of a double layer potential as in (4.11). The fundamental solution is calculated in the boundary, so $s = 0$. The solution is repeated below,

$$N(X,T)=\int_0^{T_a} R_s(X,T;s=0,\tau)\,\phi(\tau)\,d\tau - R(X,T;s=0,T_a)\,\phi(T_a)\,\frac{\partial}{\partial X}T_a \tag{4.21}$$

where

$$T_a = T - X \tag{4.22}$$

The Riemann function $R(X,T;s,\tau)$ is obtained from (3.86). For the case of a flat bottom without bottom friction, the Riemann function is

$$R(X,T;s,\tau)=1 \tag{4.23}$$

If we substitute (4.23) into (4.21), then we can write the solution as

$$N(X,T)=\phi(T-X) \tag{4.24}$$

The density ϕ is determined by the boundary condition at $X=0$:

$$\phi(T)=F(T) \tag{4.25}$$

This result allows us to express $N(X,T)$ as

$$N(X,T)=F(T-X) \tag{4.26}$$

For the case of a sinusoidal function in (4.18), the solution can be written as,

$$N(X,T)=\sin(2\pi(T-X)) \tag{4.27}$$

And for the case of Weierstrass function in (4.19), the solution can be written as

$$N(X,T)=\sum_{k=1}^{\infty}\lambda^{(\gamma-2)k}\sin\left(\lambda^{k}(T-X)\right) \tag{4.28}$$

The water depth for the problems with sinusoidal and Weierstrass function-generated waves is 2.5 meters. The ocean data can be entered directly into (4.26). Figures 4.2a – 4.2c show the results of (4.27) in dimensional form.

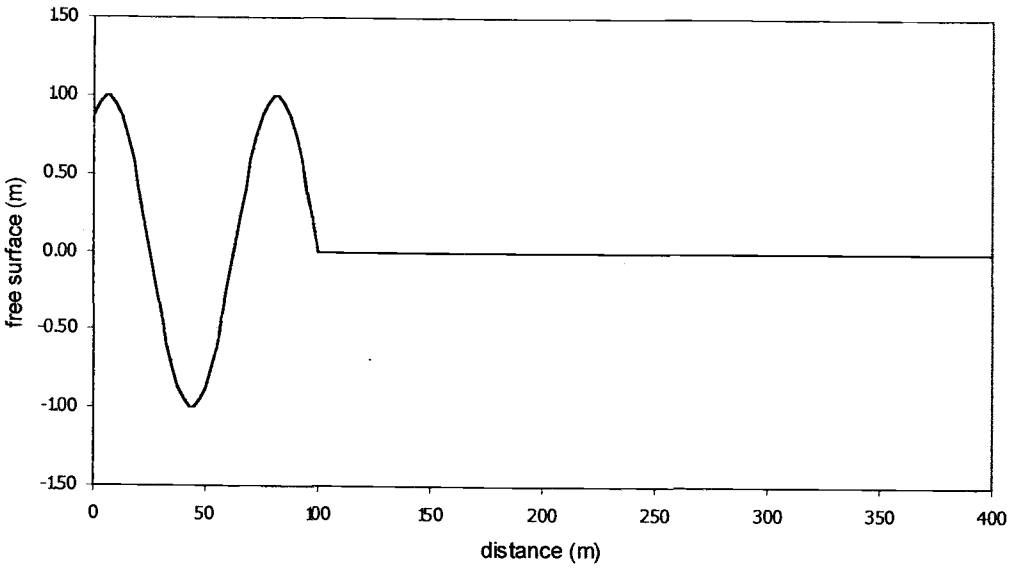

Figure 4.2a. Propagation of sinusoidal waves at $t=20\,\text{sec}$, celerity is 5 m/sec

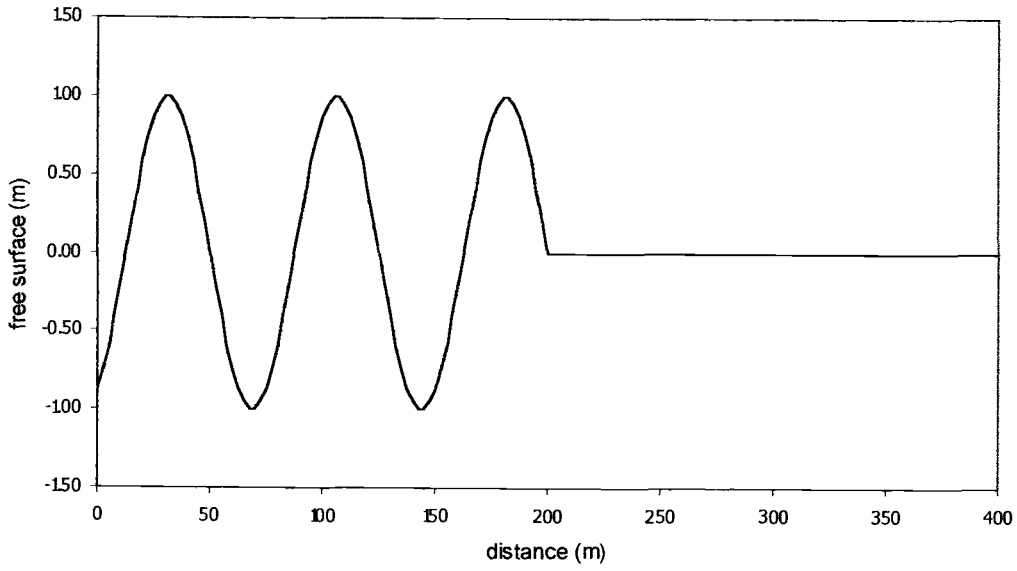

Figure 4.2b. Propagation of sinusoidal waves at $t = 40\,\text{sec}$

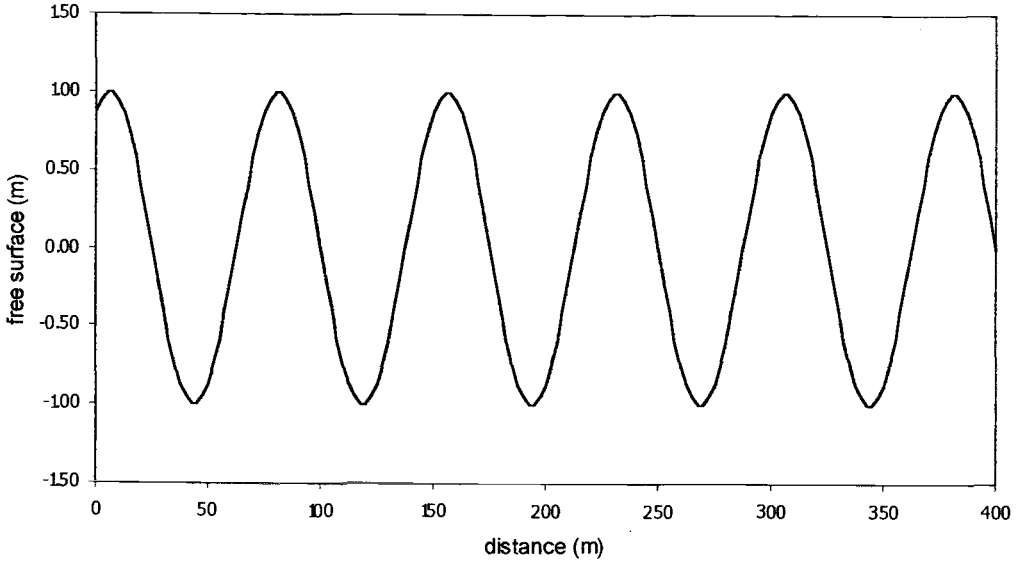

Figure 4.2c. Propagation of sinusoidal waves at $t = 80\,\text{sec}$

Figures 4.2a-c show that the sinusoid propagates without any change in frequency. The energy flux is also conserved.

The next figures show the solution to the fractal-shaped Weierstrass function-generated waves. It is seen that the shape of the propagating wave form is constant.

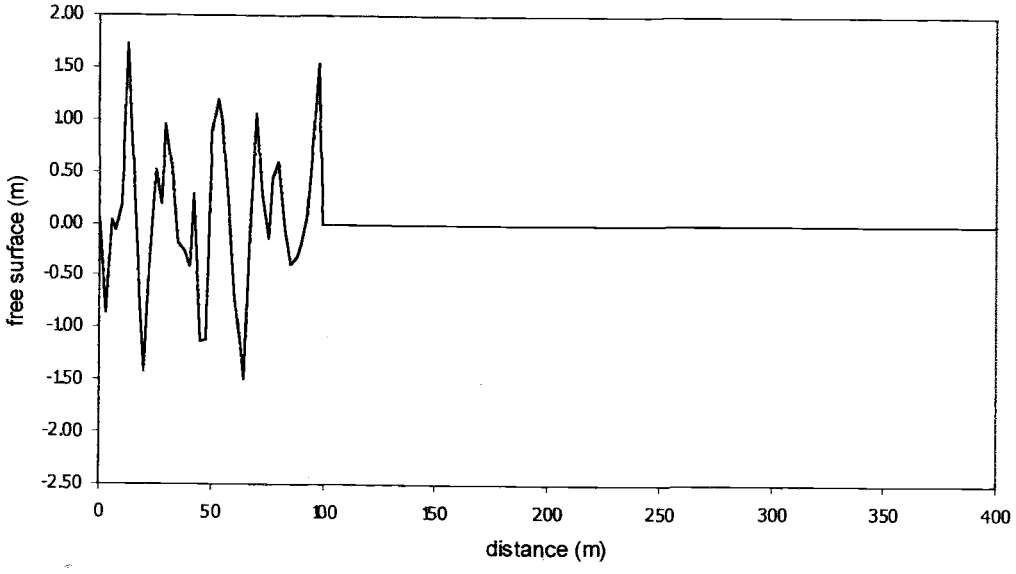

Figure 4.3a. Propagation of fractal Weierstrass function-generated waves at $t = 20\,\text{sec}$.

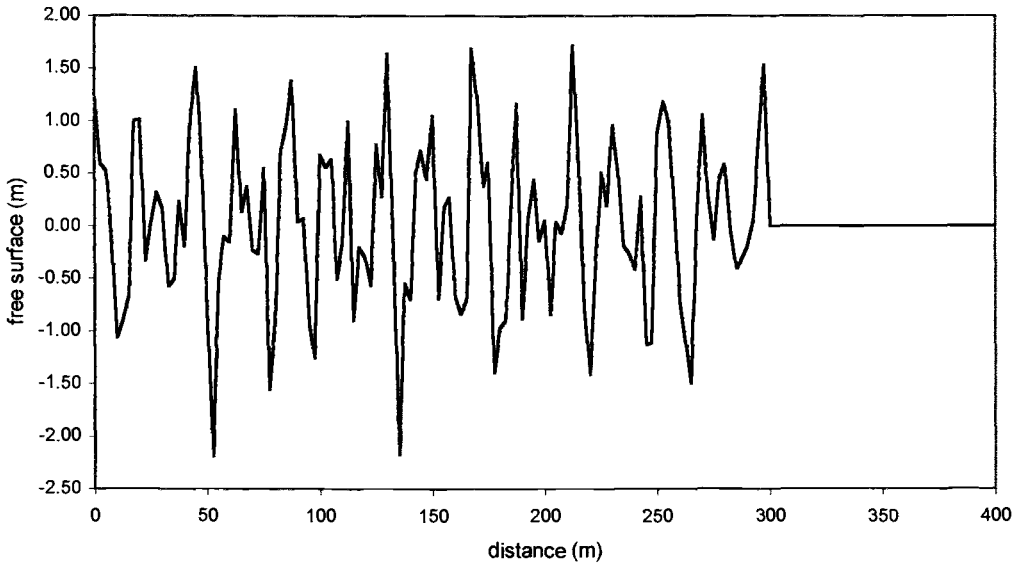

Figure 4.3b. Propagation of fractal Weierstrass function-generated waves at $t = 60\,\text{sec}$

The next figures show the results using the wave data as the input. The ocean wave data are taken from Sandy Duck, Field Research Facility in North Carolina, 1997. The sampling rate is 2 Hz. The time series is taken at a water depth h of approximately 1.9 meters. The wavelength L_0 is approximately 30 meters. The ratio h/L_0 is larger than $1/20$, which is not a shallow water condition. Therefore, the data are shoaled and filtered to a depth of 0.9 meter with the procedure described above. Figures 4.4a – 4.4c show the propagation of waves on a flat bottom without bottom friction.

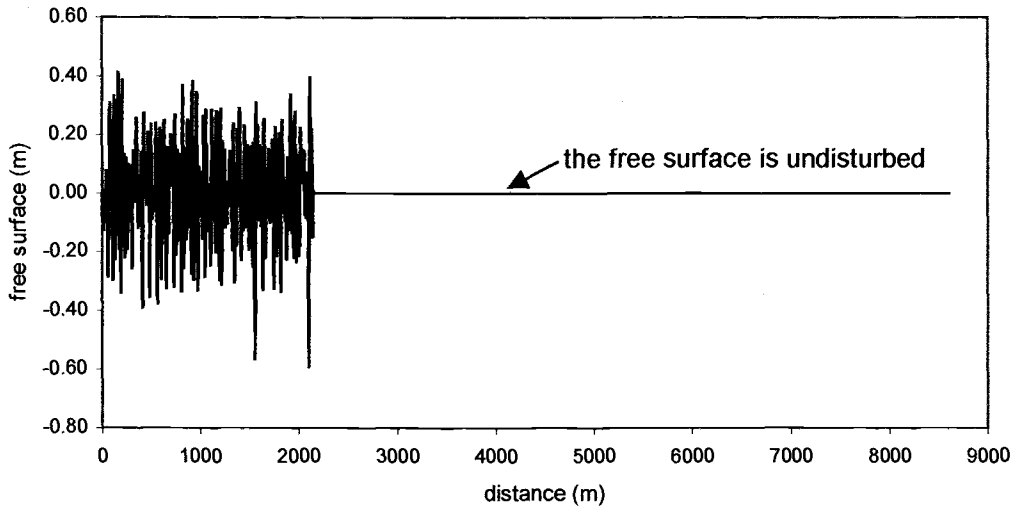

Figure 4.4a. The solution of the wave equation at $t = 716\,\text{sec}$ with ocean waves taken from Sandy Duck Field Research Facility, North Carolina, 1997.

From Figures 4.4a-c, we can see that the solution exhibits what we see in the field, that the waves take time to reach certain point. In other words, the solution gives finite speed of wave propagation. While the waves are propagating, the body of water in front of the waves is undisturbed. Other shallow water solutions give infinite speed of wave propagation. That is the solutions for a certain time t are also defined for the entire distance x.

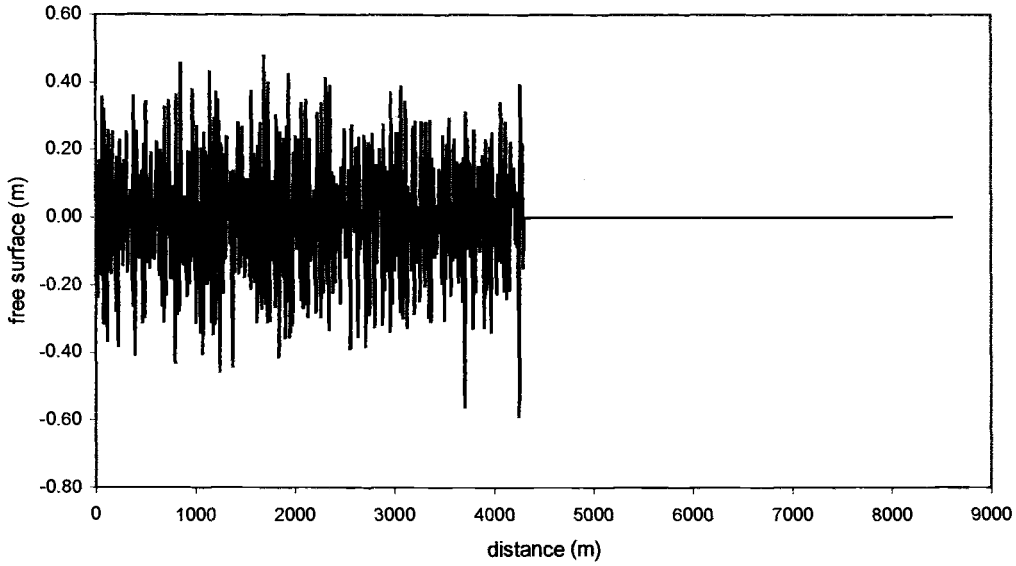

Figure 4.4b. The propagation of ocean waves at $t = 1430\,\text{sec}$

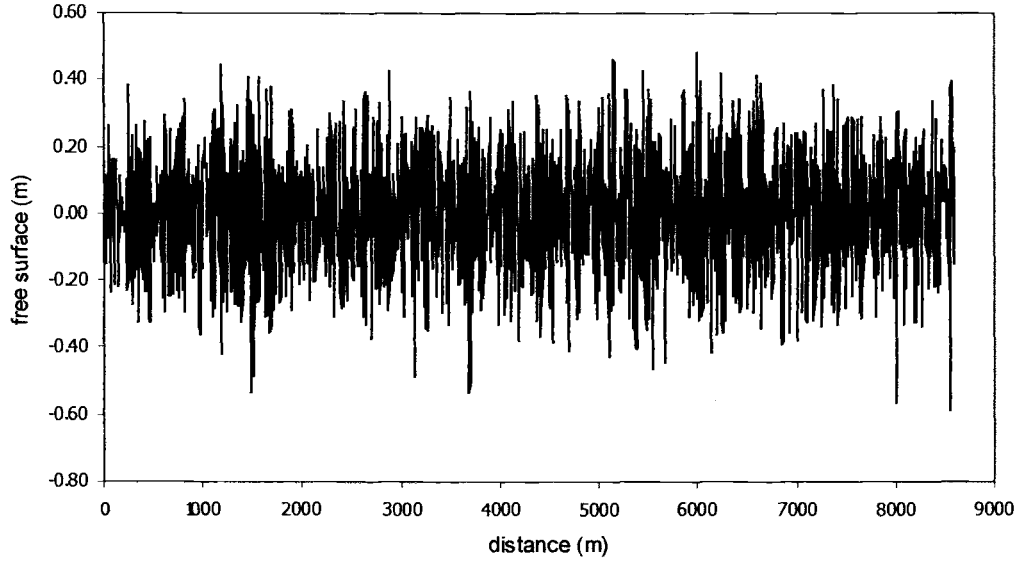

Figure 4.4c The propagation of ocean waves at $t = 2150\,\text{sec}$

The effect of propagation on fractal dimension is determined from the time series of the solution. Figures 4.5 and 4.5b show the solutions in the time domain.

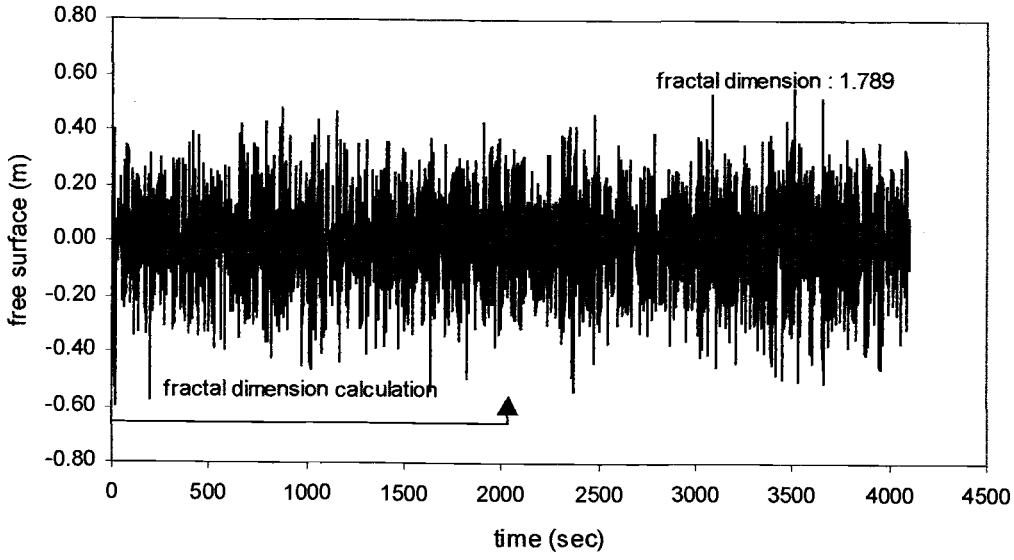

Figure 4.5a. The time history of the solution at $x = 0$, fractal dimension is 1.789.

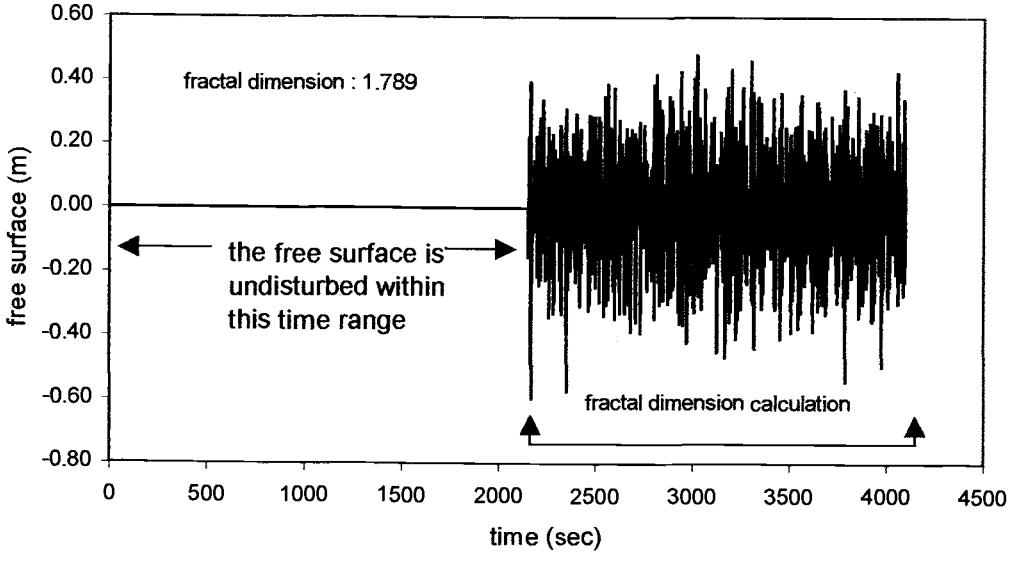

Figure 4.5b. The time series of the solution in the middle of the domain. We can see that there is time range that the free surface is undisturbed.

Figures 4.5a and 4.5b show that the solution of the linear equations for the case of a flat bottom without bottom friction predicts a fractal dimension that is constant in time. This is the result of a linear analysis. Figure 4.5b also shows the time range in which the free surface is undisturbed after the waves pass the middle of domain. Figures 4.5a and 4.5b demonstrate the ability of the solution to reveal finite speed of wave propagation in the time domain. Figures 4.6a and 4.6b show the energy spectrum calculated from the solution at two different locations. It is seen that there is no change in the frequency content. The total area under the energy spectrum curves is identical, indicating that energy flux is conserved for the flat bottom.

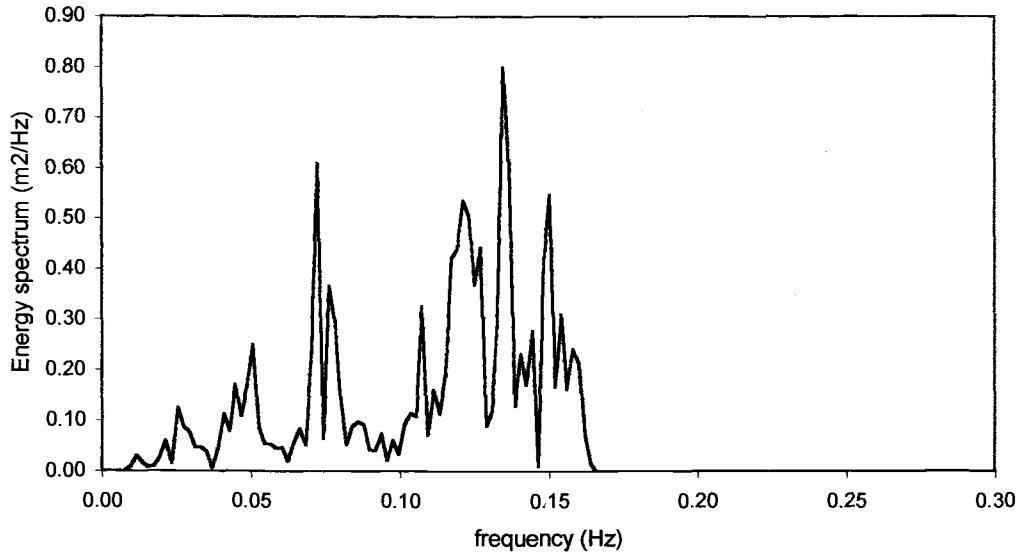

Figure 4.6a Energy spectrum of the time series at $x = 0$ calculated using 4000 points of the time series

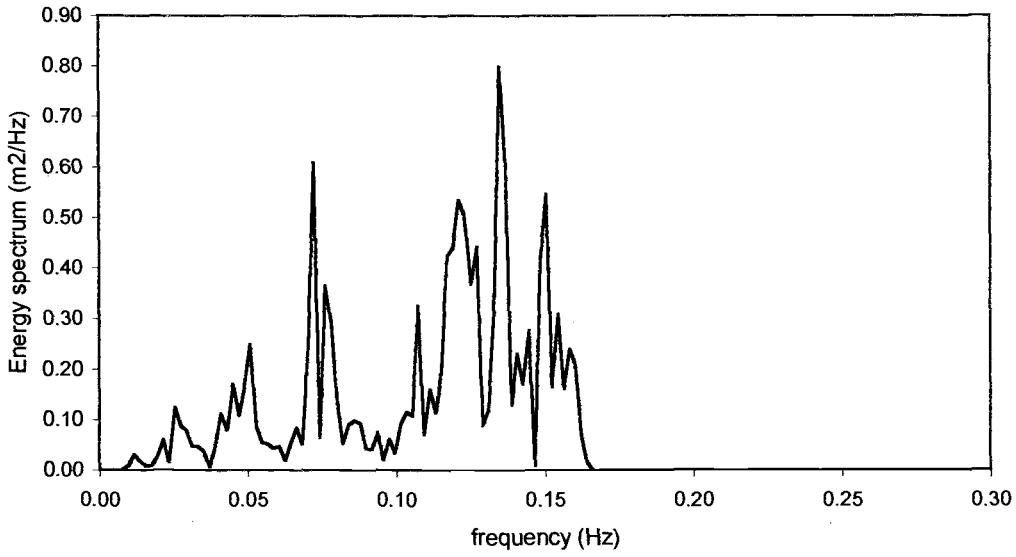

Figure 4.6b. Energy spectrum of the time series near the middle of the domain

4.2 FLAT BOTTOM WITHOUT BOTTOM FRICTION WITH REFLECTIVE WALL

This section focuses on the fractal dimension when the waves interact with a reflective wall. The reflective wall is assumed to be non-porous and vertical. Figure 4.7 shows the sketch of the problem.

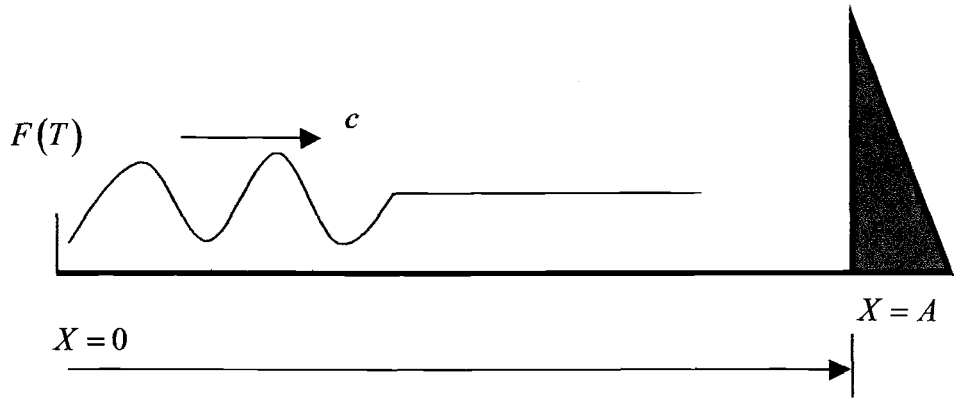

Figure 4.7. Wave propagation on a flat bottom with a reflective wall, without bottom friction.

The reflective wall is located at $X = A$. The boundary value problem is the same as (4.20), with additional boundary conditions at $X = A$,

$$N_X(X = A, T) = 0 \qquad T \geq 0 \tag{4.29}$$

Because there are two boundary conditions, the solution is written in the form of *double* and *single layer potentials*, as in (4.16). The solution can be rewritten as

$$\begin{aligned} N(X,T) = & \int_0^{T_a} R_s(X,T;s=0,\tau)\ \phi(\tau)\, d\tau \\ & - R(X,T;s=0,T_a)\ \phi(T_a)\ \frac{\partial}{\partial X} T_a \\ & + \int_0^{S_a} R(X,T;s=A,\tau)\ \psi(\tau)\, d\tau \end{aligned} \tag{4.30}$$

where T_a is $T - X$ and S_a is $T + X - A$. The Riemann function has the same value as the case in Section 4.1, $R(X,T;s,\tau) = 1$. By substituting T_a, S_a and $R(X,T;s,\tau)$ into (4.30), we can write the solution as

$$N(X,T) = \phi(T - X) + \int_0^{T+X-A} \psi(\tau)\, d\tau \tag{4.31}$$

By applying the boundary condition at $X = 0$, we can write (4.31) as

$$N(0,T) = F(T) = \phi(T) + \int_0^{T-A} \psi(\tau)\ d\tau \tag{4.32}$$

The density $\phi(T)$ is obtained by solving (4.32):

$$\phi(T) = F(T) - \int_0^{T-A} \psi(\tau)\ d\tau \tag{4.33}$$

By differentiating (4.31), we can get

$$\begin{aligned} N_X(X,T) &= -\phi_X(T-X) + \frac{\partial}{\partial X} \int_0^{S_a=T+X-A} \psi(\tau)\ d\tau \\ &= -\phi_X(T-X) + \int_0^{S_a=T+X-A} \psi_X(\tau)\ d\tau + \psi(T+X-A)\frac{\partial S_a}{\partial X} \\ &= -\phi_X(T-X) + \psi(T+X-A) \end{aligned} \tag{4.34}$$

By applying the boundary conditions (4.29) at $X = A$, we can write the density $\psi(T)$ as

$$\psi(T) = \phi_X(T-A) \tag{4.35}$$

By defining $\sigma = T - A$, we can write (4.35) as

$$\phi_X(\sigma) = \psi(\sigma + A) \tag{4.36}$$

Integration of (4.36) gives

$$\begin{aligned} \int_0^{\sigma} \phi'(\sigma)\ d\sigma &= \int_0^{\sigma} \psi(\sigma + A)\ d\sigma \\ \phi(\sigma) &= \int_0^{\sigma=T-A} \psi(\sigma + A)\ d\sigma \end{aligned} \tag{4.37}$$

A change of variable gives

$$\int_0^{T-A} \psi(\tau + A)\, d\tau = \phi(T - A) \tag{4.38}$$

By shifting the arguments of ψ and ϕ by $(-A)$, we can rewrite (4.38) as

$$\int_0^{T-A} \psi(\tau)\, d\tau = \phi(T - 2A) \tag{4.39}$$

The substitution of (4.39) into (4.33) implies that

$$\phi(T) = F(T) - \phi(T - 2A) \tag{4.40}$$

If we reconstruct (4.40) by substituting the density ϕ recursively, then we can write the density ϕ as

$$\phi(T) = F(T) - F(T - 2A) + F(T - 4A) - ..... \tag{4.41}$$

or

$$\phi(T) = \sum_{n=1}^{\infty} (-1)^{n-1}\, F(T - (2n-2)A) \tag{4.42}$$

The substitution of (4.35) into (4.31) will result in the solution $N(X,T)$.

$$N(X,T) = \phi(T - X) + \int_0^{T+X-A} \phi'(\tau - A)\, d\tau \tag{4.43}$$

To evaluate the integral term on the right hand side, we make a change of variable

$$\sigma = \tau - A \tag{4.44}$$

By differentiating with respect to τ, we can get

$$\frac{d\sigma}{d\tau} = 1 \tag{4.45}$$

With the change of variable $\sigma = \tau - A$, the integral term in (4.43) becomes

$$\begin{aligned}
\int_{0}^{S_a=T+X-A} \phi'(\tau - A)\, d\tau &= \int_{-A}^{T+X-2A} \phi'(\sigma)\, d\sigma \\
&= \phi(\sigma)_{\sigma=T+X-A} - \phi(\sigma)_{\sigma=-A} \\
&= \phi(T+X-2A) - \phi(-A) \\
&= \phi(T+X-2A)
\end{aligned} \tag{4.46}$$

The density ϕ with negative argument is zero. The substitution of (4.46) into (4.43) gives the solution $N(X,T)$ as

$$N(X,T) = \phi(T-X) + \phi(T+X-2A) \tag{4.47}$$

If we substitute (4.42) into (4.47), then we can write a solution $N(X,T)$ as

$$N(X,T)=\sum_{n=1}^{\infty}(-1)^{n-1}F\left(T-X-(2n-2)A\right)+\sum_{n=1}^{\infty}(-1)^{n-1}F\left(T+X-2A-(2n-2)A\right) \tag{4.48}$$

Figures 4.8a-c and 4.9a-c show the solutions for the sinusoidal and Weierstrass function waves, respectively. The water depth is taken to be 2.5 meters.

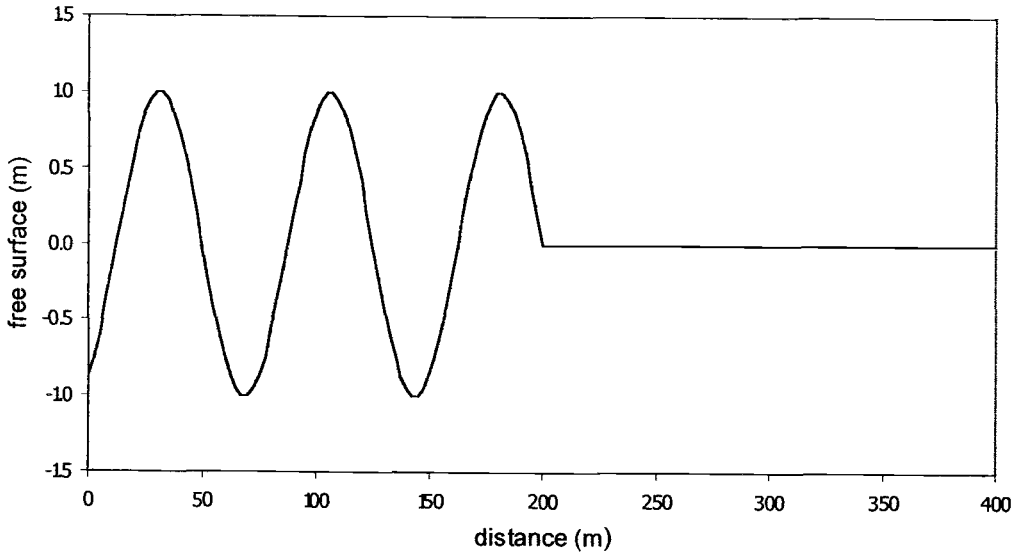

Figure 4.8a. Sinusoidal wave at $t=40\,\text{sec}$. The location of the wall is at $x=400$ m

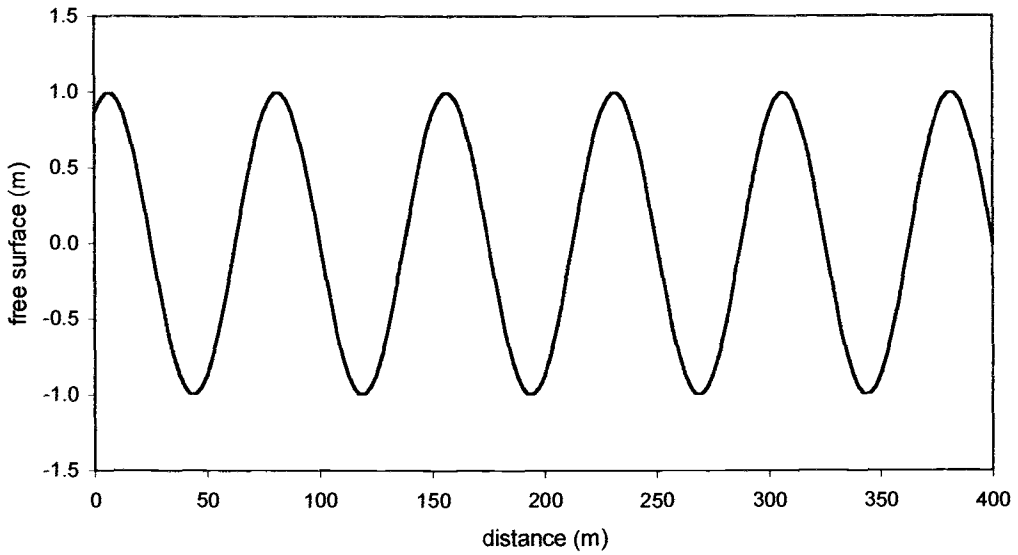

Figure 4.8b. Sinusoidal wave at $t = 80\,\text{sec}$. The wave is hitting the reflective wall at $x = 400$ m

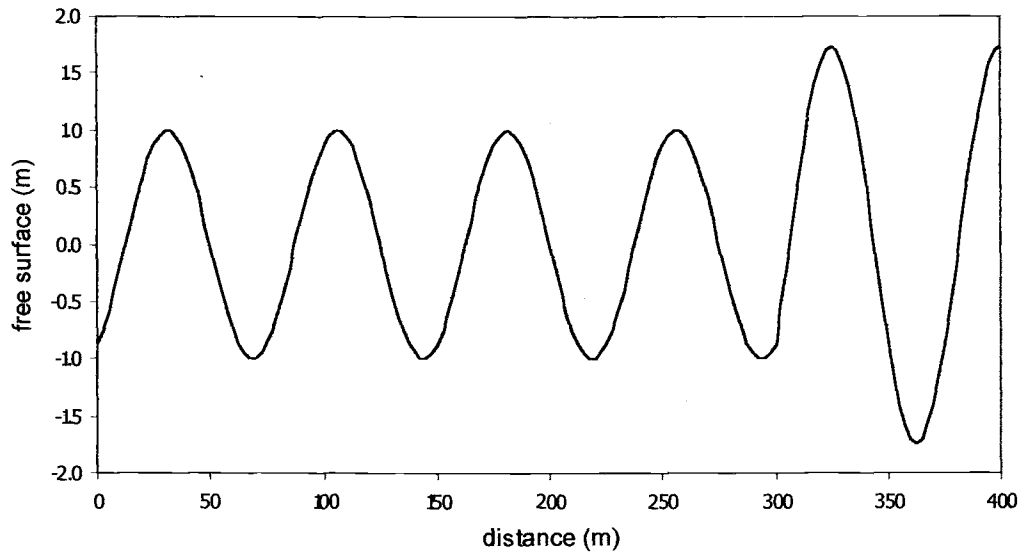

Figure 4.8c. Sinusoidal wave at $t = 100$ sec. The wave is reflected by the wall.

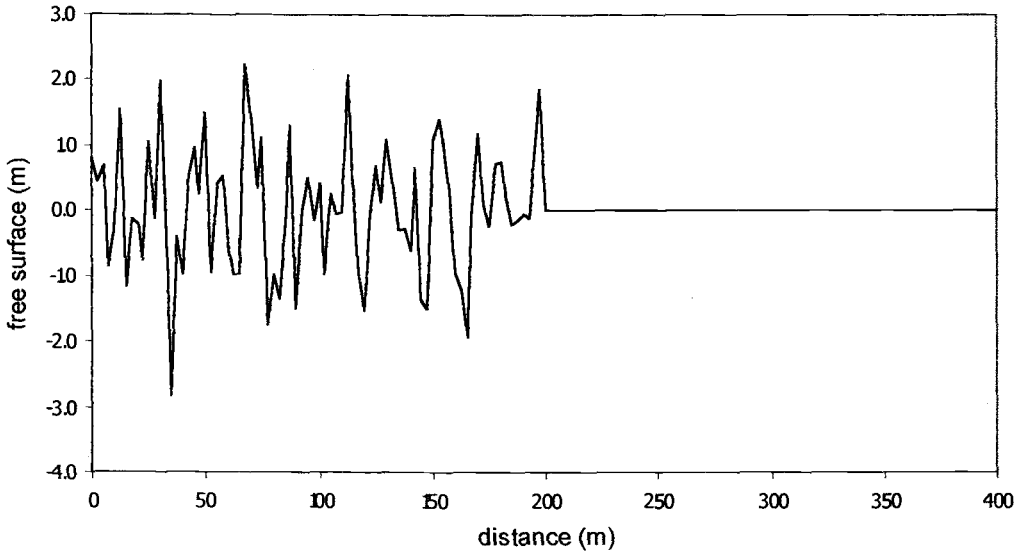

Figure 4.9a Fractal Weierstrass function-generated waves propagation on a flat bottom at $t = 40\,\text{sec}$. The wave celerity is 5 m/sec. The location of the wall is at $x = 400$ m

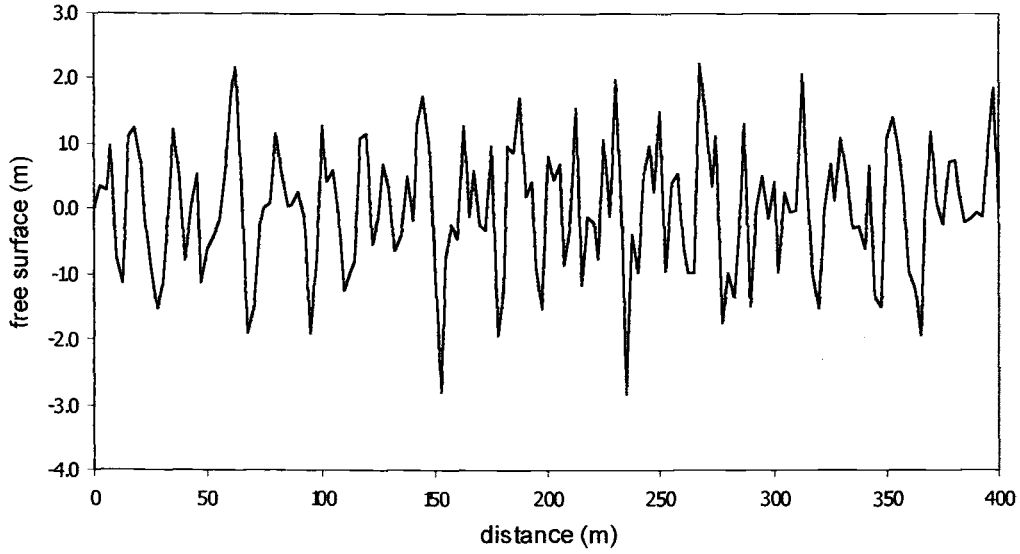

Figure 4.9b. Fractal Weierstrass function-generated waves propagation on a flat bottom at $t = 80\,\text{sec}$. The wave celerity is 5 m/sec

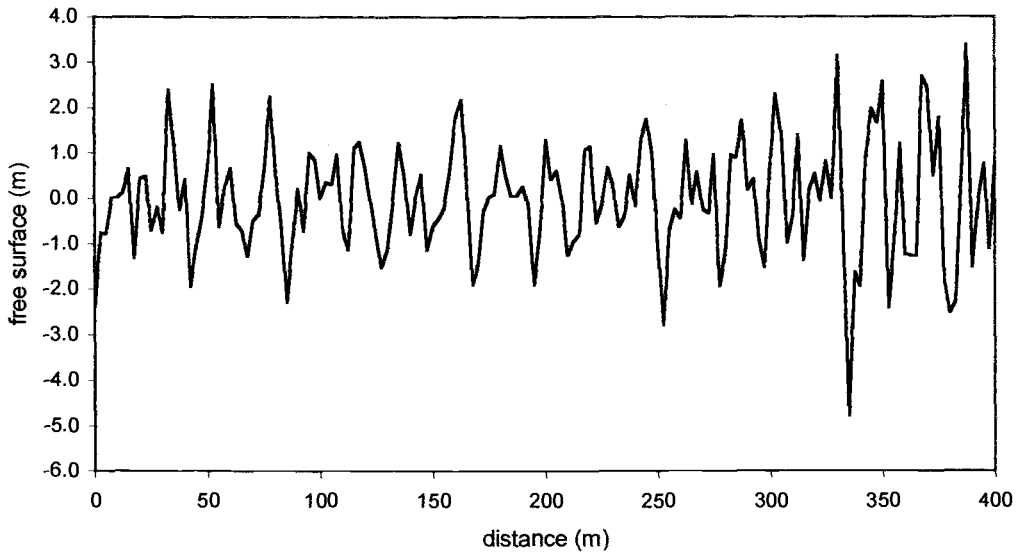

Figure 4.9c. Fractal Weierstrass function-generated waves propagation on a flat bottom at $t = 100\,\text{sec}$. The wave celerity is 5 m/sec . The wave has been reflected and creates a standing wave.

Figures 4.8a – c at $t > 80\,\text{sec}$ show that standing waves occur when the waves are reflected by the wall. The results show an interaction between the incident waves with the reflected waves. Figure 4.10a-d show time series of the ocean wave data at 4 locations. Standing waves are evident in Figures 4.10b-d. The fractal dimension was calculated using 4000 data points at $x = 0$ and $x = 6144$ meters. The resulting fractal dimension is 1.789 and does not change.

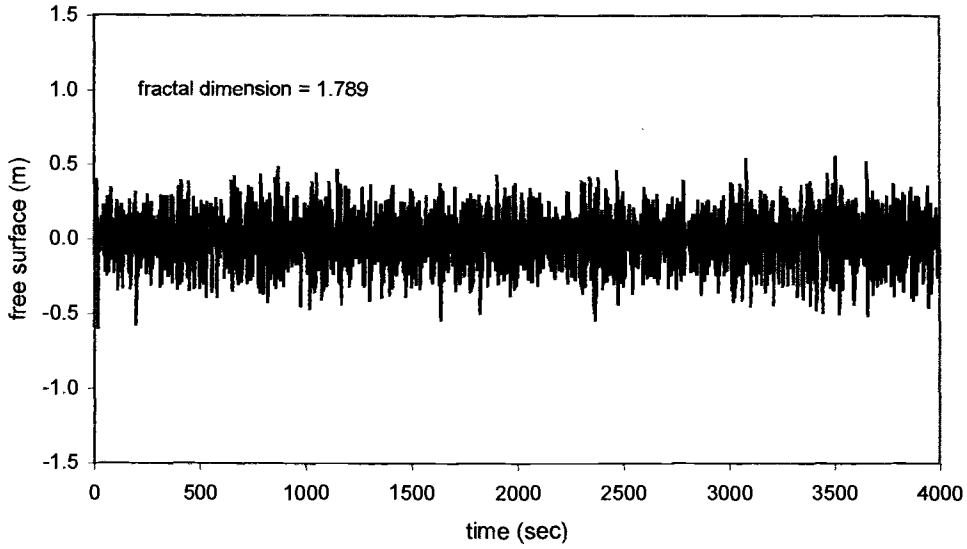

Figure 4.10a. Time history of ocean waves (from Sandy Duck, North Carolina, 1997) observed at $x = 0$ m ; fractal dimension is 1.789.

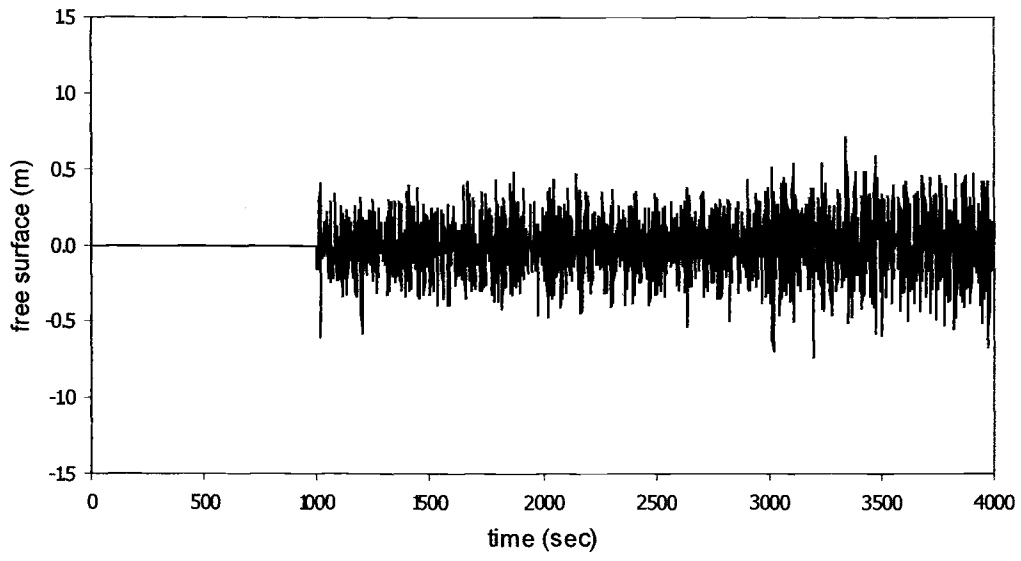

Figure 4.10b. Time history of ocean waves (from Sandy Duck, North Carolina, 1997) observed at $x = 3072$ m (middle of the space domain).

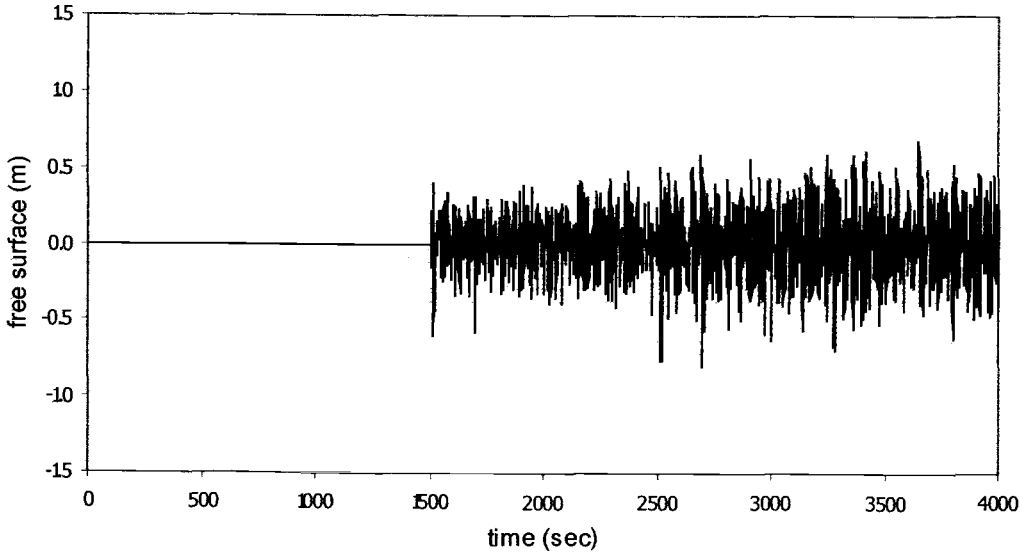

Figure 4.10c. Time history of ocean waves (from Sandy Duck, North Carolina, 1997) observed at $x = 4608$ m ($\frac{3}{4}$ of the space domain).

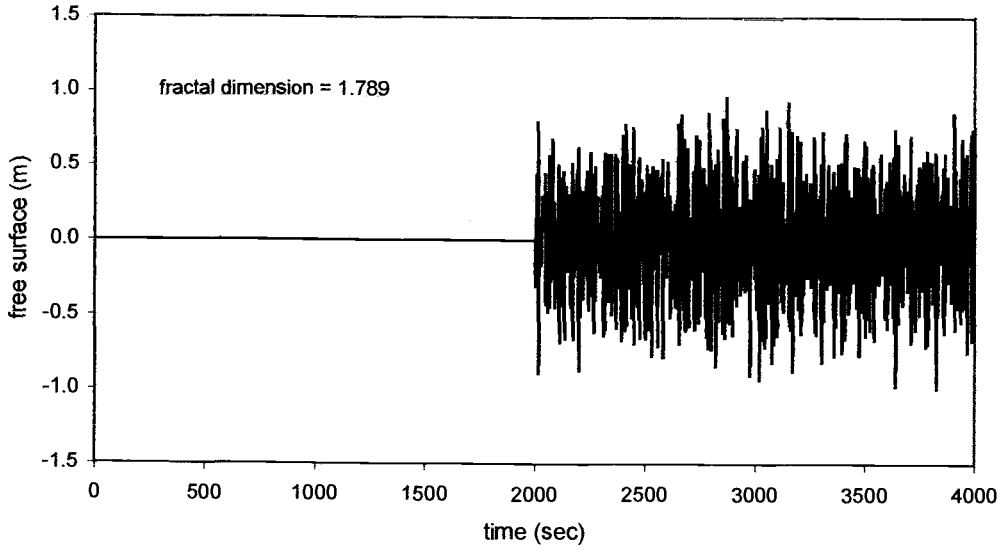

Figure 4.10d. Time history of ocean waves (from Sandy Duck, North Carolina, 1997) observed at the end of the space domain ($x = 6144$ m); fractal dimension is 1.789.

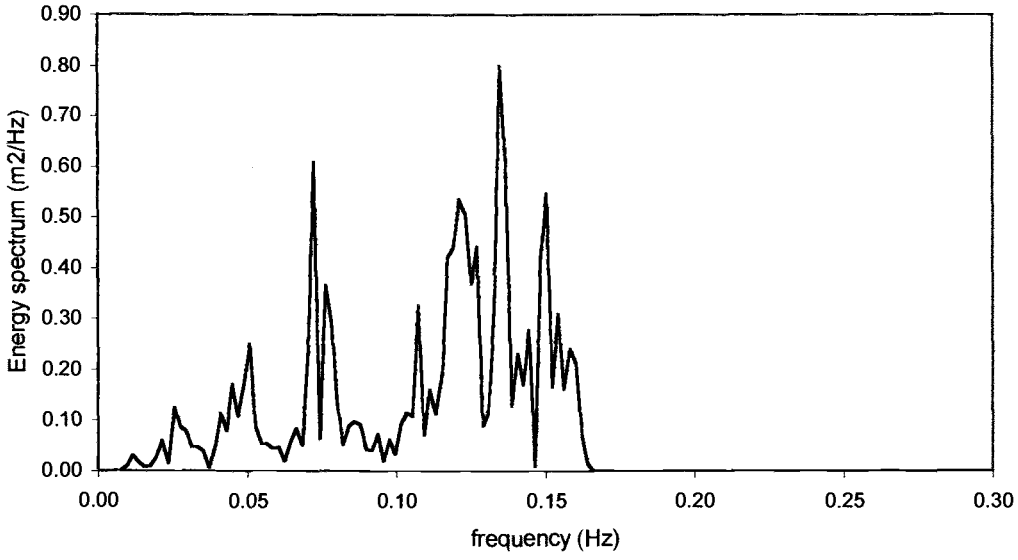

Figure 4.11a. Energy spectrum of the first 4000 data points in Figure 4.10a.

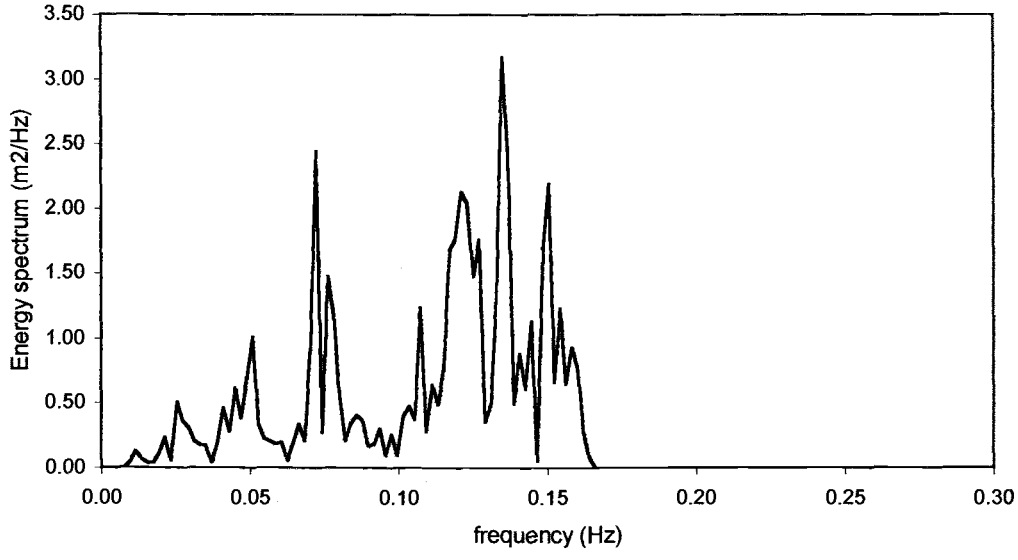

Figure 4.11b. Energy spectrum of the data points in Figure 4.10d.

Figures 4.11a-b show the energy spectrum calculated from 4000 data points for the solutions at $x = 0$ m and at the wall. The figures are intended to show how the energy changes as the waves are reflected. Since the waves are 100% reflected, the standing wave height is twice the incident wave height, and the standing wave energy spectrum is four times the incident wave energy spectrum. The total area under the energy spectrum curves in Figure 4.11a and 4.11b are 13.1 m^2 and 52.4 m^2, respectively. Figures 4.12 show the results in the spatial domain.

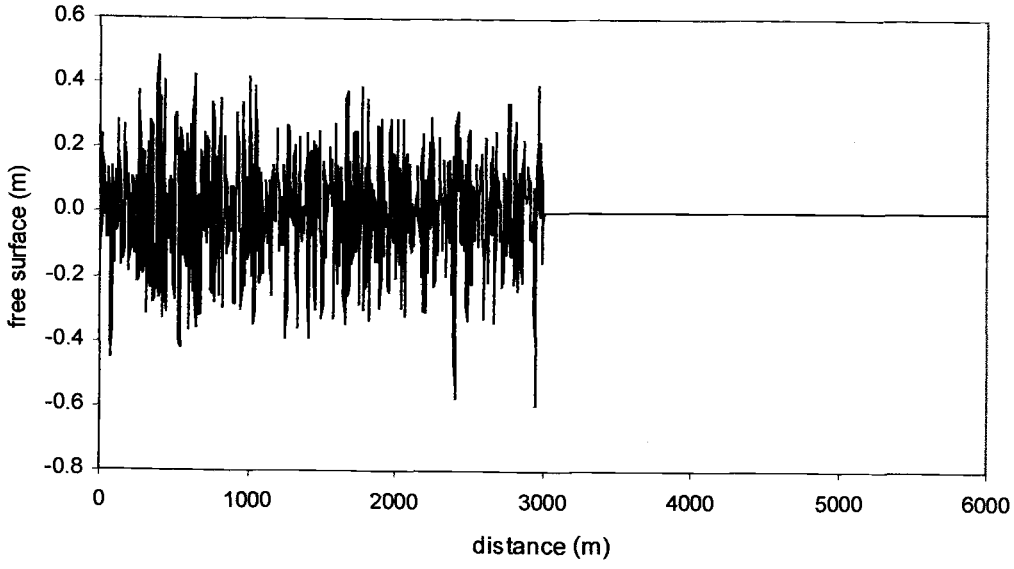

Figure 4.12a. The propagation of the ocean waves (from Sandy Duck, North Carolina, 1997) at $t = 1024$ sec

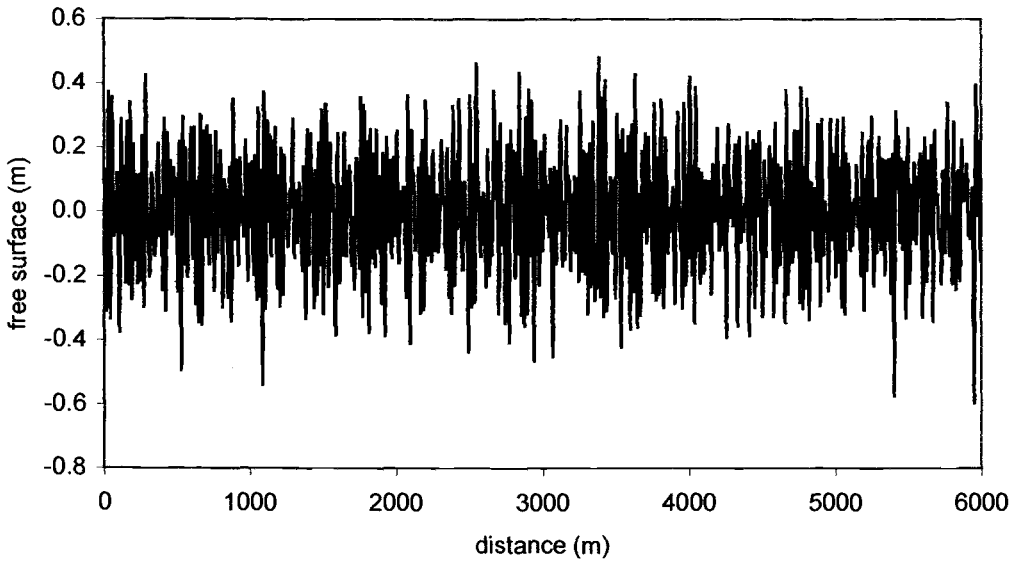

Figure 4.12b. The propagation of the ocean waves (from Sandy Duck, North Carolina, 1997) at $t = 2048\,\text{sec}$

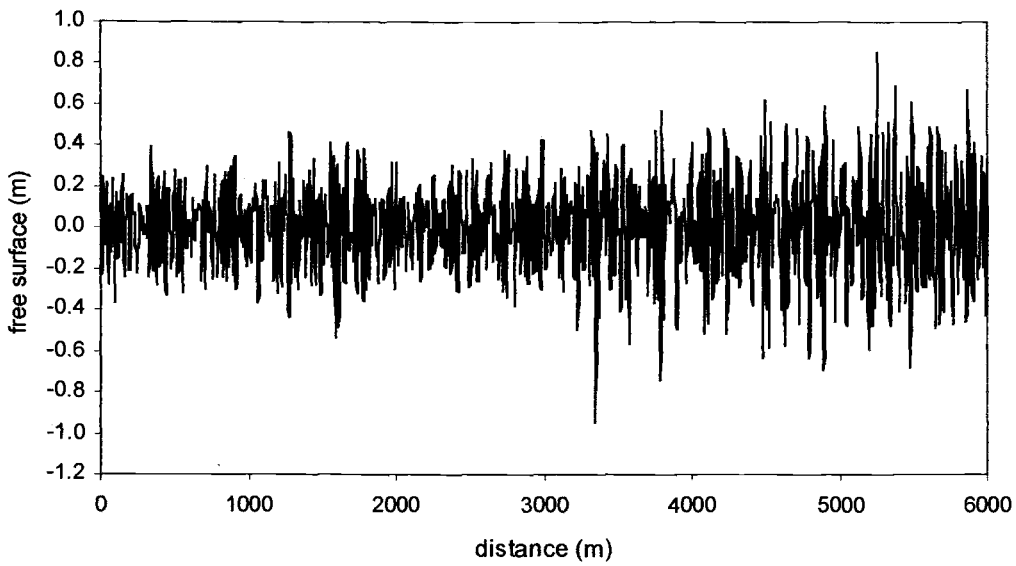

Figure 4.12c. The propagation of the ocean waves (from Sandy Duck, North Carolina, 1997) at $t = 2970\,\text{sec}$**. Location of the wall is at** $x = 6000$ m**. It is seen that there is a standing wave in front of the wall.**

4.3 FLAT BOTTOM WITH BOTTOM FRICTION ON SEMI-INFINITE DOMAIN

This section focuses on the effect of interactions between the propagated waves and the beach on the fractal dimension of the waves. The governing equation follows (3.44). The initial and boundary conditions are the same as the conditions in Section 4.1. Data from the Grays Harbor Wave Refraction Experiment, Washington, 1999 are used for the ocean wave data input. The energy spectra of the ocean waves are analyzed, and the fractal dimension is calculated. Figure 4.13 shows the sketch of the domain.

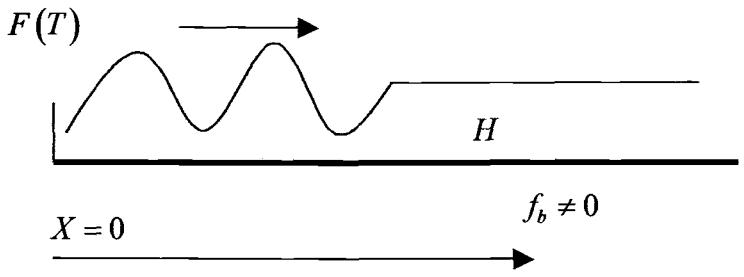

Figure 4.13 Wave propagation on a flat bottom with bottom friction.

The boundary value problem with the governing equation (3.44) can be summarized as follows,

$$
\begin{aligned}
&W_{TT} - \frac{b^2}{4} W = W_{XX} && X \geq 0, \quad T \geq 0 \\
&W(X,0) = W_T(X,0) = 0 \\
&W(0,T) = \exp(-\delta T) F(T)
\end{aligned}
\tag{4.49}
$$

where $N(X,T)=\exp(\delta T)W(X,T)$. The value of δ is obtained from (3.42). Because the boundary condition is of the Dirichlet-type, the solution to (4.49) is written in the form of a *double layer potential.* By evaluating the value κ in (3.66), and substituting it into (3.86), we can find the Riemann function that is a kernel for the integral equation. By matching the governing equation written in (4.49) with (3.53), where the variable W replaces N, we can find the value k as

$$\kappa=\frac{b^2}{16} \tag{4.50}$$

From (3.43),

$$b=\frac{F_b U_m}{3\pi} \tag{4.51}$$

Equation (4.50) is substituted into (3.86). By using the transformations in (4.5) to (4.8), we can write the Riemann function in terms of variables $(X,T;s,\tau)$ as

$$R(X,T;s,\tau)=I_o\left(\frac{b}{2}\sqrt{(X-s+T-\tau)(s-X+T-\tau)}\right) \tag{4.52}$$

The solution to the boundary value problem in (4.49) is written in the form of a double layer potential as

$$\begin{aligned} W(X,T)=&\int_0^{T_a}\left(\frac{\partial}{\partial s}I_o\left(\frac{b}{2}\sqrt{(X-s+T-\tau)(s-X+T-\tau)}\right)\right)_{s=0}\phi(\tau)\,d\tau \\ &-I_o\left(\frac{b}{2}\sqrt{(X-s+T-T_a)(s-X+T-T_a)}\right)_{s=0}\phi(T_a) \end{aligned} \tag{4.53}$$

We can rewrite (4.53) as

$$W(X,T)=\frac{b}{2}\int_0^{T_a}\left(\frac{X-s}{\sqrt{(X-s+T-\tau)(s-X+T-\tau)}}\cdot I_1\left(\frac{b}{2}\sqrt{(X-s+T-\tau)(s-X+T-\tau)}\right)\right)_{s=0}\phi(\tau)\,d\tau + I_o\left(\frac{b}{2}\sqrt{(X-s+T-T_a)(s-X+T-T_a)}\right)\phi(T_a) \tag{4.54}$$

If we substitute $s=0$ into (4.54), then we can write $W(X,T)$ as

$$W(X,T)=\frac{b}{2}\int_0^{T_a}\left(\frac{X}{\sqrt{(X+T-\tau)(-X+T-\tau)}}\cdot I_1\left(\frac{b}{2}\sqrt{(X+T-\tau)(-X+T-\tau)}\right)\phi(\tau)\,d\tau\right) + I_o\left(\frac{b}{2}\sqrt{(X+T-T_a)(-X+T-T_a)}\right)\phi(T_a) \tag{4.55}$$

where $T_a=T-X$. The boundary condition at $X=0$ is applied to solve the density ϕ. As X approaches zero, T_a becomes T, and the Bessel function $I_0(\ )$ becomes one. The density $\phi(T)$ can be written as

$$\begin{aligned}\phi(T)&=\exp(-\delta\,T)F(T) \quad ; \quad T\geq 0\\ \phi(T)&=0 \quad ; \quad T<0\end{aligned} \tag{4.56}$$

$\phi(T) = 0$ for $T < 0$. The substitution of (4.56) into (4.55) gives

$$W(X,T) = X \frac{b}{2} \int_0^{T_a = T-X} \frac{I_1\left(\frac{b}{2}\sqrt{(X+T-\tau)(-X+T-\tau)}\right)}{\sqrt{(X+T-\tau)(-X+T-\tau)}} e^{-\delta\tau} F(\tau)\, d\tau + I_o\left(\frac{b}{2}\sqrt{(X+T-T_a)(-X+T-T_a)}\right) e^{-\delta T_a} F(T_a) \tag{4.57}$$

If we substitute $T_a = T - X$ into (4.57), then we can write $W(X,T)$ as

$$W(X,T) = X\frac{b}{2} \int_0^{T-X} \left(\frac{I_1\left(\frac{b}{2}\sqrt{(X+T-\tau)(-X+T-\tau)}\right)}{\sqrt{(X+T-\tau)(-X+T-\tau)}} e^{-\delta\tau} F(\tau)\, d\tau \right) + e^{-\delta(T-X)} F(T-X) \tag{4.58}$$

We can transform $W(X,T)$ to $N(X,T)$ by using the following relation,

$$N(X,T) = \exp(\delta T) W(X,T) \tag{4.59}$$

As in the previous chapter, the solution (4.59) is verified using smooth sinusoidal waves and the Weierstrass function-generated waves in (4.27) and (4.28). We take the water depth to be 2.5 meters, and bottom friction coefficient, f^b to be 0.1. Figures 4.14a – d show the results of the sinusoidal waves run. Figures 4.15a – b show the results of the Weierstrass function-generated waves. Figures 4.16a – d

show the results of the ocean wave data run. The water depth for the ocean wave model is 5.5 meters.

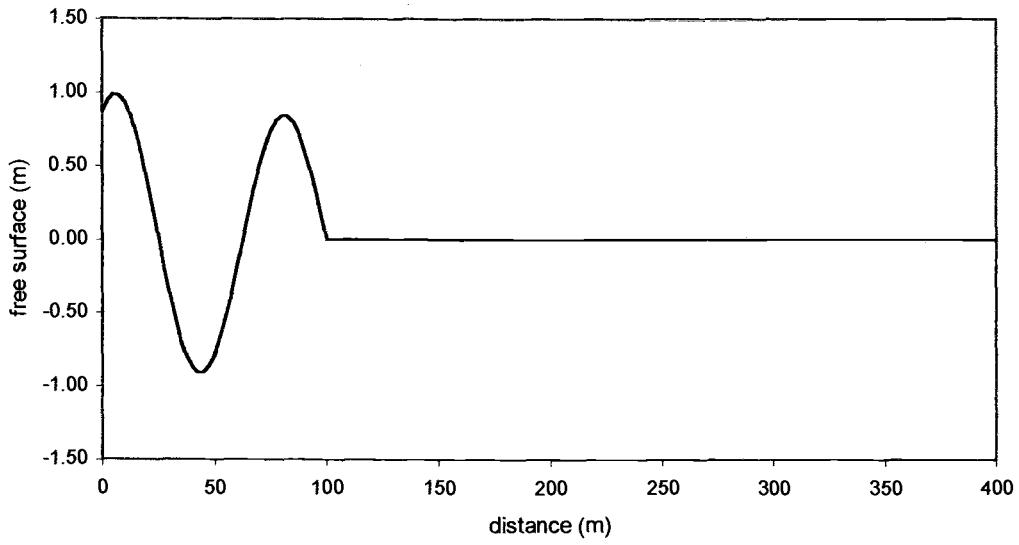

Figure 4.14a. Sinusoidal waves with bottom friction on flat bottom at $t = 20\,\text{sec}$

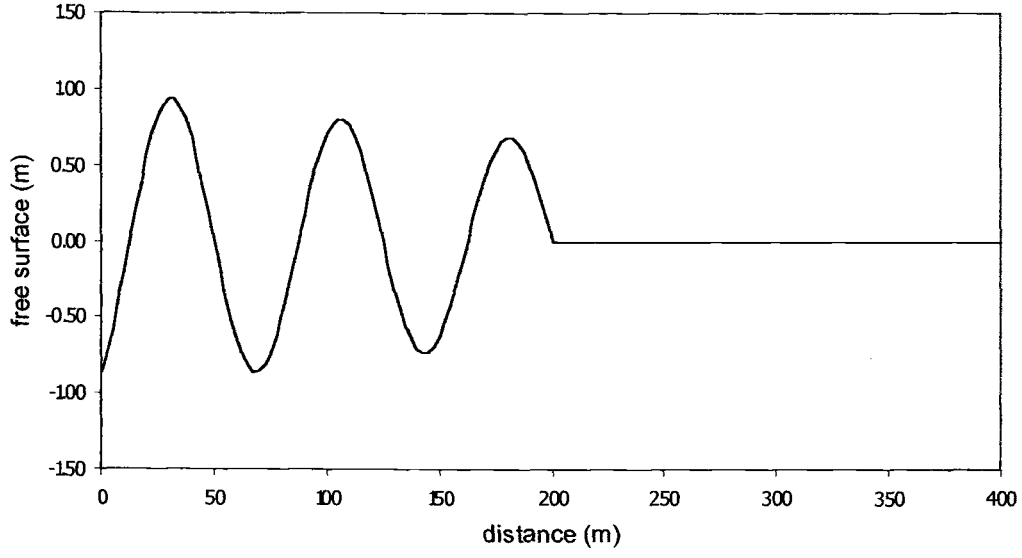

Figure 4.14b. Sinusoidal waves with bottom friction on flat bottom at $t = 40\,\text{sec}$.

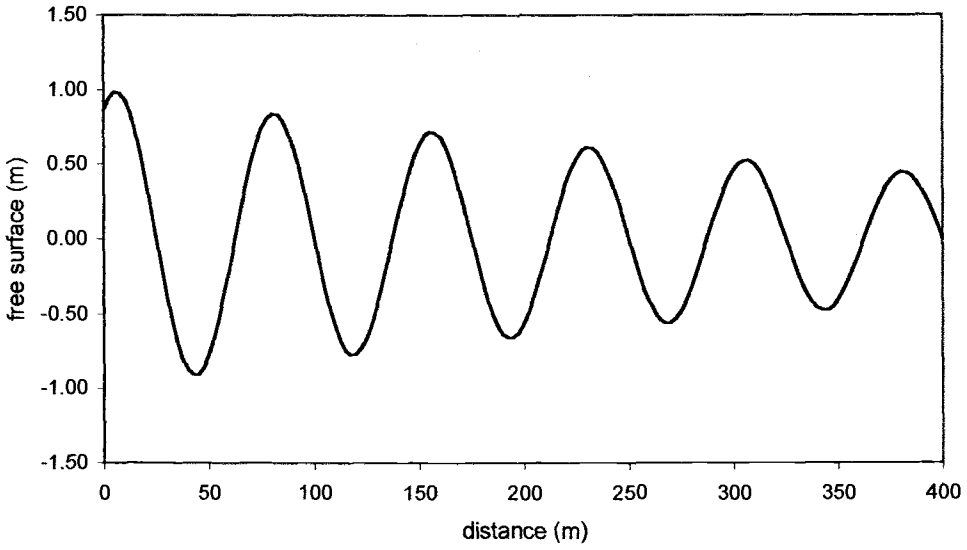

Figure 4.14c. Sinusoidal waves with bottom friction on flat bottom at $t = 80\,\text{sec}$

Figure 4.14d shows the same waves as in Figure 4.14c with the wave envelope curve drawn.

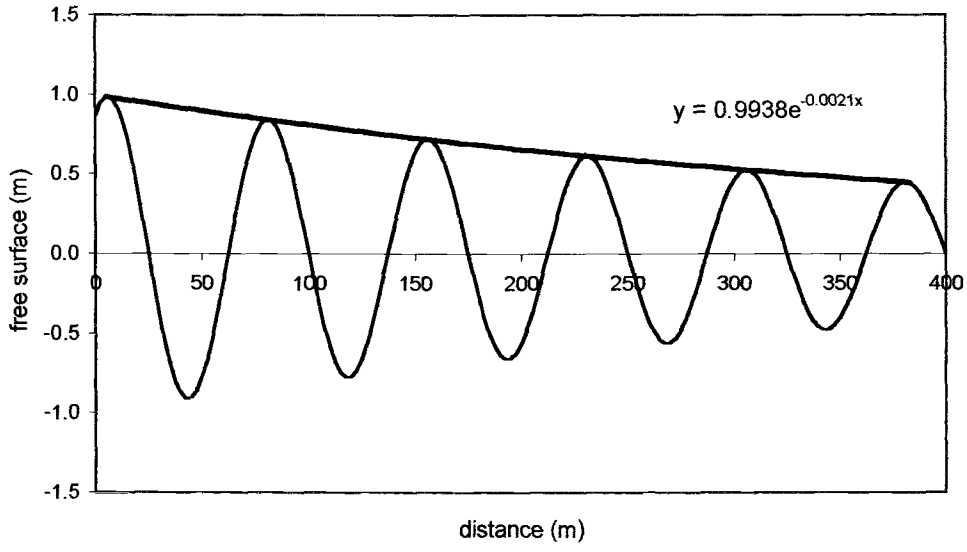

Figure 4.14d. Wave envelope of waves in Figure 4.14c

The trendline of the upper envelope as written in the figure is

$$y = 0.9938\ \exp(-0.0021x) \approx \exp(-0.0021x) \tag{4.60}$$

The energy loss is proportional to the squared wave height decrease. The ratio of the wave energy loss to the initial wave energy is

$$\frac{\Delta E}{E} \propto \left(\frac{\left(1-\exp(-0.0021x)\right)^2}{1} \right). 100\% \tag{4.61}$$

where x is dimensional distance. For this case, the energy loss as the waves reach the end of domain at $x = 400$ m is around 80%. Figures 4.16a – d show the time series of the ocean wave data at several locations. The data were taken from Grays Harbor Wave Refraction Experiment, Washington, 1999, in water depth 11 meters. These data are shoaled and filtered to adjust to shallow water conditions. The wave data are shoaled to a water depth of 5.5 meters according to procedure described in page 47. The data has a sample rate of 2 Hz, and a peak wave period of 19.7 seconds. The bottom friction coefficient is taken to be 0.01. The fractal dimension calculation is taken for a block of 4000 data using rescaled range analysis.

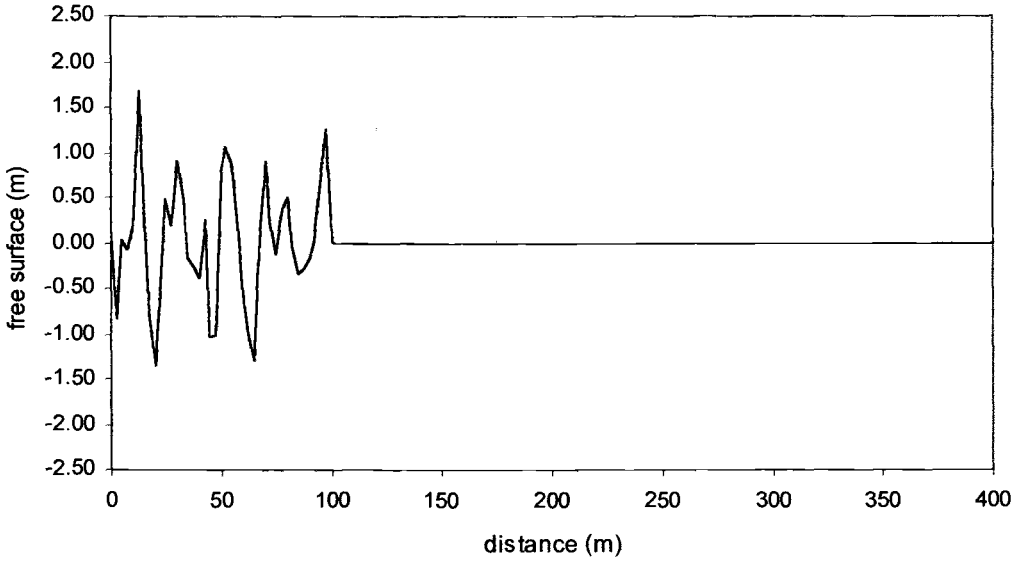

Figure 4.15a. Propagation of Weierstrass function-generated waves at $t = 20\,\text{sec}$

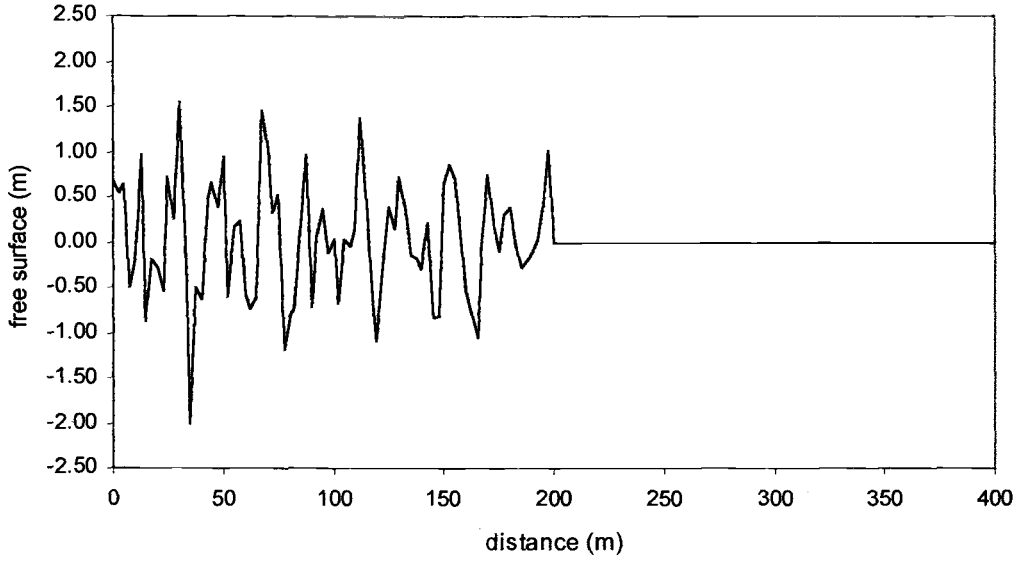

Figure 4.15b. Propagation of Weierstrass function-generated waves at $t = 40\,\text{sec}$

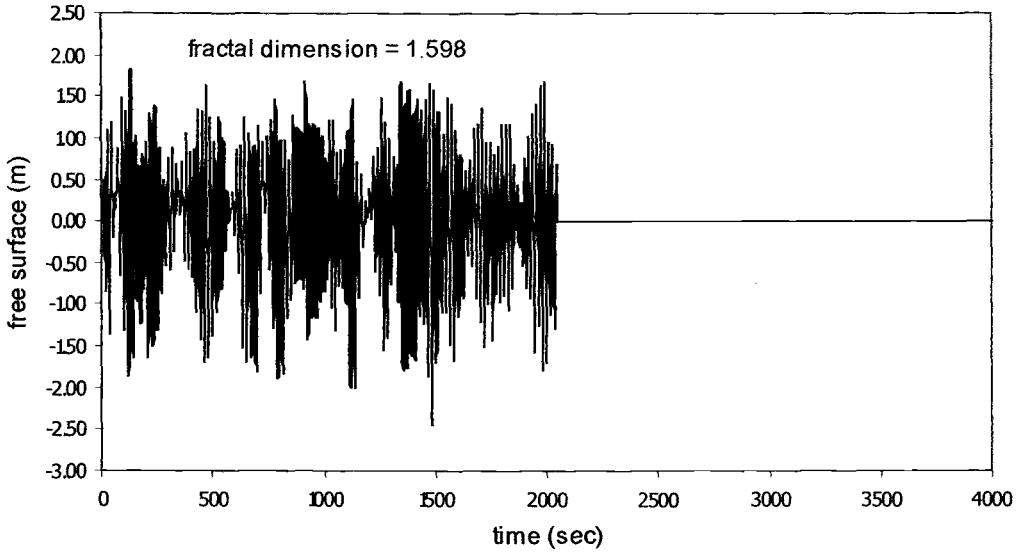

Figure 4.16a. Ocean wave data at $x = 0$ m ; fractal dimension is 1.598

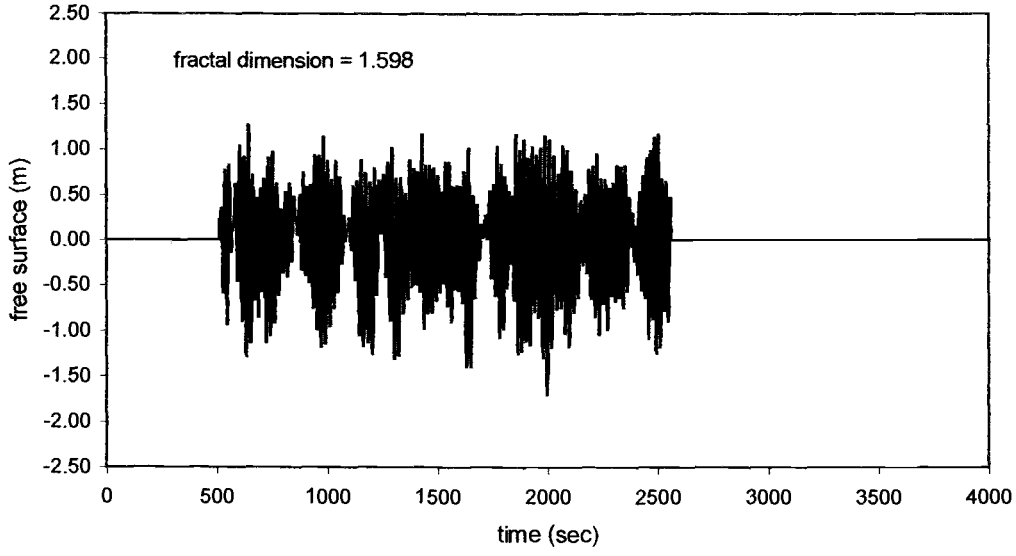

Figure 4.16b. Ocean wave data at ¼ of the domain; fractal dimension is 1.598

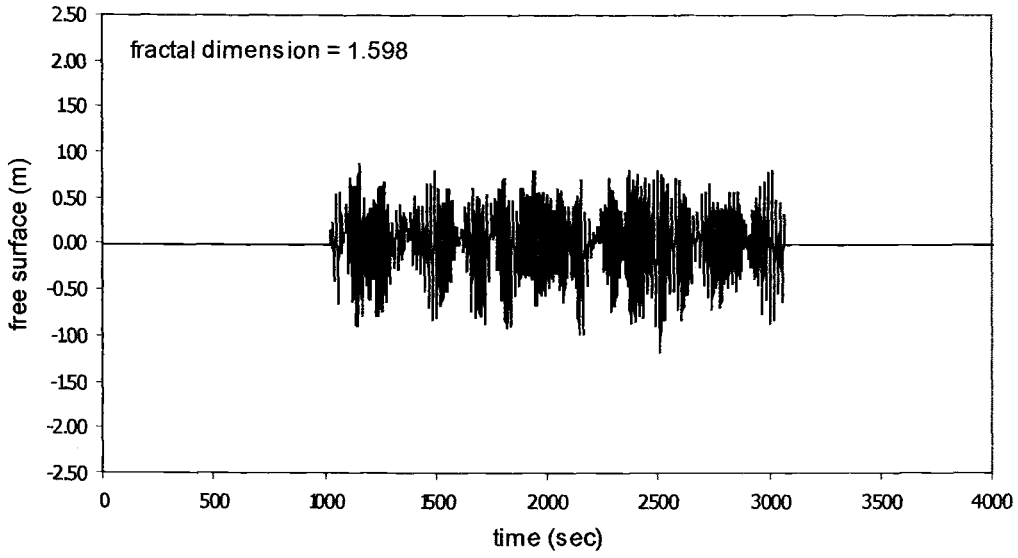

Figure 4.16c. Ocean wave data from the middle of the domain; fractal dimension is 1.598

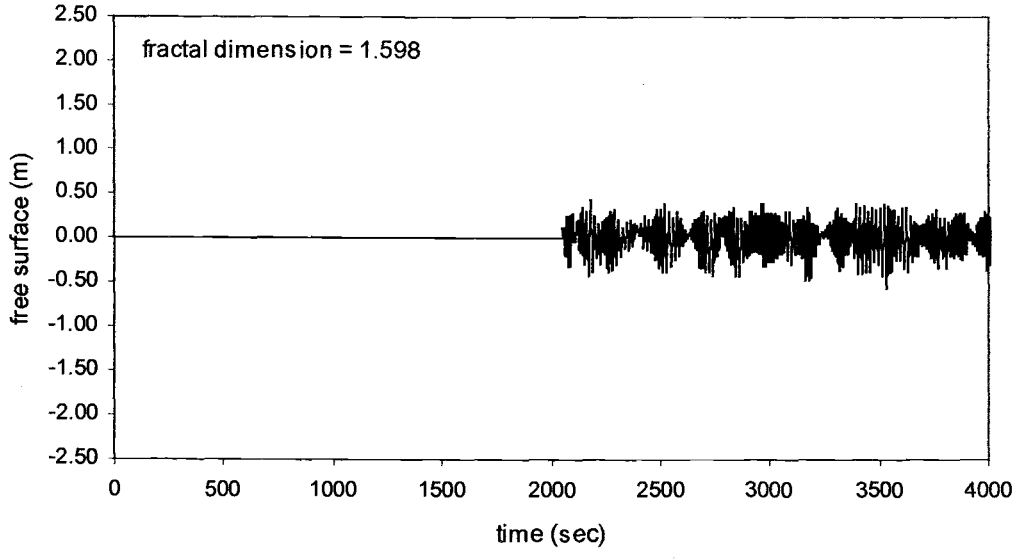

Figure 4.16d. Ocean wave data at the end of the domain; fractal dimension is 1.598

Figures 4.16a – d show that the bottom friction decreases the wave amplitude as the wave propagates. However, the bottom friction does not affect the fractal dimension of the waves. Figures 4.17a – b show the energy spectra of the waves.

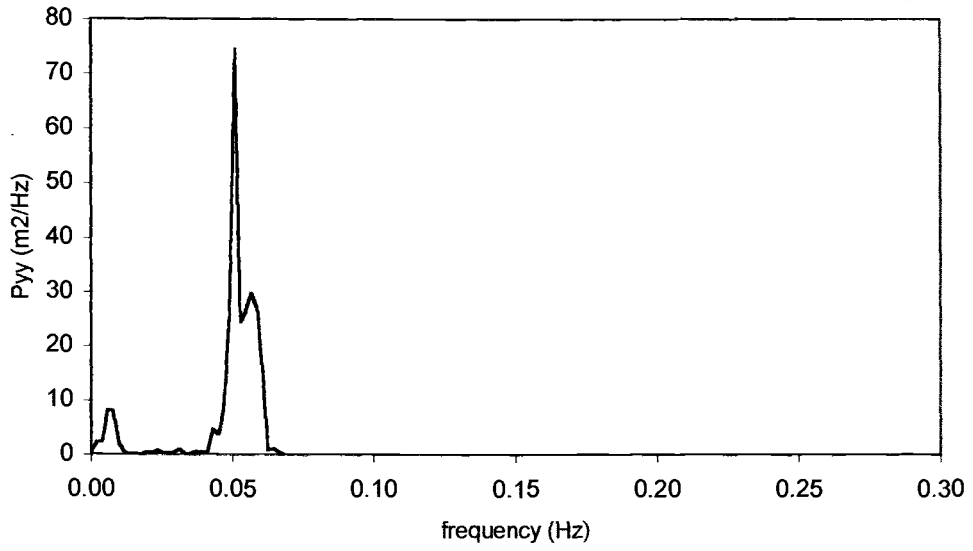

Figure 4.17a. Energy spectrum of ocean wave data observed at $x = 0$ m

Figures 4.17a – 4.17b show that the bottom friction does not affect the frequency contents of the waves. However, the amplitude of the energy decreases due to the bottom friction. The total are under the energy spectrum curve in Figure 4.17a is 0.528 m^2 ($x = 0$), and that of Figure 4.17b is 0.029 m^2 (the end of domain). The total energy loss is 94.5%.

Equation (4.58) shows that the frequency of the waves is explicitly written in the function $F(T)$, and the bottom friction term δ is written as an exponential term. Assuming the linear superposition within the solution for any time dependent boundary condition $F(T)$, it is clear that the friction term does not affect the frequency content of the solution. To investigate whether the linear superposition assumption holds true, 3 sinusoidal waves with different periods (5sec, 10sec and

15sec) are tested. The test is done by running the model individually with $F(T)=\sin\left(\frac{2\pi}{T_p}T_cT\right)$, and the 3 solutions are superposed.

The second test is to run the wave signal function $F(T)=\sin\left((2\pi/5)T_cT\right)+\sin\left((2\pi/10)T_cT\right)+\sin\left((2\pi/15)T_cT\right)$. The two solutions are compared in Figures 4.18a – d and 4.19a – d. The results between the superposition of the sinusoidal waves and the wave signal are identical. This means the linear relationship assumption between the friction term and the frequency term in (4.58) holds true.

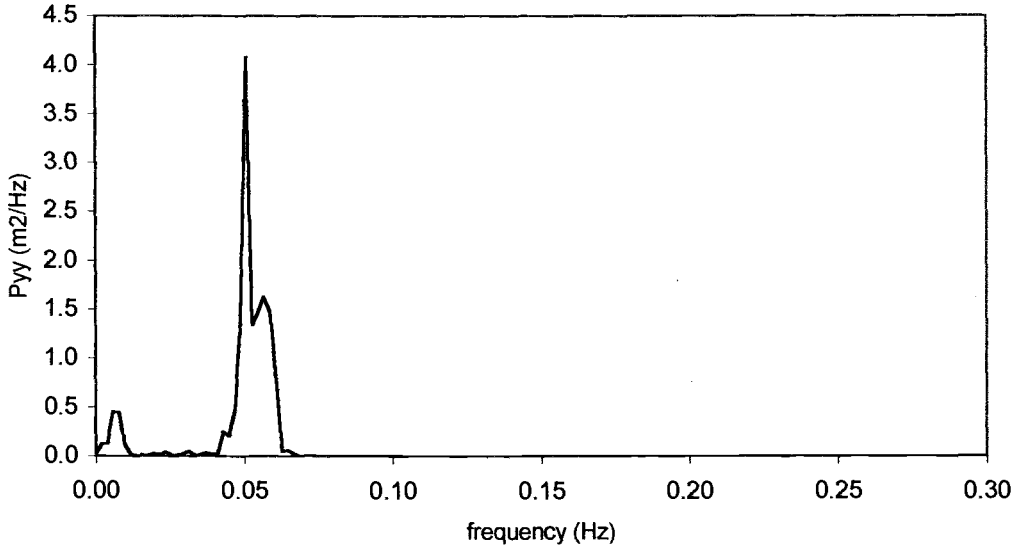

Figure 4.17b. Energy spectrum of ocean wave data observed at the end of the domain

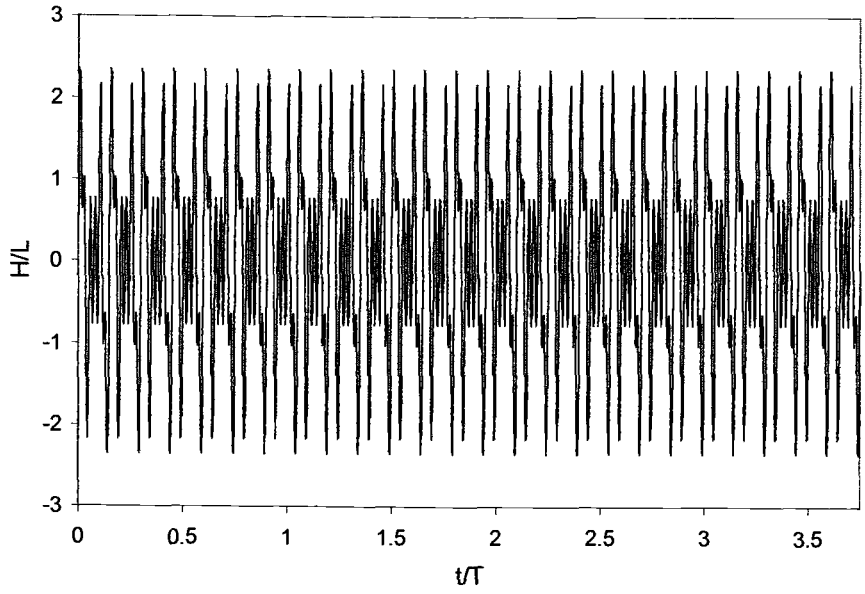

Figure 4.18a. Superposition of 3 solutions to 3 sinusoidal waves with periods of 5, 10, 15 sec at $x = 0$.

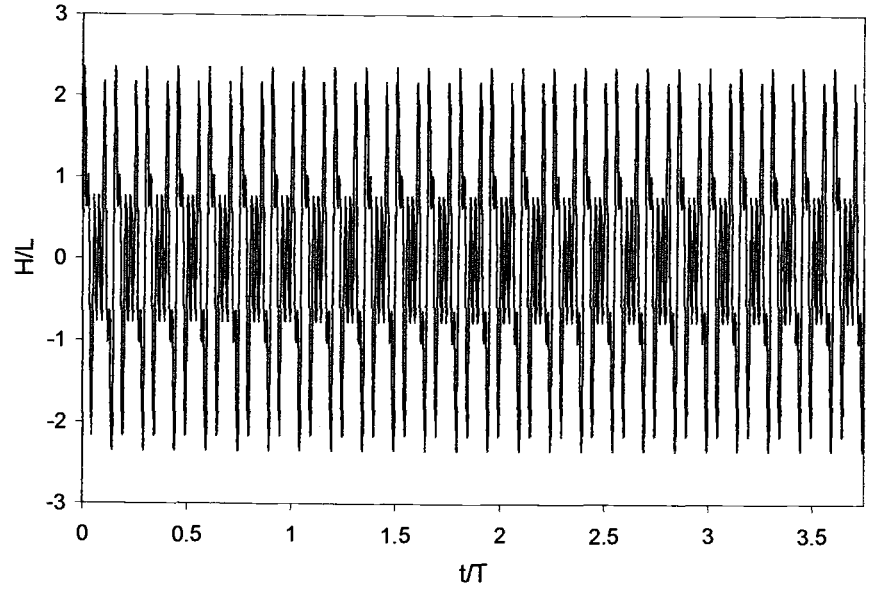

Figure 4.18b. Solutions of signals of 3 sinusoidal waves with periods of 5, 10, 15 sec at $x = 0$. Note that the graph is identical to Figure 4.18a.

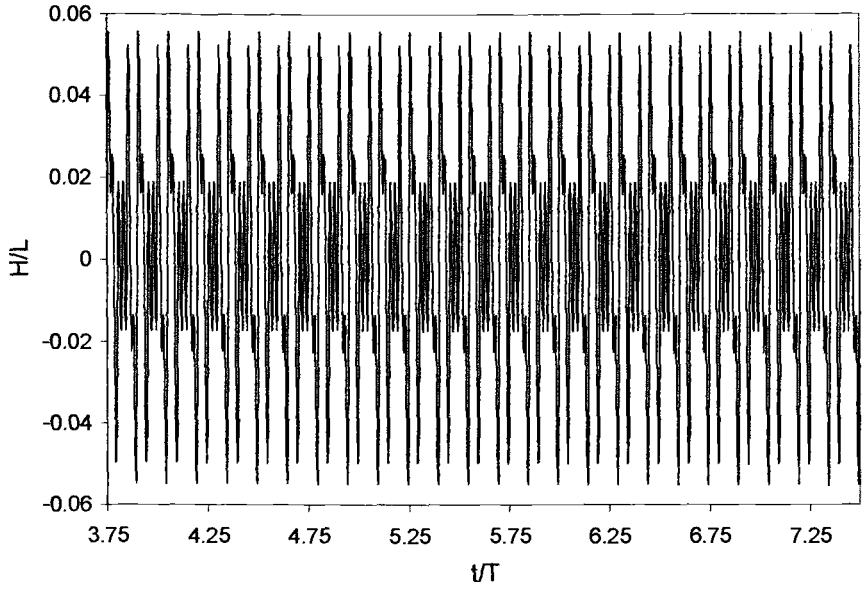

Figure 4.18c. Superposition of 3 solutions to 3 sinusoidal waves with periods of 5, 10, 15 sec at the end of domain.

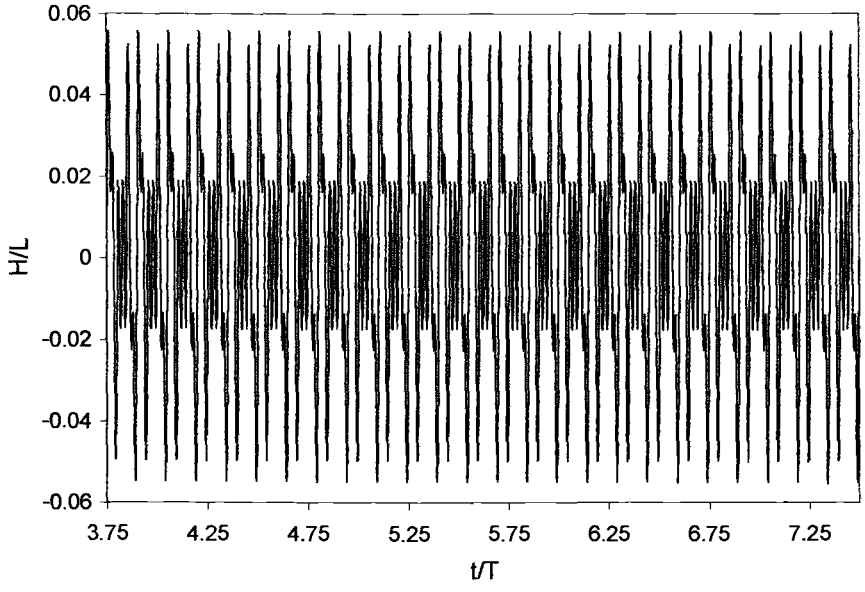

Figure 4.18d. Solutions of signals of 3 sinusoidal waves with periods of 5, 10, 15 sec at the end of domain. Note that the graph is identical to Figure 4.18c.

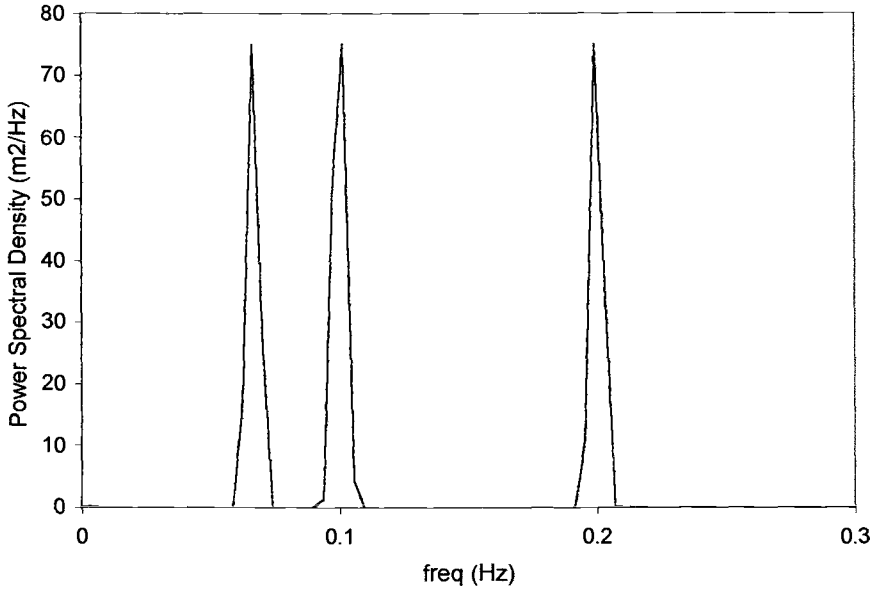

Figure 4.18e. The energy spectrum of the superposition of 3 solutions of sinusoidal waves with periods of 5, 10 and 15 sec, at x= 0 m

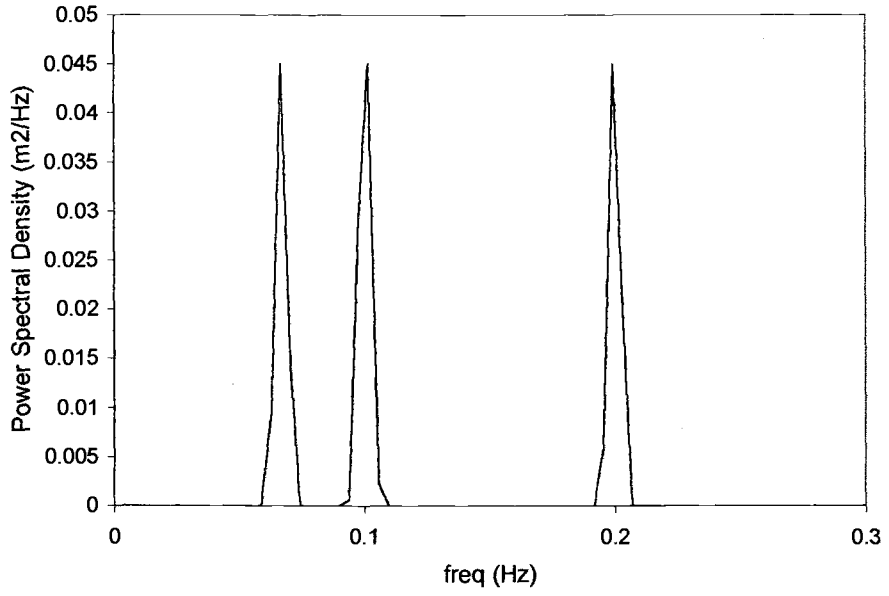

Figure 4.18f. The energy spectrum of signal waves with periods of 5, 10 and 15 sec, at $x = 0$ m. Note that the energy content is identical with the case of superposition in Figure 4.18e.

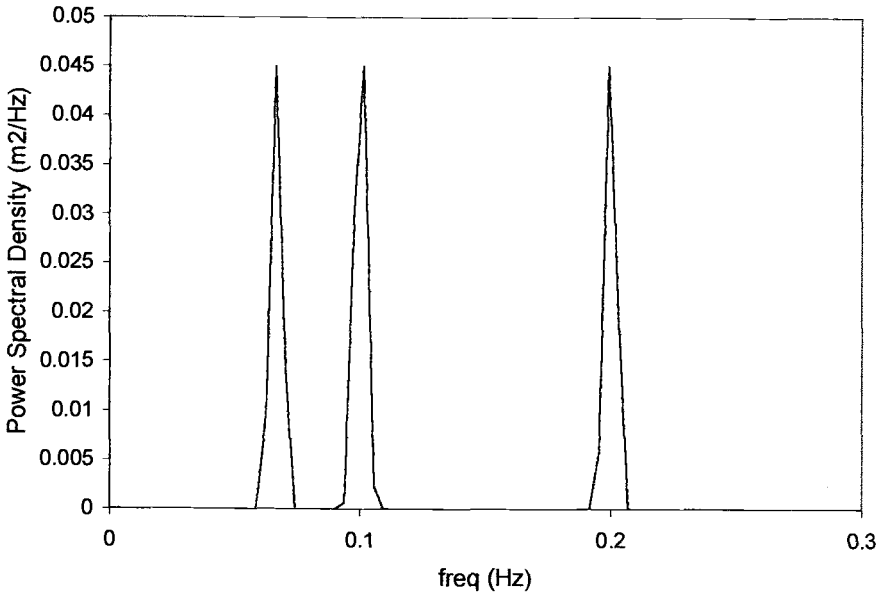

Figure 4.18g. The energy spectrum of the superposition of 3 solutions of sinusoidal waves with periods of 5, 10 and 15 sec, at the end of the domain.

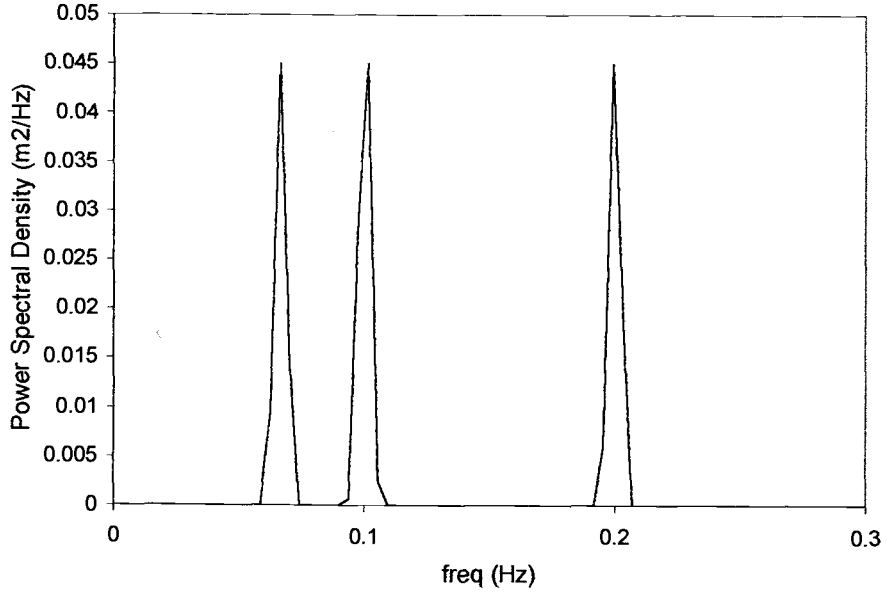

Figure 4.18h. The energy spectrum of signal waves with periods of 5, 10 and 15 sec, at the end of the domain. Note that the energy content is identical with the case of the superposition in Figure 4.18g.

4.4 FLAT BOTTOM WITH BOTTOM FRICTION CONSTRAINT WITH REFLECTIVE WALL

This section focuses on the effects of wave reflections and bottom friction on the fractal dimension of the waves. The boundary value problem is the same as Section 4.3, written in (4.49), with an additional of the reflective boundary at $X = A$. The reflective boundary can be written as

$$W_X(X = A, T) = 0 \qquad T \geq 0 \qquad (4.62)$$

Figure 4.20 shows the domain of the problem.

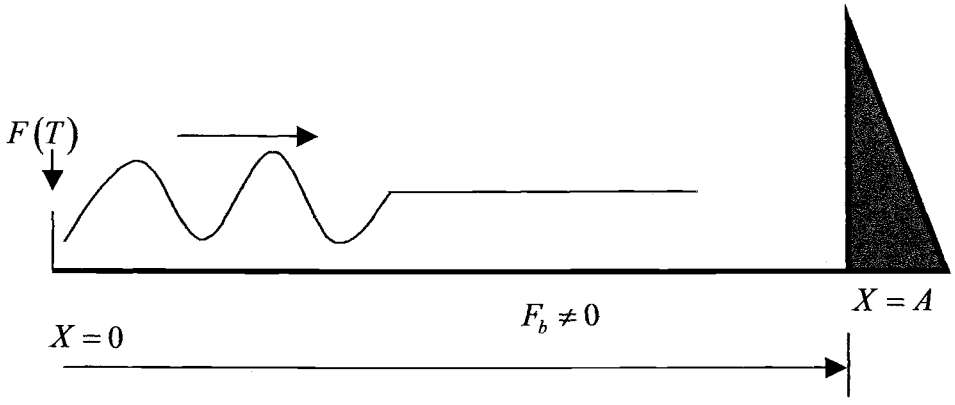

Figure 4.20. Wave propagation on a flat bottom with bottom friction constraints with reflective wall

For the case with two boundary conditions of Dirichlet and Neumann-type, the solution is written in the form of double and single layer potentials . The solution can be written

$$W(X,T) = \int_0^{T_a} R_s(X,T;s=0,\tau)\,\phi(\tau)\,d\tau - R(X,T;s=0,T_a)\,\phi(T_a)\,\frac{\partial}{\partial X}T_a + \int_0^{S_a} R(X,T;s=A,\tau)\,\psi(\tau)\,d\tau \tag{4.63}$$

where the Riemann function R will have the same value as in Section 4.3 since the governing equation is the same. The Riemann function can be obtained from (4.52). We take $\phi(T)$ and $\psi(T) = 0$ for $T \le 0$. The substitution of the Riemann function in (4.52) into (4.63) gives

$$W(X,T) = \int_0^{T_a} \left(\frac{\partial}{\partial s} I_0\left(\frac{b}{2}\sqrt{(X-s+T-\tau)(s-X+T-\tau)}\right)\phi(\tau)\right)_{s=0} d\tau - I_0\left(\frac{b}{2}\sqrt{(X-s+T-T_a)(s-X+T-T_a)}\right)\Big|_{s=0} \phi(T_a) + \int_0^{S_a} I_0\left(\frac{b}{2}\sqrt{(X-s+T-\tau)(s-X+T-\tau)}\right)\Big|_{s=A} \psi(\tau)\,d\tau \tag{4.64}$$

We can rewrite $W(X,T)$ as

$$W(X,T) = \frac{b}{2}\int_0^{T_a} \frac{X\, I_1\left(\frac{b}{2}\sqrt{(X+T-\tau)(-X+T-\tau)}\right)}{\sqrt{(X+T-\tau)(-X+T-\tau)}}\,\phi(\tau)d\tau - I_0\left(\frac{b}{2}\sqrt{(X+T-T_a)(-X+T-T_a)}\right)\phi(T_a) + \int_0^{S_a} I_0\left(\frac{b}{2}\sqrt{(X-A+T-\tau)(A-X+T-\tau)}\right)\psi(\tau)\,d\tau \tag{4.65}$$

The boundary conditions are

$$W(X=0,T)=e^{-\delta T}F(T) \tag{4.66}$$

and

$$W_X(X=A,T)=0 \tag{4.67}$$

Using (4.66), we solve the density $\phi(T)$.

$$\phi(T)=-\exp(-\delta T)F(T)\ + \int_0^{S_a=T-A} I_0\left(\frac{b}{2}\sqrt{(-A+T-\tau)\ (A+T-\tau)}\right)\psi(\tau)\,d\tau \tag{4.68}$$

where $\phi(T)=0$ for $T\le 0$. The density $\psi(T)$ can be solved using (4.67). The first derivative of $W(X,T)$ with respect to X is

$$W_X(X=A,T)=\frac{\partial}{\partial X}\ \frac{b}{2}\int_0^{T_a}\left(\frac{X}{\sqrt{(X+T-\tau)(-X+T-\tau)}}\right. \left. I_1\left(\frac{b}{2}\sqrt{(X+T-\tau)(-X+T-\tau)}\right)\ \phi(\tau)\right)d\tau$$

$$-\frac{\partial}{\partial X}\left(I_0\left(\frac{b}{2}\sqrt{(X+T-T_a)(-X+T-T_a)}\right)\ \phi(T_a)\right) \tag{4.69}$$

$$+\ \frac{\partial}{\partial X}\int_0^{S_a} I_0\left(\frac{b}{2}\sqrt{(X-A+T-\tau)(A-X+T-\tau)}\right)\ \psi(\tau)\,d\tau$$

where $T_a = T - X$ and $S_a = T + X - A$. If we substitute T_a and S_a into (4.69), then we can rewrite (4.69) as

$$W_X(X = A, T) = \frac{\partial}{\partial X} \frac{b}{2} \int_0^{T-X} \left(\frac{X}{\sqrt{(X+T-\tau)(-X+T-\tau)}} \right. \\ \left. I_1\left(\frac{b}{2} \sqrt{(X+T-\tau)(-X+T-\tau)} \right) \phi(\tau) \right) d\tau$$

$$- \frac{\partial}{\partial X} \phi(T-X) \qquad (4.70)$$

$$+ \frac{\partial}{\partial X} \int_0^{T+X-A} I_0\left(\frac{b}{2} \sqrt{(X-A+T-\tau)(A-X+T-\tau)} \right) \psi(\tau)\, d\tau$$

We evaluate the first term of (4.70) using the Leibnitz rule,

$$1^{st}\text{term} = \frac{b}{2} \int_0^{T-X} \frac{\partial}{\partial X} \left(\frac{X}{\sqrt{(X+T-\tau)(-X+T-\tau)}} \right. \\ \left. I_1\left(\frac{b}{2} \sqrt{(X+T-\tau)(-X+T-\tau)} \right) \varphi(\tau) \right) d\tau$$

(4.71)

$$+ \frac{b}{2} \left(\frac{X}{\sqrt{(X+T-(T-X))(-X+T-(T-X))}} \right. \\ \left. I_1\left(\frac{b}{2} \sqrt{(X+T-(T-X))(-X+T-(T-X))} \right) \phi(T-X) \frac{\partial(T-X)}{\partial X} \right)$$

If the argument of the modified Bessel function of order one approaches zero, then

$$\lim_{X\to 0}\frac{I_1\left(\sqrt{X}\right)}{X}=\frac{1}{2} \tag{4.72}$$

(4.71) can be written

$$1^{st}\text{term} = \frac{b}{2}\int_0^{T-X}\left(\frac{I_1\left(\frac{b}{2}\sqrt{\Omega}\right)}{\sqrt{\Omega}}-\frac{X^2 b}{2}\frac{I_0\left(\frac{b}{2}\sqrt{\Omega}\right)}{\Omega}+\frac{2X^2}{\Omega}\frac{I_1\left(\frac{b}{2}\sqrt{\Omega}\right)}{\sqrt{\Omega}}\right)\phi(\tau)\,d\tau \tag{4.73}$$

$$- \frac{b\,X\,\phi(T-X)}{4}$$

where,

$$\Omega=(X+T-\tau)(-X+T-\tau) \tag{4.74}$$

The second term of (4.70) is

$$2^{nd}\text{ term}=-\frac{\partial}{\partial X}\phi(T-X)=\phi'(T-X) \tag{4.75}$$

By using the Leibnitz rule, we can rewrite the 3rd term of (4.70) as

$$3^{rd}\,\text{term} = \int_0^{S_a=T+X-A} \frac{\partial}{\partial X}\left(I_0\left(\frac{b}{2}\sqrt{(X-A+T-\tau)(A-X+T-\tau)}\right)\ \psi(\tau)\right) d\tau$$

$$+\quad I_0\left(\frac{b}{2}\sqrt{(X-A+T-S_a)(A-X+T-S_a)}\right)\ \psi(S_a)\ \frac{\partial S_a}{\partial X} \tag{4.76}$$

If we substitute $S_a = T+X-A$ into (4.76), then we can rewrite (4.76) as

$$3^{rd} = \frac{b}{2}\int_0^{T+X-A}\left((A-X)\frac{I_1\left(\frac{b}{2}\sqrt{(X-A+T-\tau)(A-X+T-\tau)}\right)}{\sqrt{(X-A+T-\tau)(A-X+T-\tau)}}\ \psi(\tau)\right) d\tau$$

$$+\ \psi(T+X-A) \tag{4.77}$$

By combining all of the terms, we can rewrite (4.70) as

$$W_X(X,T) = \frac{b}{2}\int_0^{T-X}\left(\frac{I_1\left(\frac{b}{2}\sqrt{\Omega}\right)}{\sqrt{\Omega}} - \frac{X^2 b}{2}\frac{I_0\left(\frac{b}{2}\sqrt{\Omega}\right)}{\Omega} + \frac{2X^2}{\Omega}\frac{I_1\left(\frac{b}{2}\sqrt{\Omega}\right)}{\sqrt{\Omega}}\right)\phi(\tau)\,d\tau$$

$$-\frac{bX\phi(T-X)}{4}\quad +\ \phi'(T-X) + \psi(T+X-A)$$

$$+\int_0^{S_a=T+X-A}\left((A-X)\ \frac{I_1\left(\frac{b}{2}\sqrt{(X-A+T-\tau)(A-X+T-\tau)}\right)}{\sqrt{(X-A+T-\tau)(A-X+T-\tau)}}\ \psi(\tau)\right) d\tau \tag{4.78}$$

Applying the boundary condition (4.67) at $X = A$, we have

$$\psi(T) = -\frac{b}{2}\int_0^{T-A}\left(\frac{I_1\left(\frac{b}{2}\sqrt{\Omega_A}\right)}{\sqrt{\Omega_A}} - \frac{A^2 b}{2}\frac{I_0\left(\frac{b}{2}\sqrt{\Omega_A}\right)}{\Omega_A} + 2\frac{A^2}{\Omega_A}\frac{I_1\left(\frac{b}{2}\sqrt{\Omega_A}\right)}{\sqrt{\Omega_A}}\right)\phi(\tau)\,d\tau \tag{4.79}$$

$$+ \frac{bA}{4}\phi(T-A) - \phi'(T-A)$$

where

$$\Omega_A = (A+T-\tau)\,(-A+T-\tau) \tag{4.80}$$

$\psi(T) = 0$ for $T \le 0$. In summary,

$$\text{for } 0 \le T \le A: \quad \phi(T) = -\exp(-\delta T)\,F(T) = -\mu(T)$$
$$\psi(T) = 0 \tag{4.81}$$

$$\text{for } A < T < 2A: \tag{4.82}$$

$$\phi(T) = -e^{-\delta T}F(T) + \int_0^{T-A} I_0\left(\frac{b}{2}\sqrt{(-A+T-\tau)(A+T-\tau)}\right)\psi(\tau)\,d\tau$$

and,

$$\psi(T) = -\frac{b}{2}\int_0^{T-A}\left(\left(\frac{I_1\left(\frac{b}{2}\sqrt{\Omega_A}\right)}{\sqrt{\Omega_A}} - \frac{A^2 b}{2}\frac{I_0\left(\frac{b}{2}\sqrt{\Omega_A}\right)}{\Omega_A} + 2\frac{A^2}{\Omega_A}\frac{I_1\left(\frac{b}{2}\sqrt{\Omega_A}\right)}{\sqrt{\Omega_A}}\right)\right. \tag{4.83}$$
$$\left.\phi(\tau)\,d\tau\right)$$
$$+ \frac{Ab}{4}\phi(T-A) - \phi'(T-A)$$

The density $\psi(T)$ in the second term of (4.82) is calculated over $0 < T < A$, where from (4.81), $\psi(T) = 0$. Thus (4.82) can be rewritten as,

$$\phi(T) = -\exp(-\delta T)\, F(T) = -\mu(T) \tag{4.84}$$

The solution in the domain of $0 \le T \le A$ is

$$W(X,T) = -\frac{b}{2}\int_0^{T-X} \frac{X\, I_1\left(\frac{b}{2}\sqrt{(X+T-\tau)(-X+T-\tau)}\right)}{\sqrt{(X+T-\tau)(-X+T-\tau)}}\,\mu(\tau)\,d\tau + \mu(T-X) \tag{4.85}$$

If,

$$\Omega_\sigma = \left(\frac{A}{L}+\tau-\sigma\right)\left(-\frac{A}{L}+\tau-\sigma\right) \tag{4.86}$$

then the solution $W(X,T)$ in the domain of $A < T \le 2A$ is

$$W(X,T) =$$

$$-\frac{b}{2}\int_0^{T-X}\frac{X}{\sqrt{(X+T-\tau)(-X+T-\tau)}}I_1\left(\frac{b}{2}\sqrt{(X+T-\tau)(-X+T-\tau)}\right)\mu(\tau)d\tau$$

$$+\mu(T-X)$$

$$+\frac{b}{2}\int_0^{T+X-A} I_0\left(\frac{b}{2}\sqrt{(X-A+T-\tau)(A-X+T-\tau)}\right)$$

$$\int_0^{\tau-A}\left(\frac{I_1\left(\frac{b}{2}\sqrt{\Omega_\sigma}\right)}{\sqrt{\Omega_\sigma}}-\frac{A^2b}{2}\frac{I_0\left(\frac{b}{2}\sqrt{\Omega_\sigma}\right)}{\sqrt{\Omega_\sigma}}+\frac{2A^2}{\Omega_\sigma}\frac{I_1\left(\frac{b}{2}\sqrt{\Omega_\sigma}\right)}{\sqrt{\Omega_\sigma}}\right)\mu(\sigma)\,d\sigma\,d\tau$$

$$-\int_0^{T+X-A} I_0\left(\frac{b}{2}\sqrt{(X-A+T-\tau)(A-X+T-\tau)}\right)\ \frac{Ab}{4}\,\mu(\tau-A)\ d\tau \qquad (4.87)$$

$$+\int_0^{T+X-A} I_0\left(\frac{b}{2}\sqrt{(X-A+T-\tau)(A-X+T-\tau)}\right)\ \mu'(\tau-A)\ d\tau$$

The last term in (4.87), $\mu'(\tau-A)$, is a first derivative term. We can rewrite the derivative term by letting

$$\tau - A = \vartheta \ \rightarrow\ \tau = \vartheta + A \ \rightarrow\ \frac{d\tau}{d\vartheta} = 1 \qquad (4.88)$$

The limits of integration transform to

$$\begin{aligned} \tau &= 0 && \rightarrow\ \vartheta = -A \\ \tau &= T+X-A && \rightarrow\ \vartheta = T+X-2A \end{aligned} \qquad (4.89)$$

Denoting the last term of (4.87) as LT

$$\begin{aligned} \text{LT} &= \int_{-A}^{T+X-2A} I_0\left(\frac{b}{2}\sqrt{(X+T-\vartheta-2A)(-X+T-\vartheta)}\right)\mu'(\vartheta)\,d\vartheta \\ &= \int_{-A}^{T+X-2A} I_0\left(\frac{b}{2}\sqrt{(X+T-\vartheta-2A)(-X+T-\vartheta)}\right)\,d\mu(\vartheta) \end{aligned} \tag{4.90}$$

By using integral by parts, (4.90) can be rewritten as

$$\begin{aligned} \text{LT} &= \mu(\vartheta)\, I_0\left(\frac{b}{2}\sqrt{(X+T-\vartheta-2A)(-X+T-\vartheta)}\right)\Bigg|_{-A}^{T+X-2A} \\ &\quad - \int_{-A}^{T+X-2A} \mu(\vartheta)\, dI_0\left(\frac{b}{2}\sqrt{(X+T-\vartheta-2A)(-X+T-\vartheta)}\right) \end{aligned} \tag{4.91}$$

The substitution of ϑ in (4.89) into (4.91) gives

$$\begin{aligned} \text{LT} &= \mu(T+X-2A)\;\; I_0\left(\frac{b}{2}\sqrt{0}\right) \\ &\quad + \mu(-A)\;\; I_0\left(\frac{b}{2}\sqrt{(X+T-A)(-X+T+A)}\right) \\ &\quad - \int_{-A}^{T+X-2A} \mu(\vartheta)\, dI_0\left(\frac{b}{2}\sqrt{(X+T-\kappa-2A)(-X+T-\kappa)}\right) \end{aligned} \tag{4.92}$$

Since μ vanishes for a negative argument, the lower limit of the integral term in (4.92) can be shifted to zero. We can rewrite (4.92) as

$$\mathrm{LT} = \mu(T+X-2A) - \int_0^{T+X-2A} \mu(\vartheta)\,(A-T+\vartheta)\,\frac{I_1\left(\sqrt{(-X+T-\vartheta)(X+T-\vartheta-2A)}\right)}{\sqrt{(-X+T-\vartheta)(X+T-\vartheta-2A)}}\,d\kappa \tag{4.93}$$

If we substitute LT into (4.87) , then we get a solution $W(X,T)$. $W(X,T)$ is transformed back to $N(X,T)$ by using

$$N(X,T) = \exp(\delta T)\; W(X,T) \tag{4.94}$$

The sinusoidal and Weierstrass functions-generated waves are used to check if the model works well with smooth and fractal-shaped functions. Figures 4.21a–b and 4.22a–b show the results of sinusoidal waves and Weierstrass function-generated waves. The bottom friction coefficient is taken to be 0.12, the water depth is 2.5 meters.

The ocean wave data are taken from Grays Harbor Experiment, Washington, 1999. The bottom friction of the ocean wave model is 0.01, the water depth is 5.5 meters. Figures 4.23a – d show the propagation of ocean wave. The fractal dimension of the ocean waves is determined before and after hitting the wall. The results of the ocean wave data are presented in time history charts. The energy contents of the time series are checked as a verification of the model.

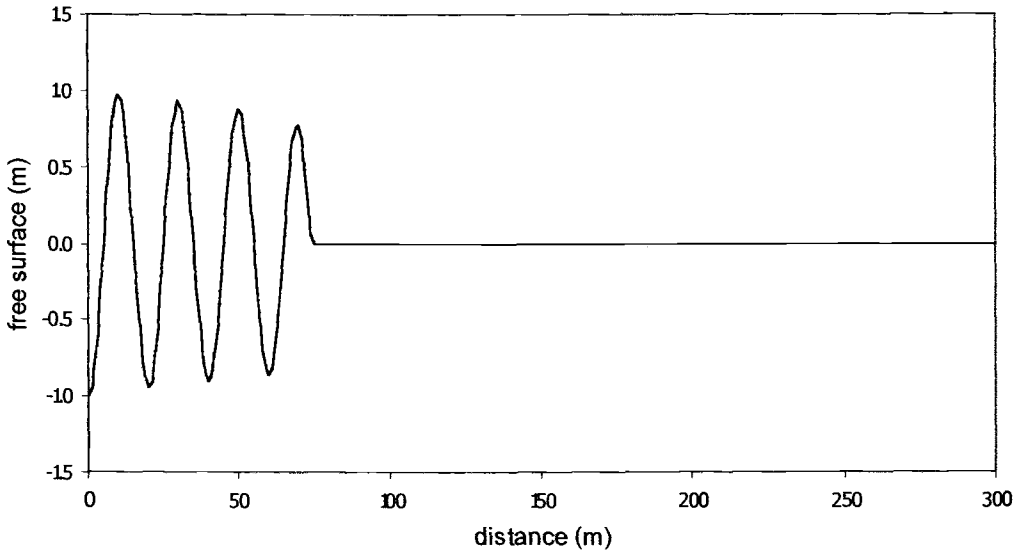

Figure 4.21a. Propagation of a sinusoidal wave on a flat bottom with friction at $t = 15\,\text{sec}$. The location of the wall is at $x = 300\ \text{m}$.

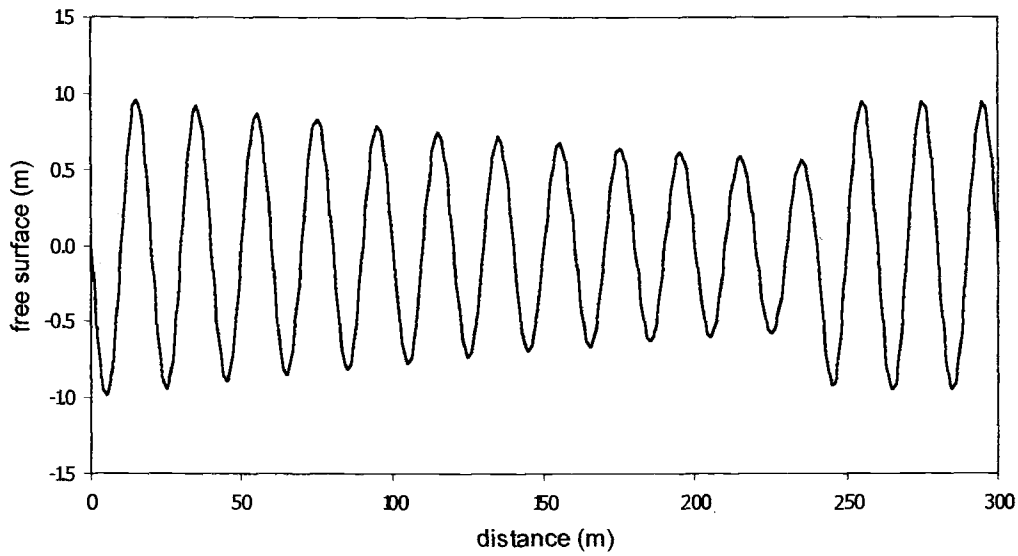

Figure 4.21b. Propagation of a sinusoidal wave on a flat bottom with friction at $t = 72\,\text{sec}$. The effect of reflected waves is shown.

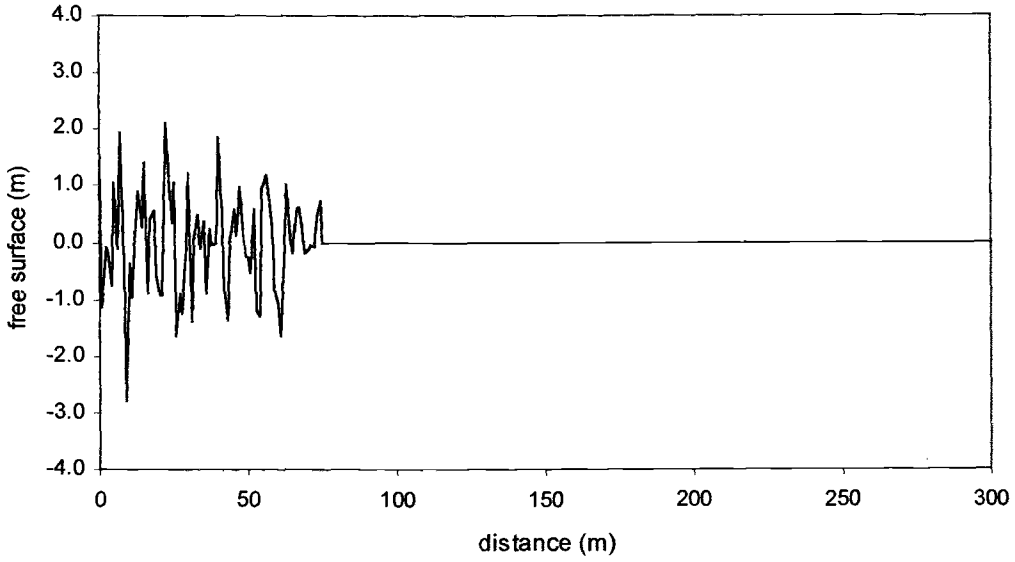

Figure 4.22a. Propagation of a Weierstrass function wave on a flat bottom with friction $t = 15\,\text{sec}$. The location of the wall is at $x = 300\ \text{m}$.

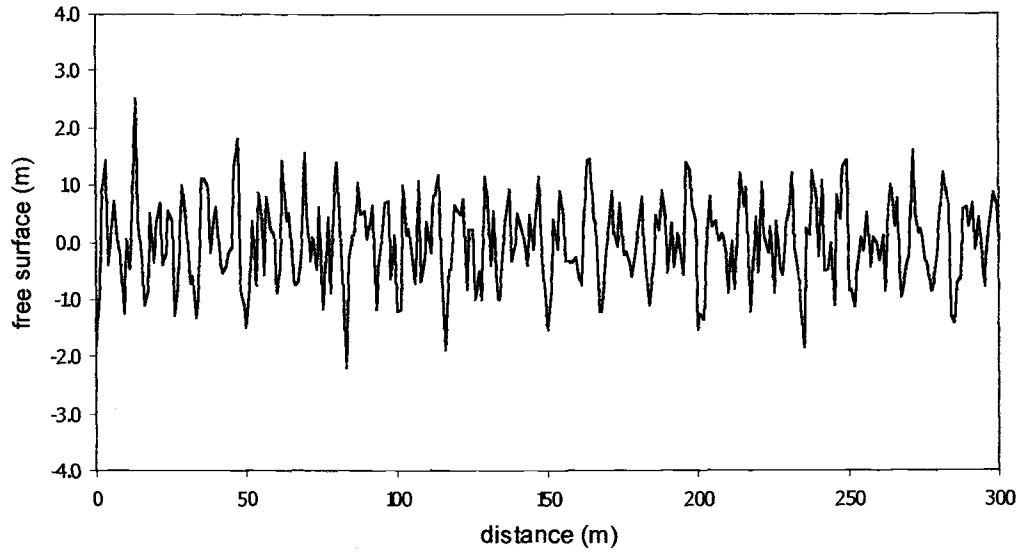

Figure 4.22b. Propagation of a Weierstrass function wave on a flat bottom with friction $t = 90\,\text{sec}$. The waves have been reflected by the wall. The location of the wall is at $x = 300\ \text{m}$.

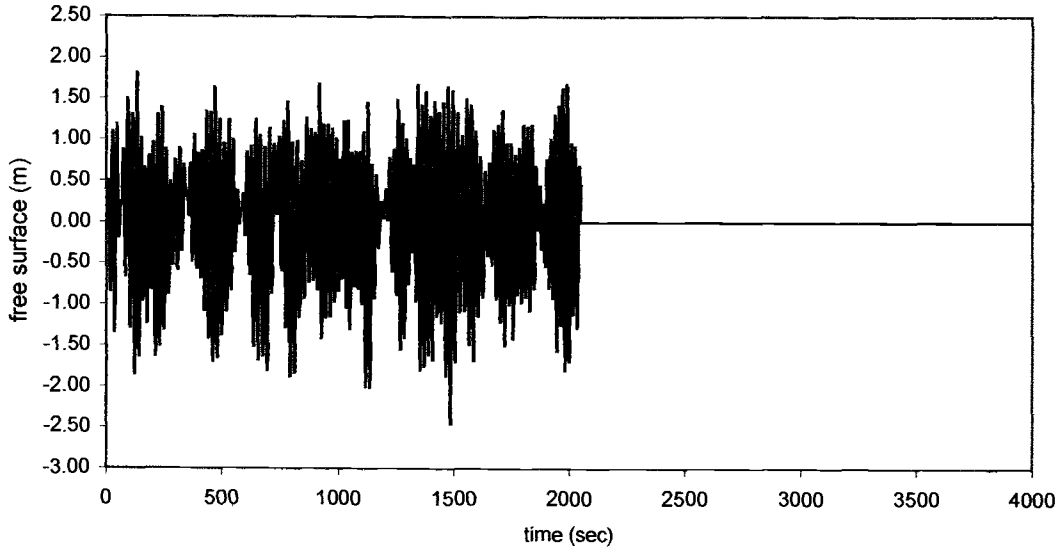

Figure 4.23a. Time history of ocean waves at $x = 0$ m. Fractal dimension is 1.598

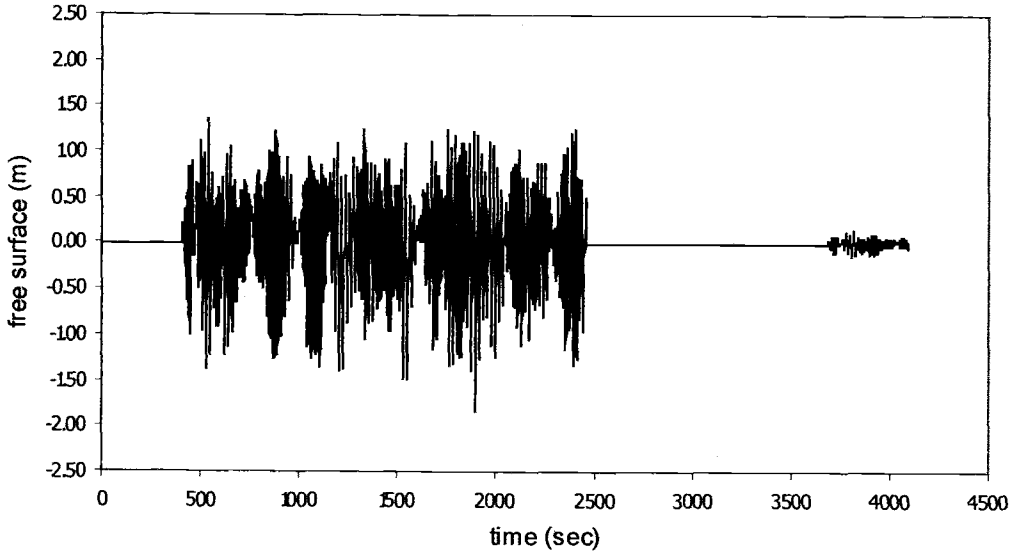

Figure 4.23b. Time history of ocean waves at a location of 1/5 of the domain.

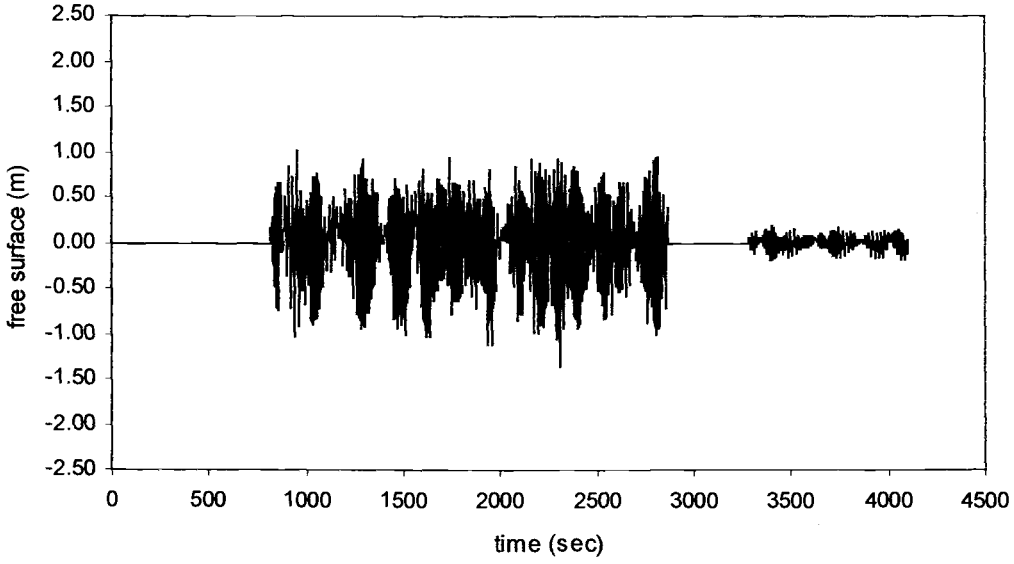

Figure 4.23c. Time history of ocean waves at a location of 2/5 of the domain.

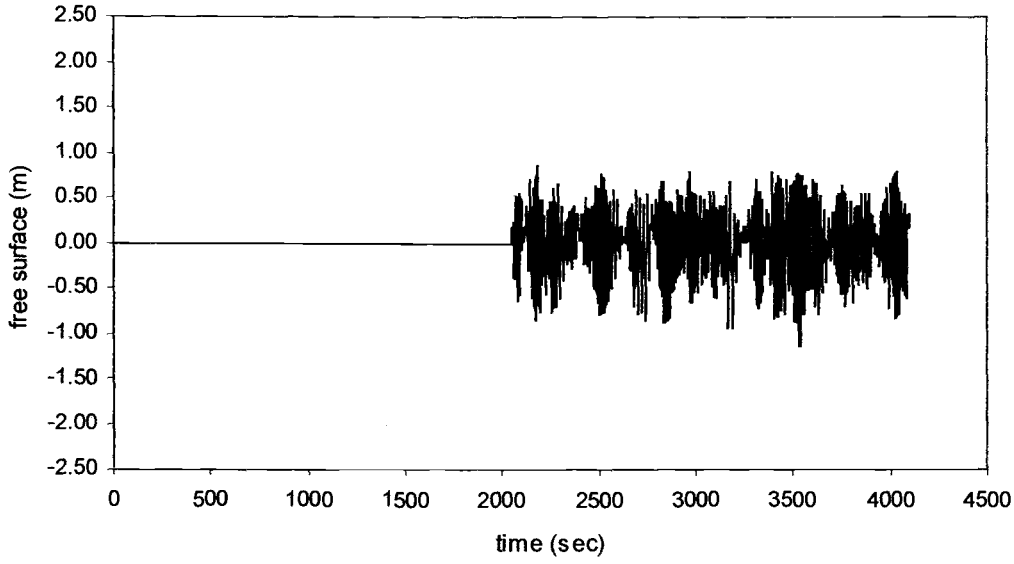

Figure 4.23d. Time history of ocean waves at the location of the wall. The waves are being reflected. Fractal dimension is 1.598.

Figures 4.24a-b show the energy spectra for the solutions in Figure 4.23a and 4.23d. The total area under the energy spectrum at $x = 0$ in Figure 4.24a is 0.528 m^2, and the total area at $x = a$ m in Figure 4.24b is 0.116 m^2. The energy loss is around 22%. By using the results without a reflective wall in Figure 4.17b, the total area under the energy spectrum curve, when the waves reach $x = a$ m, is 0.029 m^2. The values can be analyzed as follows,

$$\frac{E_{total}(\text{with wall})}{E_{total}(\text{without wall})} = \frac{0.116}{0.029} = 4 \tag{4.95}$$

The energy is proportional to the squared wave height.

$$\frac{(H_i + H_r)^2}{H_i^2} = 4 \tag{4.96}$$

where H_i is incident wave height, and H_r is reflected wave height. If we calculate further, then we can rewrite (4.96) as

$$1 + \frac{H_r}{H_i} = 2 \tag{4.97}$$

The reflection coefficient of the wall is

$$K_{r\,\text{wall}} = \frac{H_r}{H_i} = 1 \tag{4.98}$$

The value of one fulfills the assumption of the model that the wall is completely reflective. Figures 4.23a and 4.23d also show that the fractal dimension of the waves does not change with the bottom friction and reflective wall interactions.

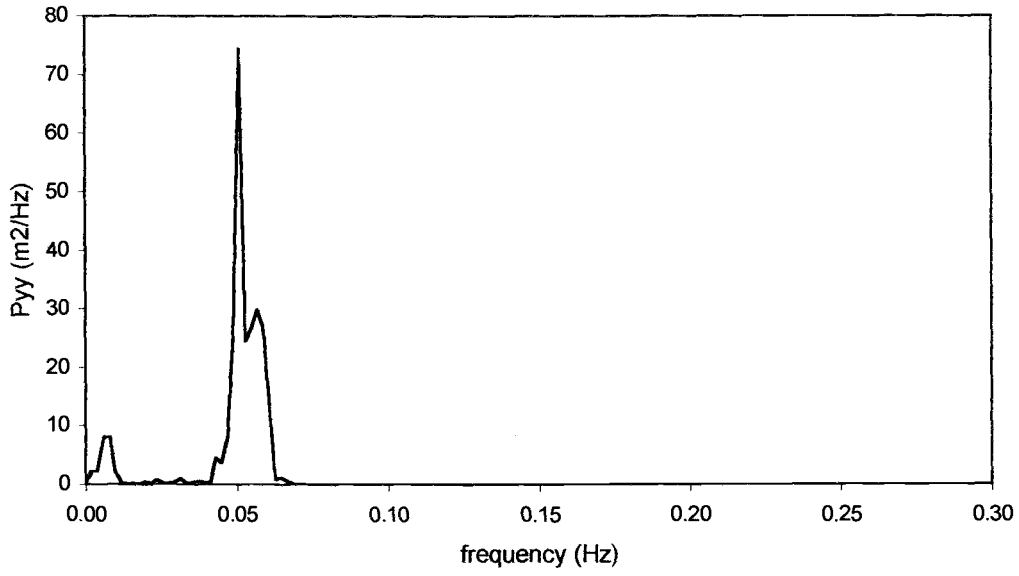

Figure 4.24a. The energy spectrum of data points in Figure 4.23a

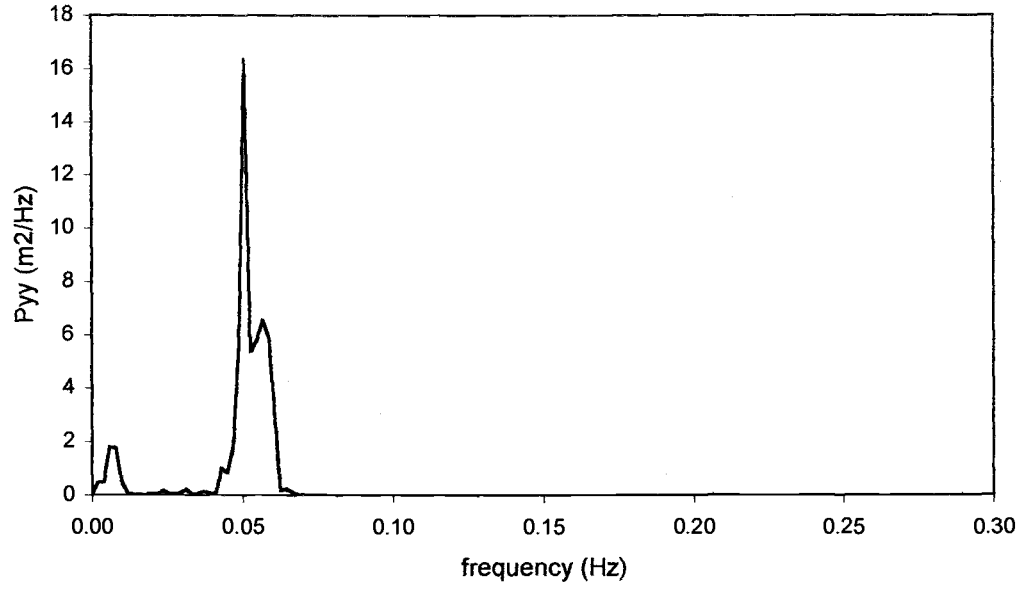

Figure 4.24b. The energy spectrum of data points in Figure 4.23d

4.5 A SLOPING BOTTOM WITHOUT BOTTOM FRICTION

This section focuses on the effects of interactions between waves and sloping bottom on the fractal dimension of the waves. The problem does not include bottom friction, thus, $F^b = 0$. The model does not consider the depth-limited breaking waves, so the computer run ends when the wave height reaches a threshold corresponding to the breaking wave height cutoff.

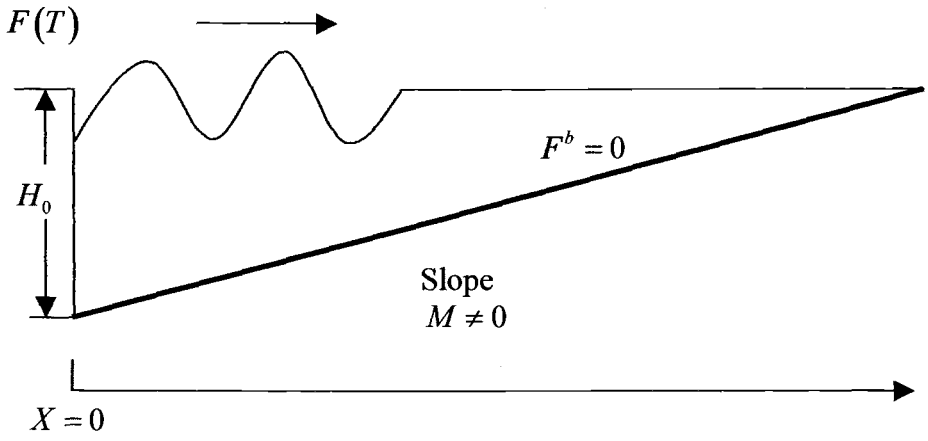

Figure 4.25. Sketch of the domain for a sloping bottom without bottom friction

The governing equation is written in (3.52). We assume that the slope is small as defined in (3.48). The boundary value problem can be written as

$$\begin{aligned} &W_{TT} + \frac{M^2}{4} W = W_{XX} && X \geq 0, \quad T \geq 0 \\ &W(X,0) = W_T(X,0) = 0 \\ &W(0,T) = F(T) \end{aligned} \tag{4.103}$$

where $N(X,T)=\exp(\delta X)\,W(X,T)$, and $\delta=-\frac{M}{2}$. We assume that bottom depth over domain changes by less than 10%. We also assume that the value of 10% is small enough that the governing equation in (3.52) is valid for the model with sloping bottom. If we write the step width as X_s, then the assumption can be rewritten in different form as

$$X^s \le \frac{0.1}{M} \tag{4.104}$$

where X^s is the width of the small step. The solution at the end of each step of width X^s becomes the boundary condition for the next step with the same step width X^s. Decreasing step width X^s may give better results, however, the smaller step will add to computer run time. The model moves forward to any total distance as desired. The model should be stopped before the wave breaks. Using the same method as described in Chapter 3, the Riemann function R is

$$R(X,T;s,\tau)=J_0\left(\frac{M}{2}\sqrt{(X-s+T-\tau)(-X+s+T-\tau)}\right) \tag{4.105}$$

For the Dirichlet-type boundary condition written in (4.103), the solution is written in terms of *double layer potential*.

$$\begin{aligned} W(X,T)=\int_0^{T_a} & \frac{\partial}{\partial s}J_0\left(\frac{M}{2}\sqrt{(X-s+T-\tau)(-X+s+T-\tau)}\right)\Bigg|_{s=0}\phi(\tau)\,d\tau \\ & -J_0\left(\frac{M}{2}\sqrt{(X-s+T-T_a)(-X+s+T-T_a)}\right)\Bigg|_{s=0}\phi(T_a)\frac{\partial}{\partial X}T_a \end{aligned} \tag{4.106}$$

where $T_a = T - X$. By carrying out the derivation of (4.106), we can rewrite (4.106) as

$$W(X,T) = -\frac{M}{2}\int_0^{T_a} \frac{X\, J_1\left(\frac{M}{2}\sqrt{(X+T-\tau)(-X+T-\tau)}\right)}{\sqrt{(X+T-\tau)(-X+T-\tau)}}\ \phi(\tau)\, d\tau$$
$$+J_0\left(\frac{M}{2}\sqrt{(X+T-(T-X))(-X+T-(T-X))}\right)\phi(T-X) \tag{4.107}$$

Applying the boundary condition at $X = 0$,

$$\phi(T) = F(T) \tag{4.108}$$

The substitution of (4.108) into (4.107) gives

$$W(X,T) = -X\frac{M}{2}\int_0^{T-X} \frac{J_1\left(\frac{M}{2}\sqrt{(X+T-\tau)(-X+T-\tau)}\right)}{\sqrt{(X+T-\tau)(-X+T-\tau)}}\ F(\tau)\, d\tau$$
$$+\ F(T-X) \tag{4.109}$$

To get the original solution $N(X,T)$, we use a change of variable

$$N(X,T) = \exp(\delta X)\ W(X,T) \tag{4.110}$$

where $\delta = -\frac{M}{2}$. The solution $N(X,T)$ in (4.110) is repeated over the entire domain in every small step X^s. Figures 4.26a-b show the results for the sinusoidal waves with a boundary condition at $x = 0$ m. The wave period is 10 seconds, and

the bottom slope is 0.02. The water depth at the beginning of the domain is 1.9 meters. By using (4.104), we calculate the step width to be 9.5 meters. Figures 4.27a-b show the results for the ocean waves taken from Grays Harbor, Washington, 1999. The original data were taken in a water depth of 11 meters. To adjust to shallow water conditions, the data are shoaled and filtered to a water depth of 5.5 meters according to procedure described in page 46. For the ocean wave data run, the small step width is 27.5 meters.

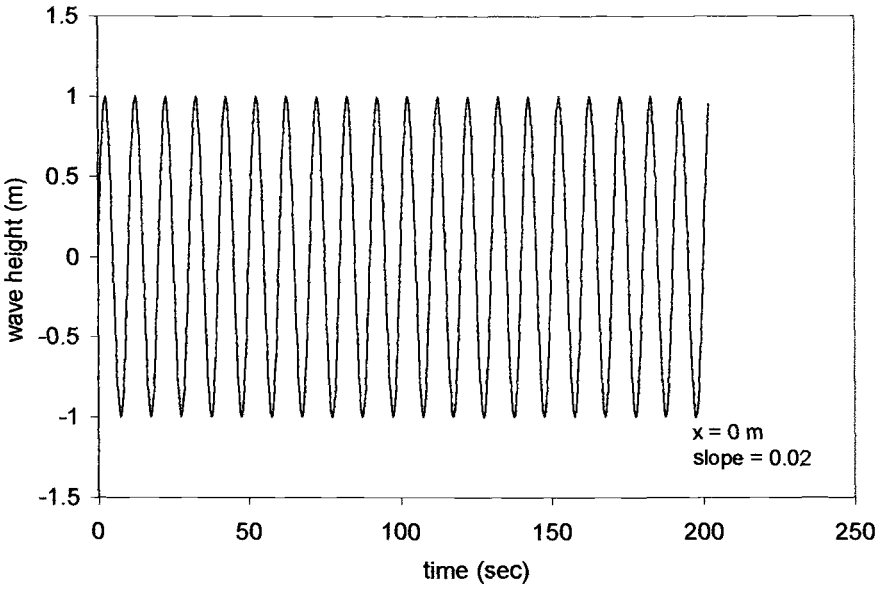

Figure 4.26a Sinusoidal waves on a sloping bottom at $x = 0$ m

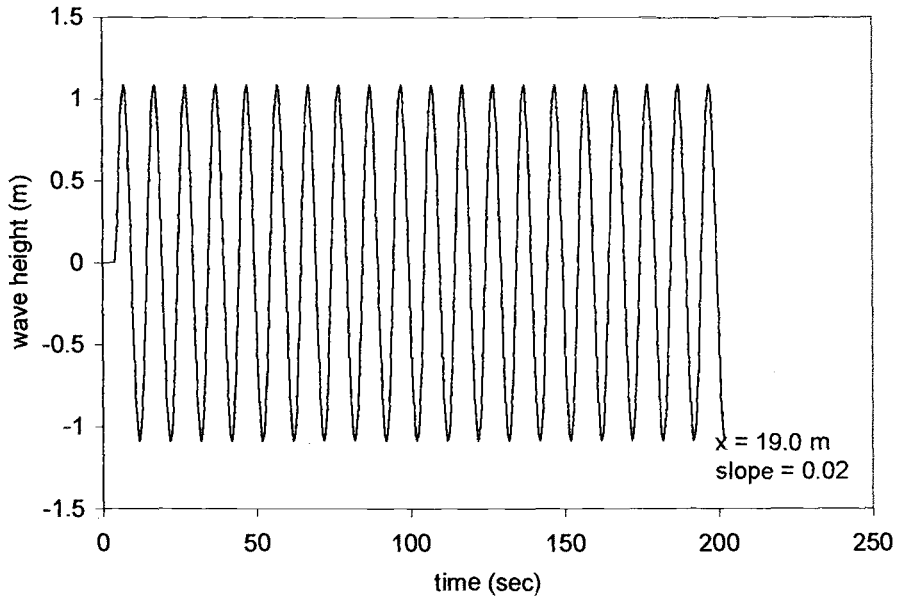

Figure 4.26b. Sinusoidal waves on a sloping bottom at x = 19 m. Notice that the waves increase in height as it propagates.

The energy flux of the waves can be written as

$$\text{Flux}_i = E_i C_{gi} \tag{4.111}$$

where the total energy $E_i = 1/8\ \rho g H_i^2$ and for shallow water the group velocity is the same as the celerity. We evaluate the ratio between energy flux at x = 19 m and x = 0 m.. The ratio can be written as

$$\frac{\text{Flux}_{x=19m}}{\text{Flux}_{x=0m}} = \frac{H_{x=19m}^{\ 2}}{H_{x=0m}^{\ 2}} \sqrt{\frac{h_{x=19m}}{h_{x=0m}}} = \frac{1.08^2}{1^2} \sqrt{\frac{1.52}{1.9}} = 1.04 \tag{4.112}$$

The value of 1.04 shows that the solutions of the sloping model do not conserve energy flux. The fact that the ratio is not equal to one may indicate that there is an

error in this technique. Figures 4.27a – b show the propagation of ocean waves over the sloping bottom. Figures 4.28a – b show the energy spectrum of the data points in Figures 4.27a – b.

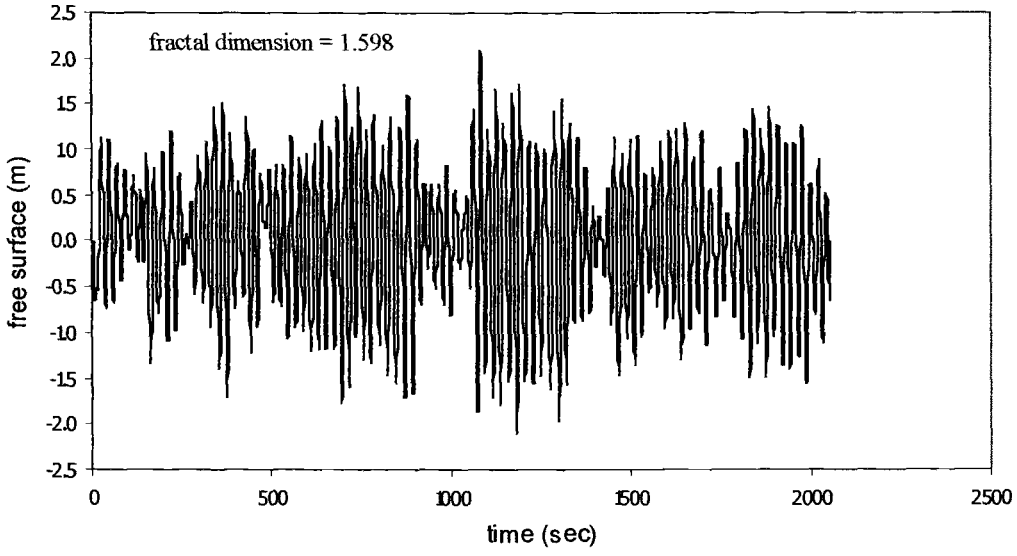

Figure 4.27a. The time history of ocean waves at $x = 0$. The data are taken from Grays Harbor Wave Refraction Experiment, Washington, 1999. The slope of the bottom *m* is 0.02.

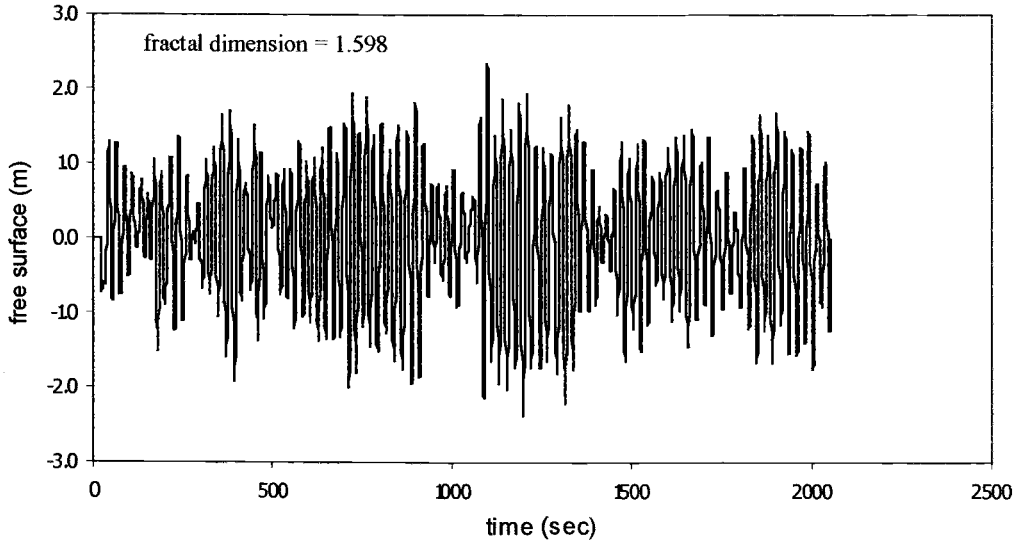

Figure 4.27b. The time history ocean waves at $x = 27.5$ m. The data are taken from Grays Harbor Wave Refraction Experiment, Washington, 1999. The slope of the bottom is 0.02

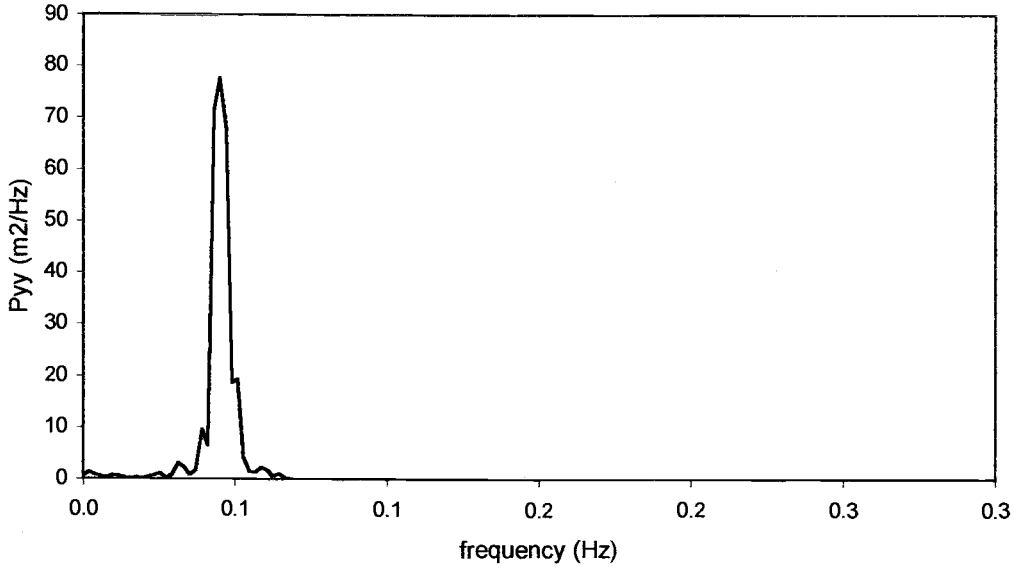

Figure 4.28a. The energy spectrum for the data points in Figure 4.27a

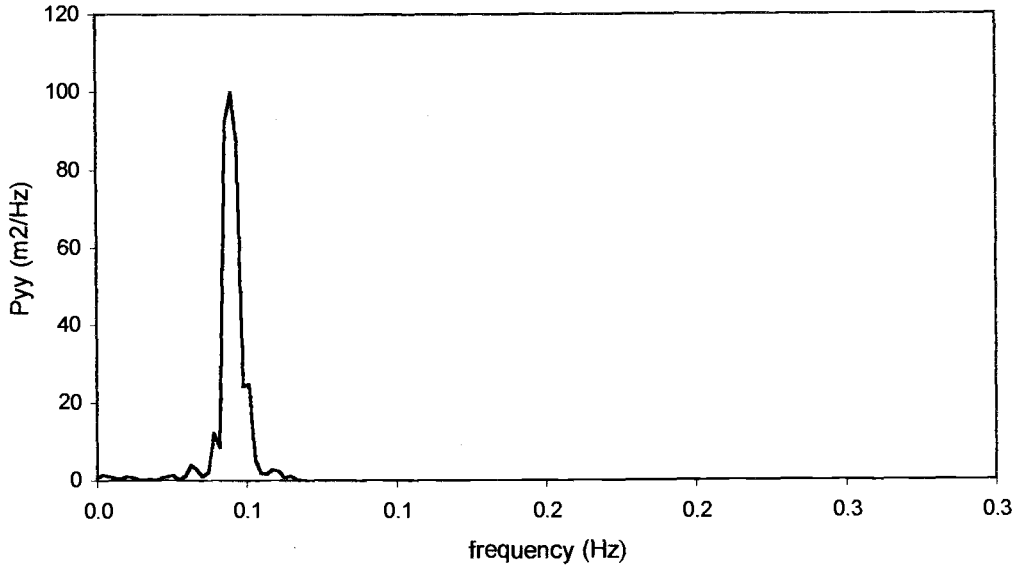

Figure 4.28b. The energy spectrum for the data points in Figure 4.27b

Figures 4.27a – b show that a linear analysis of wave propagation over sloping bottom does not reproduce the expected change of fractal dimension of the waves. The fractal dimension of the waves is 1.589 at all locations. The propagation of the waves does not change the frequency contents either, as shown in Figures 4.28a – 4.28b. The linear solution on sloping bottom using (4.109) and (4.110) does not conserve energy flux. This may be caused by the small slope assumption in (3.48) that lead us to a constant coefficient PDE for the case of sloping bottom. To deal with the problem, we will apply the linear solution on flat bottom without bottom friction written in (4.21) to a series of small steps. The model will be discussed in Chapter 6.

Solutions from a linear model have been considered in Sections 4.1-4.5. The integral solutions exhibit one important point that the solution gives finite

speed of wave propagation. The solutions show the area in which the body of water is undisturbed. However, these solutions predict a constant fractal dimension, in contrast to the changing fractal dimension observed in real oceanic data. The next step is to perform a nonlinear analysis.

CHAPTER 5. NONLINEAR LONG WAVE EQUATION

The linear solutions derived in Chapter 4 do not reproduce the change in fractal dimension observed in ocean waves. The observation made in Chapter 2 that fractal dimension is correlated with the degree of nonlinearity of the waves suggests that nonlinear effects need to be retained. Thus, we develop a nonlinear analysis using the nonlinear wave equation derived in Chapter 3.

We consider wave propagation over a flat bottom without bottom friction. To provide insight into the nonlinear problem, we first approach the problem using an implicit finite difference method. We apply a smooth half-sinusoidal wave as the initial condition.

In our second approach, we use the Runge-Kutta numerical integration method, with the same initial condition. The results are then compared with the results from the finite difference method.

We start with the equations for conservation of mass and momentum, (3.5) and (3.14). Letting

$$\zeta = h + \eta \tag{5.1}$$

and

$$v = u(h+\eta), \tag{5.2}$$

(3.5) and (3.14) can be expressed as

$$\zeta_t + v_x = 0 \tag{5.3}$$

and

$$v_t + uv_x = -g\zeta(\zeta - h)_x \tag{5.4}$$

For a flat bottom, the momentum equation in (5.4) is reduced to

$$v_t + uv_x + g\zeta\zeta_X = 0 \tag{5.5}$$

where

$$u = \frac{v}{\zeta} \tag{5.6}$$

These equations can be written in matrix form as

$$\begin{pmatrix} \zeta_t \\ v_t \end{pmatrix} + \begin{bmatrix} 0 & 1 \\ g\zeta & \dfrac{v}{\zeta} \end{bmatrix} \begin{pmatrix} \zeta_x \\ v_x \end{pmatrix} = \begin{pmatrix} 0 \\ 0 \end{pmatrix} \tag{5.7}$$

5.1 THE FINITE DIFFERENCE METHOD

The method uses a backward difference in time and a central difference in space. The conservation of mass in (5.3) can be written in difference form as

$$\frac{\zeta_i^j - \zeta_i^{j-1}}{\Delta t} + \frac{v_{i+1}^j - v_{i-1}^j}{2\Delta x} = 0 \tag{5.8}$$

where subscript i denotes spatial points, and subscript j denotes time points. Equation (5.8) can be rewritten as

$$\zeta_i^j = \zeta_i^{j-1} - \frac{1}{2}\frac{\Delta t}{\Delta x}\left(v_{i+1}^j - v_{i-1}^j\right) \tag{5.9}$$

The conservation of momentum in (5.5) can be modified to

$$v_t + \frac{1}{\zeta}\left(\frac{v^2}{2}\right)_x = -g\left(\frac{\zeta^2}{2}\right)_x \tag{5.10}$$

Equation (5.10) is written in difference form as follows

$$\frac{v_i^j - v_i^{j-1}}{\Delta t} + \frac{1}{2\zeta_i^j}\left(\frac{\left(v_{i+1}^j\right)^2 - \left(v_{i-1}^j\right)^2}{2\Delta x}\right) = -\frac{1}{2}g\left(\frac{\left(\zeta_{i+1}^j\right)^2 - \left(\zeta_{i-1}^j\right)^2}{2\Delta x}\right) \quad (5.11)$$

or

$$v_i^j = v_i^{j-1} - \frac{1}{4\zeta_i^j}\frac{\Delta t}{\Delta x}\left(\left(v_{i+1}^j\right)^2 - \left(v_{i-1}^j\right)^2\right) - \frac{\Delta t}{4\Delta x}g\left(\left(\zeta_{i+1}^j\right)^2 - \left(\zeta_{i-1}^j\right)^2\right) \quad (5.12)$$

Figure 5.1 shows the domain of the computer model.

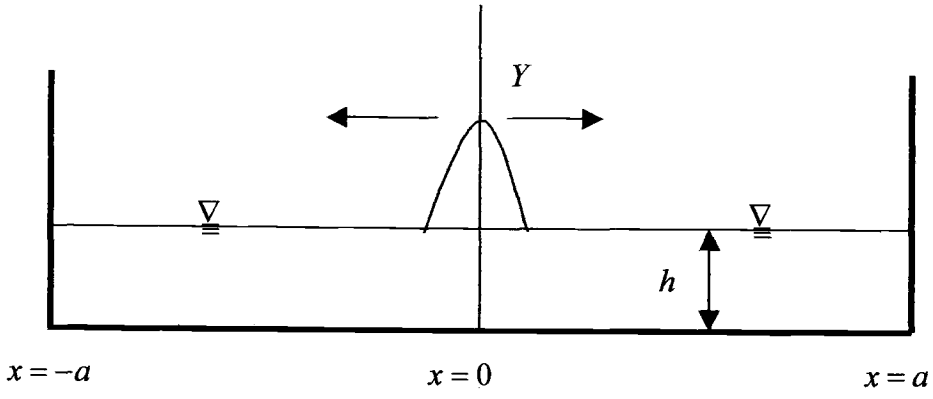

Figure 5.1 Sketch of the domain of the model

We assume a reflective boundary at $x = a$ and $x = -a$. At the boundary, we expect

$$\frac{\partial \zeta}{\partial x} = \frac{\zeta_{i+1}^j - \zeta_{i-1}^j}{2\Delta x} = 0 \tag{5.13}$$

or

$$\zeta_{i+1}^j = \zeta_{i-1}^j \tag{5.14}$$

The velocity at the end boundaries is zero.

$$v_i^j = 0 \tag{5.15}$$

The following procedure is followed in our numerical analysis:

a. Estimate $\left(v_i^j\right)^0$ in (5.9) and obtain $\left(\zeta_i^j\right)^1$

b. Substitute $\left(\zeta_i^j\right)^1$ from (a) into (5.12) to obtain $\left(v_i^j\right)^1$

c. Repeat (a) by replacing $\left(v_i^j\right)^0$ with $\left(v_i^j\right)^1$ to obtain $\left(\zeta_i^j\right)^2$

d. Repeat (b) by replacing $\left(\zeta_i^j\right)^1$ with $\left(\zeta_i^j\right)^2$ to obtain $\left(v_i^j\right)^2$

e. Repeat steps (a) to (d) until $\left|\left(v_i^j\right)^{k+1} - \left(v_i^j\right)^k\right| < \varepsilon$ and $\left|\left(\zeta_i^j\right)^{k+1} - \left(\zeta_i^j\right)^k\right| < \varepsilon$

k denotes the iteration number. We take ε to be 0.01.

Figures 5.2a – b show the results with half sinusoidal function as the initial condition.

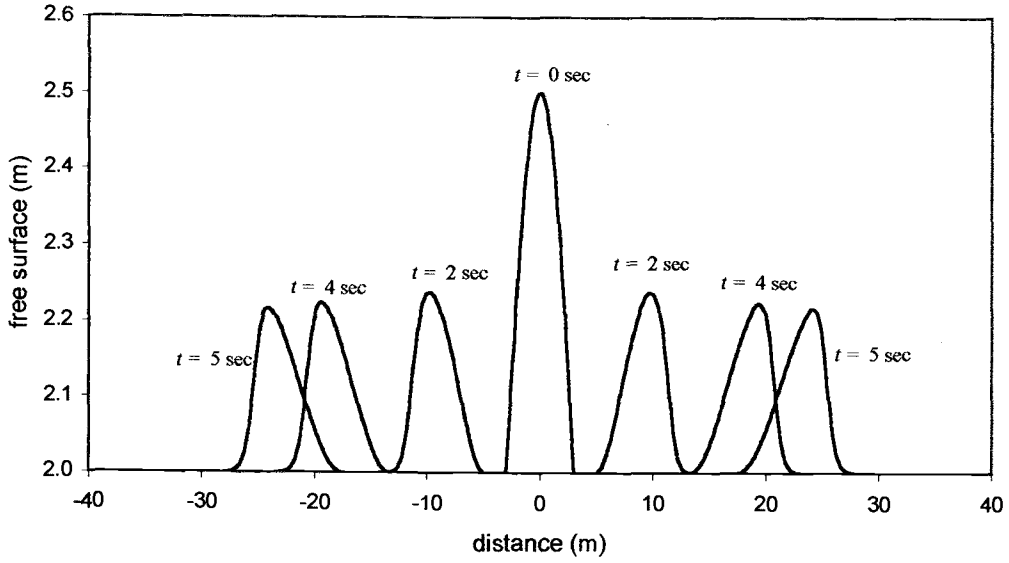

Figure 5.2a Combined plots of nonlinear wave solutions using finite difference method. We can see the decrease of surface peaks and the widening of wave bases.

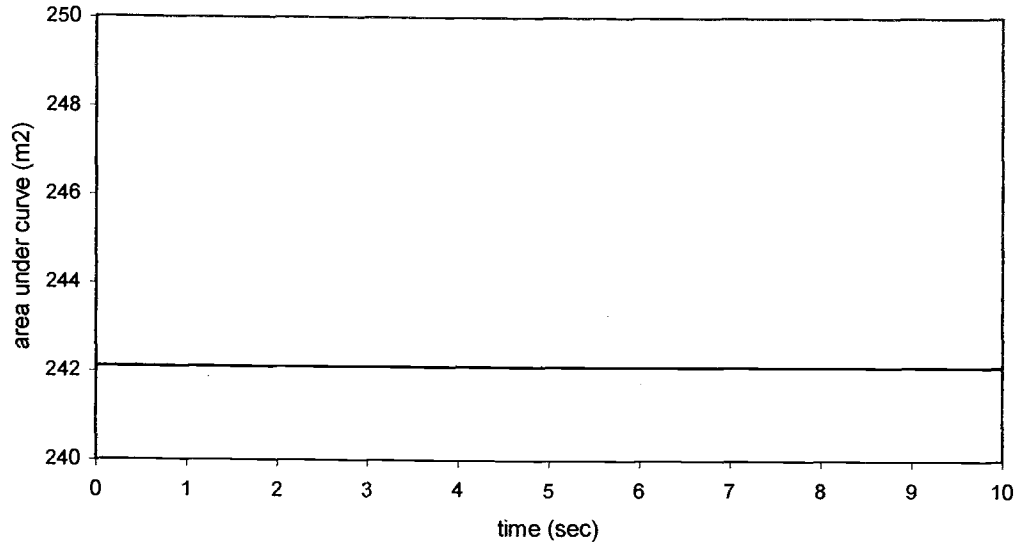

Figure 5.2b Total area under the curves of the solution to verify the conservation of mass

Figure 5.2a shows the tendency of the waves to curl over as time elapses. However, the wave surface never becomes vertical because the finite difference method does not support a multi-valued function. We can see that the wave amplitudes tend to decrease, and the wavelength increases. The peaks travel faster than the center of the wave base. Figure 5.2b shows that the solution satisfies the conservation of mass. The total area under the solution curves is constant for all times. The finite difference model does not work with a fractal-shaped function because the model uses the principle of slopes or tangents at each point. Thus, the finite difference method only works for smooth functions which are everywhere differentiable.

5.2 METHOD OF CHARACTERISTICS

The objective of this section is to develop a Runge-Kutta numerical solution to solve the nonlinear wave equations. By using the same initial condition as in Section 5.1, we can compare the results with the finite difference results. The method is suitable for a fractal-shaped function because it is based on an integral equation. The nonlinear wave equation (5.7) is transformed to new variables by introducing change of variables as follows,

$$\begin{pmatrix} \zeta \\ v \end{pmatrix} = [B] \begin{pmatrix} \alpha \\ \beta \end{pmatrix} \tag{5.16}$$

The motivation for the change of variables is to determine a matrix $[B]$ that decouples the system of equations in (5.7). The substitution of (5.16) into (5.7) gives

$$B\begin{pmatrix} \alpha_t \\ \beta_t \end{pmatrix} + B_t\begin{pmatrix} \alpha \\ \beta \end{pmatrix} + \begin{bmatrix} 0 & 1 \\ \zeta & \dfrac{v}{\zeta} \end{bmatrix} B\begin{pmatrix} \alpha_x \\ \beta_x \end{pmatrix} + \begin{bmatrix} 0 & 1 \\ \zeta & \dfrac{v}{\zeta} \end{bmatrix} B_x\begin{pmatrix} \alpha \\ \beta \end{pmatrix} = \begin{pmatrix} 0 \\ 0 \end{pmatrix} \tag{5.17}$$

We introduce a short hand notation

$$\begin{bmatrix} 0 & 1 \\ \zeta & \frac{v}{\zeta} \end{bmatrix} = \Omega \tag{5.18}$$

If we divide (5.17) through by B, we can rewrite (5.17) as

$$\begin{pmatrix} \alpha_t \\ \beta_t \end{pmatrix} + B^{-1}\Omega B \begin{pmatrix} \alpha_x \\ \beta_x \end{pmatrix} = -B^{-1}B_t \begin{pmatrix} \alpha \\ \beta \end{pmatrix} - B^{-1}\Omega B_x \begin{pmatrix} \alpha \\ \beta \end{pmatrix} \tag{5.19}$$

To decouple the left hand side of (5.19), it is necessary for $B^{-1}\Omega B$ to be a diagonal matrix.

$$B^{-1}\Omega B = \begin{pmatrix} \lambda_1 & 0 \\ 0 & \lambda_2 \end{pmatrix} \tag{5.20}$$

To get (5.20), B must be the eigenvectors of Ω. The eigenvectors of B can be written as

$$B = \begin{pmatrix} 1 & 1 \\ \lambda_1 & \lambda_2 \end{pmatrix} \tag{5.21}$$

where

$$\lambda_1 = \frac{v}{2\zeta} + \frac{1}{2}\sqrt{\left(\frac{v}{\zeta}\right)^2 + 4g\zeta}$$

$$\lambda_2 = \frac{v}{2\zeta} - \frac{1}{2}\sqrt{\left(\frac{v}{\zeta}\right)^2 + 4g\zeta} \tag{5.22}$$

λ_1 and λ_2 are the eigenvalues of the system of equations. The eigenvalues are not constant; they depend on both ζ and v. By substituting (5.20) into (5.19), we can rewrite (5.19) as

$$\alpha_t + \lambda_1 \alpha_x = -\frac{1}{\lambda_2 - \lambda_1}\left[\left(-\lambda_{1t} + \lambda_{1x}\left(\lambda_2 - \frac{v}{\zeta}\right)\right)\alpha + \left(-\lambda_{2t} + \lambda_{2x}\left(\lambda_2 - \frac{v}{\zeta}\right)\right)\beta\right] \tag{5.23}$$

$$\beta_t + \lambda_2 \beta_x = -\frac{1}{\lambda_2 - \lambda_1}\left[\left(\lambda_{1t} + \lambda_{1x}\left(-\lambda_1 + \frac{v}{\zeta}\right)\right)\alpha + \left(\lambda_{2t} + \lambda_{2x}\left(-\lambda_1 + \frac{v}{\zeta}\right)\right)\beta\right] \tag{5.24}$$

These equations are very similar with α corresponding to a wave moving to the right and β corresponding to a wave moving to the left. The initial conditions (5.23) and (5.24) can be obtained using (5.16). We can solve α and β by multiplying both sides with the inverse of matrix B.

$$\begin{pmatrix}\alpha\\ \beta\end{pmatrix} = [B]^{-1}\begin{pmatrix}\zeta\\ v\end{pmatrix} = \begin{bmatrix}1 & 1\\ \lambda_1 & \lambda_2\end{bmatrix}^{-1}\begin{pmatrix}\zeta\\ v\end{pmatrix} \tag{5.25}$$

By evaluating the inverse of B, we can write the initial conditions of α and β as

$$\alpha(x,0) = \frac{\lambda_2^0}{\lambda_2^0 - \lambda_1^0}\zeta(x,0) \tag{5.26}$$

and

$$\beta(x,0) = \frac{-\lambda_1^0}{\lambda_2^0 - \lambda_1^0}\zeta(x,0) \tag{5.27}$$

where the superscript "0" in the eigenvalues denote the initial conditions for the eigenvalues. The eigenvalues are functions of ζ and v. Equations (5.23) and (5.24)

are solved using the method of characteristics. If we look at the differential equation in terms of α in (5.23), we can write the characteristics of the equation as

$$\frac{\partial t}{\partial \tau}=1 \qquad \text{where } t(s,\tau=0)=0 \tag{5.28}$$

$$\frac{\partial x}{\partial \tau}=\lambda_1 \qquad \text{where } x(s,\tau=0)=s \tag{5.29}$$

$$\frac{\partial \alpha}{\partial \tau}=-\frac{1}{\lambda_2-\lambda_1}\left[\left(-\frac{\partial \lambda_1}{\partial t}+\frac{\partial \lambda_1}{\partial x}\left(\lambda_2-\frac{v}{\zeta}\right)\right)\alpha+\left(-\frac{\partial \lambda_2}{\partial t}+\frac{\partial \lambda_2}{\partial x}\left(\lambda_2-\frac{v}{\zeta}\right)\right)\beta\right] \tag{5.30}$$

where

$$\alpha(s,\tau=0)=\frac{\lambda_2}{\lambda_2-\lambda_1}\zeta(s,0)$$

Thus,

$$\frac{\partial \alpha}{\partial \tau}=-\frac{1}{\lambda_2-\lambda_1}\left[\left(-\frac{\partial \lambda_1}{\partial \tau}+\frac{\partial \lambda_1}{\partial \tau}\frac{\lambda_2-\frac{v}{\zeta}}{\lambda_1}\right)\alpha+\left(-\frac{\partial \lambda_2}{\partial \tau}+\frac{\partial \lambda_2}{\partial \tau}\frac{\lambda_2-\frac{v}{\zeta}}{\lambda_1}\right)\beta\right] \tag{5.31}$$

From (5.22), we can evaluate

$$\frac{\lambda_2-\frac{v}{\zeta}}{\lambda_1}=-1 \tag{5.32}$$

If we substitute (5.32) into (5.31), we can simplify $\frac{\partial \alpha}{\partial \tau}$ as

$$\frac{\partial \alpha}{\partial \tau} = \frac{\partial \lambda_1}{\partial \tau}\left(\frac{2\alpha}{\lambda_2 - \lambda_1}\right) + \frac{\partial \lambda_2}{\partial \tau}\left(\frac{2\beta}{\lambda_2 - \lambda_1}\right) \tag{5.33}$$

The equations of characteristics $\frac{\partial t}{\partial \tau}, \frac{\partial x}{\partial \tau}$ and $\frac{\partial \alpha}{\partial \tau}$ from (5.28), (5.29) and (5.33) are ordinary differential equations. The equations have 6 unknowns: *t*, *x*, α, β, λ_1 and λ_2. 6 equations are needed to solve these 6 unknowns. Three equations are available, for $\frac{\partial t}{\partial \tau}, \frac{\partial x}{\partial \tau}$ and $\frac{\partial \alpha}{\partial \tau}$ as written in (5.28), (5.29) and (5.33). Three more equations are needed, which are $\frac{\partial \lambda_1}{\partial \tau}$, $\frac{\partial \lambda_2}{\partial \tau}$ and $\frac{\partial \beta}{\partial \tau}$. We consider the relation between the eigenvalues. The multiplication of the eigenvalues results in

$$\lambda_1 \lambda_2 = -\zeta = -(\alpha + \beta) \tag{5.34}$$

From (5.34), λ_1 can be obtained and written as

$$\lambda_1 = \frac{-(\alpha + \beta)}{\lambda_2} \tag{5.35}$$

If we take the derivative of (5.35) with respect to τ, then we can write $\frac{\partial \lambda_1}{\partial \tau}$ as

$$\frac{\partial \lambda_1}{\partial \tau} = -\left(\frac{1}{\lambda_2}\right)\frac{\partial \alpha}{\partial \tau} - \left(\frac{1}{\lambda_2}\right)\frac{\partial \beta}{\partial \tau} + \frac{(\alpha + \beta)}{\lambda_2^{\,2}}\frac{\partial \lambda_2}{\partial \tau} \tag{5.36}$$

The initial condition for λ_1 can be obtained from (5.22). λ_1 is written in the characteristic variable s as

$$\lambda_1(s,0)=\sqrt{\zeta(s,0)}=\sqrt{(h+\eta(s,0))} \tag{5.37}$$

Now, we need the equation for $\frac{\partial\lambda_2}{\partial\tau}$. We consider the summation of the two eigenvalues. We can write the summation as

$$\lambda_1+\lambda_2=\frac{v}{2\zeta} \tag{5.38}$$

λ_2 can be obtained and written as

$$\lambda_2=\frac{v}{2\zeta}-\lambda_1 \tag{5.39}$$

By substituting λ_1 obtained in (5.35), we can rewrite (5.39) as

$$\lambda_2=\frac{\lambda_1\alpha+\lambda_2\beta}{2(\alpha+\beta)}-\lambda_1 \tag{5.40}$$

If we take the derivative of λ_2 with respect to τ, we can write $\frac{\partial\lambda_2}{\partial\tau}$ as

$$\left(1-\frac{\alpha}{2(\alpha+\beta)}\right)\frac{\partial\lambda_1}{\partial\tau}+\left(1-\frac{\beta}{2(\alpha+\beta)}\right)\frac{\partial\lambda_2}{\partial\tau}$$

$$+\left(\frac{2(\lambda_1\alpha+\lambda_2\beta)}{(2\alpha+2\beta)^2}-\frac{\lambda_1}{2(\alpha+\beta)}\right)\frac{\partial\alpha}{\partial\tau} \tag{5.41}$$

$$=\left(\frac{\lambda_2}{2(\alpha+\beta)}-\frac{2(\lambda_1\alpha+\lambda_2\beta)}{(2\alpha+2\beta)^2}\right)\frac{\partial\beta}{\partial\tau}$$

By rearranging the equation, we can get $\frac{\partial \lambda_2}{\partial \tau}$. The initial condition for λ_2 is written in terms of the characteristics variable s as

$$\lambda_2(s,0) = -\sqrt{\zeta(s,0)} = -\sqrt{\left(h+\eta(s,0)\right)} \tag{5.42}$$

An equation in terms of β can be implicitly given by estimating $\beta^{(k)}$, where the superscript k denotes the iteration number k. We can write the system of ODE's in (5.28), (5.29), (5.33), (5.36) and (5.41) in matrix form,

$$\begin{pmatrix} 1 & 0 & 0 & 0 & 0 \\ 0 & 1 & 0 & 0 & 0 \\ 0 & 0 & 1 & b_{34} & b_{35} \\ 0 & 0 & b_{43} & 1 & b_{45} \\ 0 & 0 & b_{53} & b_{54} & b_{55} \end{pmatrix} \frac{\partial}{\partial \tau} \begin{pmatrix} T \\ X \\ \alpha^{(k)} \\ \lambda_1 \\ \lambda_2 \end{pmatrix} = \begin{pmatrix} 1 \\ c_2 \\ 0 \\ c_4 \\ c_5 \end{pmatrix} \tag{5.43}$$

or

$$\frac{\partial}{\partial \tau} \begin{pmatrix} T \\ X \\ \alpha^{(k)} \\ \lambda_1 \\ \lambda_2 \end{pmatrix} = \begin{pmatrix} 1 & 0 & 0 & 0 & 0 \\ 0 & 1 & 0 & 0 & 0 \\ 0 & 0 & 1 & b_{34} & b_{35} \\ 0 & 0 & b_{43} & 1 & b_{45} \\ 0 & 0 & b_{53} & b_{54} & b_{55} \end{pmatrix}^{-1} \begin{pmatrix} 1 \\ c_2 \\ 0 \\ c_4 \\ c_5 \end{pmatrix} \tag{5.44}$$

where

$$b_{34} = \frac{-2\alpha^{(k)}}{\lambda_2 - \lambda_1} \tag{5.45}$$

$$b_{35} = \frac{-2\beta^{(k)}}{\lambda_2 - \lambda_1} \tag{5.46}$$

$$b_{43} = \frac{1}{\lambda_2} \tag{5.47}$$

$$b_{45} = \frac{-\left(\alpha^{(k)} + \beta^{(k)}\right)}{\lambda_2^{\,2}} \tag{5.48}$$

$$b_{53} = \frac{2\left(\lambda_1\,\alpha^{(k)} + \lambda_2\,\beta^{(k)}\right)}{\left(2\alpha^{(k)} + 2\beta^{(k)}\right)^2} - \frac{\lambda_1}{2\left(\alpha^{(k)} + \beta^{(k)}\right)} \tag{5.49}$$

$$b_{54} = 1 - \frac{\alpha^{(k)}}{2\left(\alpha^{(k)} + \beta^{(k)}\right)} \tag{5.50}$$

$$b_{55} = 1 - \frac{\beta^{(k)}}{2\left(\alpha^{(k)} + \beta^{(k)}\right)} \tag{5.51}$$

$$c_2 = \lambda_1 \tag{5.52}$$

$$c_4 = -\frac{1}{\lambda_2}\frac{\partial \beta^{(k)}}{\partial \tau} \tag{5.53}$$

The set of ODE's for β is written in (5.24). The first 3 equations, which are the characteristics of (5.24), are

$$\frac{\partial t}{\partial \tau} = 1 \qquad t\left(s, \tau = 0\right) = 0 \tag{5.54}$$

$$\frac{\partial x}{\partial \tau} = \lambda_2 \qquad x\left(s, \tau = 0\right) = s \tag{5.55}$$

$$\frac{\partial \beta}{\partial \tau} = \frac{\partial \lambda_1}{\partial \tau}\left(\frac{-2\alpha}{\lambda_2 - \lambda_1}\right) + \frac{\partial \lambda_2}{\partial \tau}\left(\frac{-2\beta}{\lambda_2 - \lambda_1}\right) \tag{5.56}$$

where

$$\beta(s, \tau = 0) = \frac{-\lambda_1}{\lambda_2 - \lambda_1}\zeta(s, 0)$$

The equations for $\frac{\partial \lambda_1}{\partial \tau}$ and $\frac{\partial \lambda_2}{\partial \tau}$ are the same as the ODE for α. They are written in (5.36) and (5.41). We can write the ODE in a matrix form.

$$\begin{pmatrix} 1 & 0 & 0 & 0 & 0 \\ 0 & 1 & 0 & 0 & 0 \\ 0 & 0 & 1 & d_{34} & d_{35} \\ 0 & 0 & d_{43} & 1 & d_{45} \\ 0 & 0 & d_{53} & d_{54} & d_{55} \end{pmatrix} \frac{\partial}{\partial \tau}\begin{pmatrix} T \\ X \\ \beta^{(k+1)} \\ \lambda_1 \\ \lambda_2 \end{pmatrix} = \begin{pmatrix} 1 \\ e_2 \\ 0 \\ e_4 \\ e_5 \end{pmatrix} \tag{5.57}$$

or

$$\frac{\partial}{\partial \tau}\begin{pmatrix} T \\ X \\ \beta^{(k+1)} \\ \lambda_1 \\ \lambda_2 \end{pmatrix} = \begin{pmatrix} 1 & 0 & 0 & 0 & 0 \\ 0 & 1 & 0 & 0 & 0 \\ 0 & 0 & 1 & d_{34} & d_{35} \\ 0 & 0 & d_{43} & 1 & d_{45} \\ 0 & 0 & d_{53} & d_{54} & d_{55} \end{pmatrix}^{-1} \begin{pmatrix} 1 \\ e_2 \\ 0 \\ e_4 \\ e_5 \end{pmatrix} \tag{5.58}$$

where

$$d_{34} = \frac{2\alpha^{(k)}}{\lambda_2 - \lambda_1} \tag{5.59}$$

$$d_{35} = \frac{2\beta^{(k+1)}}{\lambda_2 - \lambda_1} \tag{5.60}$$

$$d_{43} = \frac{1}{\lambda_2} \tag{5.61}$$

$$d_{45} = \frac{-1\left(\alpha^{(k)} + \beta^{(k+1)}\right)}{\lambda_2^{\,2}} \tag{5.62}$$

$$d_{53} = \frac{2\left(\lambda_1\alpha^{(k)} + \lambda_2\beta^{(k+1)}\right)}{\left(2\alpha^{(k)} + 2\beta^{(k+1)}\right)} - \frac{\lambda_2}{2\left(\alpha^{(k)} + \beta^{(k+1)}\right)} \tag{5.63}$$

$$e_2 = \lambda_2 \tag{5.64}$$

$$e_4 = -\frac{1}{\lambda_2}\frac{\partial\alpha^{(k)}}{\partial\tau} \tag{5.65}$$

$$e_5 = \left(\frac{\lambda_1}{2\left(\alpha^{(k)} + \beta^{(k+1)}\right)} - \frac{2\left(\lambda_1\alpha^{(k)} + \lambda_2\beta^{(k+1)}\right)}{\left(2\alpha^{(k)} + 2\beta^{(k+1)}\right)^2}\right)\frac{\partial\alpha^{(k)}}{\partial\tau} \tag{5.66}$$

The system of equations in (5.44) and (5.58) are integrated using Runge-Kutta numerical integration. The procedure is as follows,

1. For each s, estimate $\beta^{(k)}$ for all τ and substitute $\beta^{(k)}$ into (5.44) to solve for $\alpha^{(k)}$.
2. $\alpha^{(k)}$ obtained in (1) is substituted into (5.58) to solve for $\beta^{(k+1)}$

3. $\beta^{(k+1)}$ obtained in (2) is substituted into (5.44) to get $\alpha^{(k+1)}$.
4. Repeat steps (2) – step (3) until $\left|\beta^{(k+1)}-\beta^{k}\right|<\varepsilon$ and $\left|\alpha^{(k+1)}-\alpha^{k}\right|<\varepsilon$.

Figure 5.3 shows the solution for α and β at different times. The waves separate and move away from the initial condition as expected. Figure 5.4a shows the solution in physical coordinates.

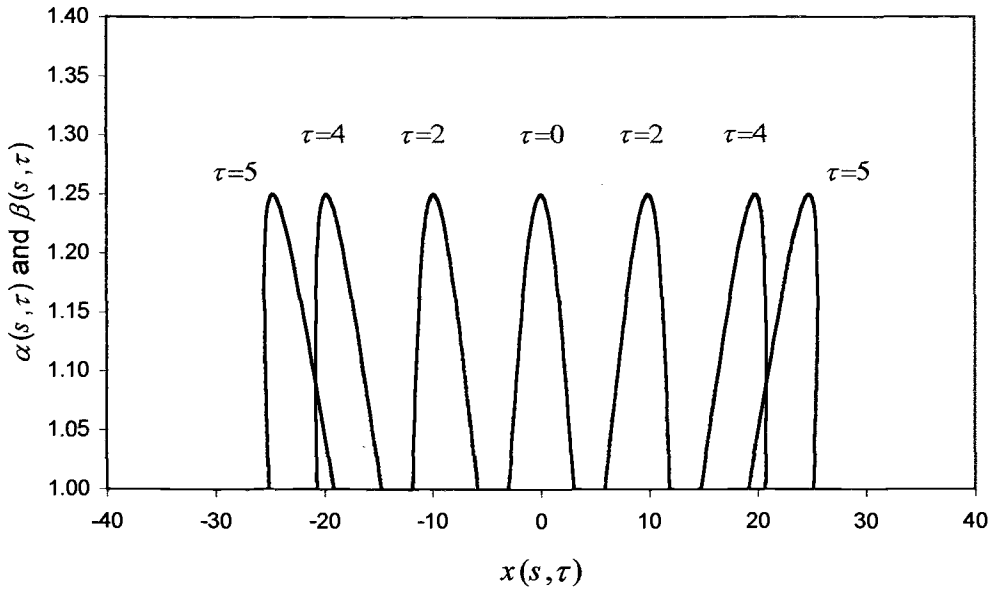

Figure 5.3. The nonlinear characteristic solution $\alpha(s,\tau)$ and $\beta(s,\tau)$ verse $x(s,\tau)$

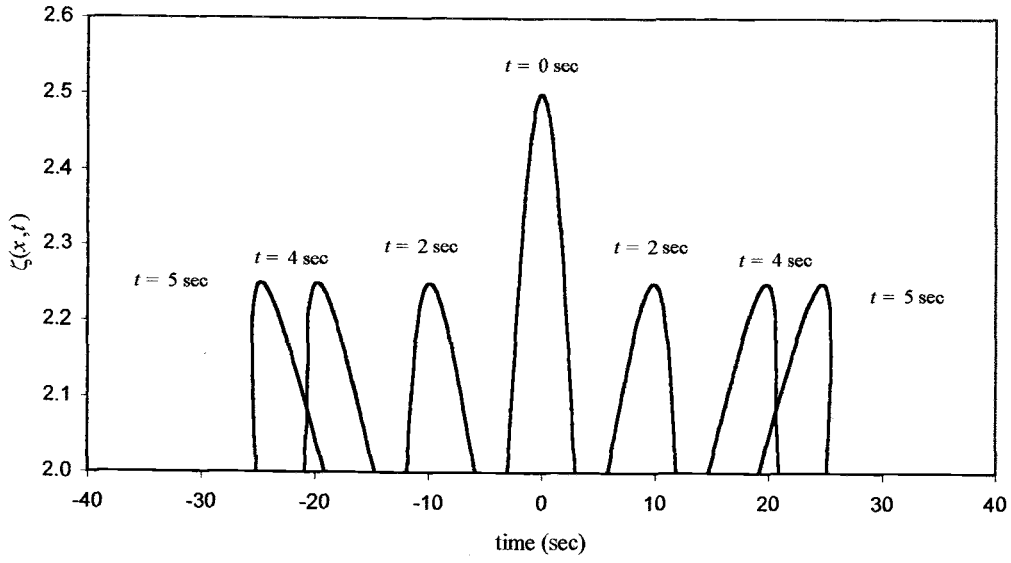

Figure 5.4a The nonlinear physical solution $\zeta(x,t)$

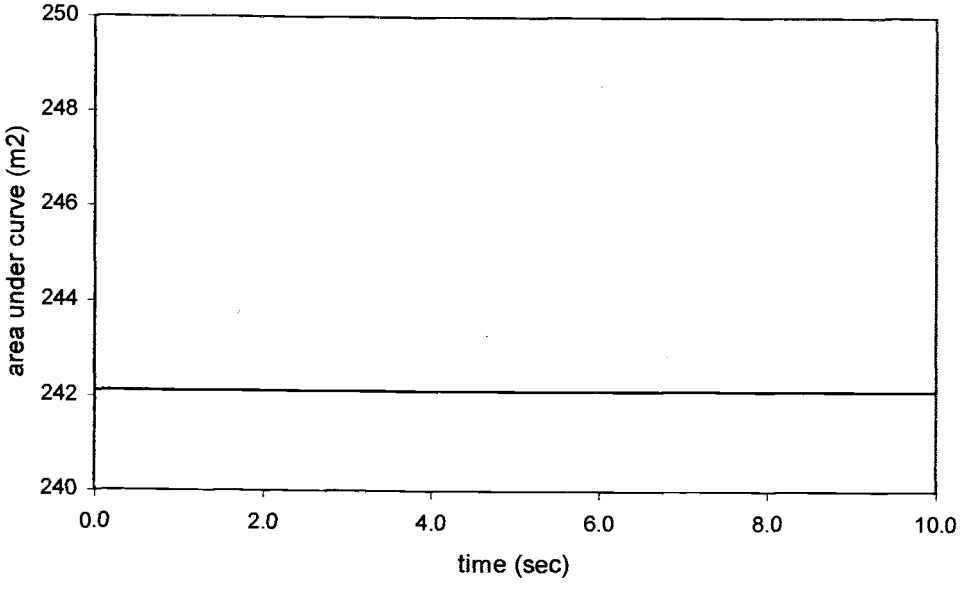

Figure 5.4b The area under the curves of $\zeta(x,t)$ with respect to time t.

The solution starts to curl over after 4.5 seconds. The term "curl over" is to describe a waveform whose leading edge extends beyond the base of the wave.

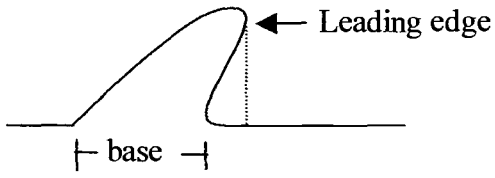

Figure 5.5 Curling over of a wave

As the wave starts to curl over, the solution $\zeta(x,t)$ becomes physically unrealistic although it is mathematically stable. Physical intuition and observations lead us to expect the wave to break once it curls over past some threshold. The solution curl over significantly at time 4.5 seconds, and this indicates the wave breaks. Figure 5.4b shows that the model conserves mass as expected.

In Chapter 2, for the time series of ocean waves examined, to evaluate the fractal dimension required a block of data of length 4000 points or greater. For 2 Hz data, this corresponds to 2000 seconds of data observation. This very long record length is not examined using the numerical model.

Comparing the results with the finite difference solution at exactly the same time and place, we see that the solutions for $t < 5\,\text{sec}$ are similar. In the finite difference solutions, the waves do not curl over, due to the fact that multi-valued functions are not supported in the finite difference method. Thus, the finite difference solution should not be used for $t > 5$ seconds.

One important point in this chapter is that the model using method of characteristics is capable of indicating when the wave begins to curl forward.

CHAPTER 6. WAVES ON A STEP BOTTOM

In this chapter a simple long wave reflection and transmission model is developed for long waves on a sloping bottom. The sloping bottom is approximated as a series of steps. The single step reflection model in Dean and Dalrymple (1984) is extended to multiple steps. The model also includes depth limited breaking. Section 6.1 focuses on the incident waves being reflected and transmitted only once. If a wave propagates over a multi-step bottom, then the reflected and transmitted waves will be re-transmitted and re-reflected. Section 6.2 focuses on modeling multi-reflected and transmitted waves. Finally, these approaches are combined to produce a composite model, in which the total energy of the reflected and transmitted waves depends on how many times the waves are reflected and transmitted.

6.1 THE PROGRESSIVE MODEL

This section focuses on waves reflected and transmitted once. Figure 6.1 shows the geometry of the depth transition region. The fluid domain is divided into Regions 1 and 2. The incoming wave H_i is assumed to propagate in the positive x-direction. At the vertical step located at $x = x_1$, a portion of the wave will be reflected, and the remainder transmitted.

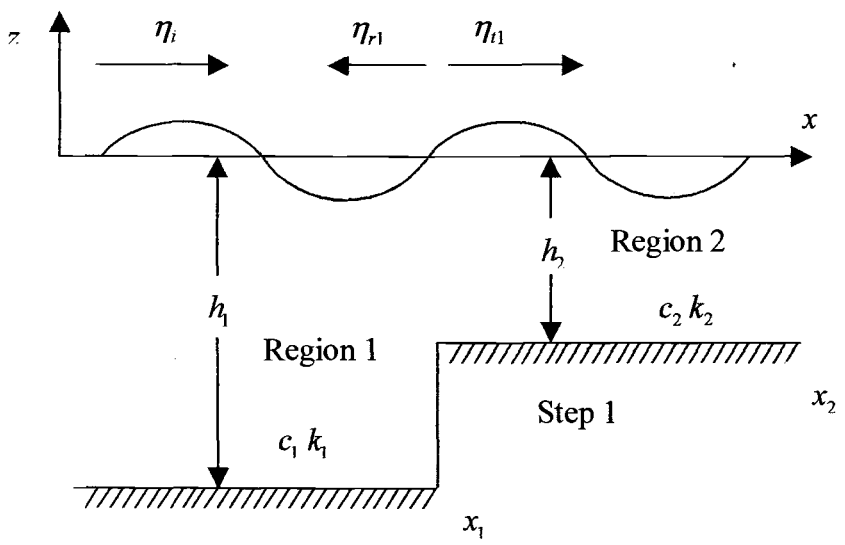

Figure 6.1 Elevation of a section of a step bottom

By assuming linear superposition, we can describe the wave in Figure 6.1 as follows:

$$\eta_1 = \eta_i + \eta_{r1} = \frac{H_i}{2}\cos\left(k_1 x - \omega\, t + \varepsilon_i\right) + \frac{H_{r1}}{2}\cos\left(k_1 x + \omega\, t + \varepsilon_{r1}\right) \quad \text{at } x < x_1$$

$$\eta_2 = \eta_{t1} = \frac{H_{t1}}{2}\cos\left(k_2 x - \omega\, t + \varepsilon_{t1}\right) \quad \text{at } x \geq x_1 \tag{6.1}$$

where η_i, η_{t1}, and η_{r1} are the incident, transmitted, and reflected waves, respectively. ε_i, ε_{t1} and ε_{r1} are the corresponding wave phases. The phases are referenced to the incident wave, whose phase is set to zero. k_1 and k_2 are the wave numbers before and after the step at $x = x_1$. The wave numbers are calculated using the long wave dispersion relation

$$k_i = \frac{2\pi}{\sqrt{g h_i}\; T_p} \tag{6.2}$$

where T_p is the wave period and h is the water depth. There are 4 unknowns: H_{t1}, H_{r1}, ε_{t1} and ε_{r1}. We impose matching boundary conditions at the location of the step as shown in Figure 4.2. The first condition is that the free surface is continuous at $x = x_1$:

$$\eta_i + \eta_{r1} = \eta_{t1} \qquad ; \quad x = x_1 \tag{6.3}$$

For the second condition, we use the linearized continuity equation

$$\frac{\partial \eta}{\partial t} = \frac{\partial (uh)}{\partial x} \tag{6.4}$$

where u is the depth-averaged horizontal velocity. From (6.3) and (6.4), it follows that the volume flux must match at the step.

$$(uh)_1 = (uh)_2 \tag{6.5}$$

For a long wave, the depth-averaged velocity can be written as (Dean and Dalrymple, 1984)

$$u = \frac{\eta c}{h} \tag{6.6}$$

where c is the wave celerity. In the direction of the wave, we can write (6.5) as

$$c_1 (\eta_i - \eta_{r1}) = c_2 \ \eta_{t1} \tag{6.7}$$

For the shallow water, the celerities are

$$\begin{aligned} c_1 &= \sqrt{g \ h_1} \\ c_2 &= \sqrt{g \ h_2} \end{aligned} \tag{6.8}$$

Equations (6.3) and (6.7) are used to solve the unknowns, $H_{t1}, H_{r1}, \varepsilon_{t1}$ and ε_{r1}. The wave heights and phases are written

$$\begin{aligned} H_{t1} &= 2\frac{c_1}{c_1+c_2}H_i \\ H_{r1} &= \frac{c_1-c_2}{c_1+c_2}H_i \end{aligned} \tag{6.9}$$

$$\begin{aligned} \varepsilon_{t1} &= k_1x_1 - k_2x_2 \\ \varepsilon_{r1} &= -2k_1x_1 \end{aligned} \tag{6.10}$$

This incident, transmitted, and reflected waves at Step 1 can be written

$$\begin{aligned} \eta_i &= \frac{H_i}{2}\cos(k_1x - \omega\, t) \\ \eta_{t1} &= \frac{c_1}{c_1+c_2}H_i\cos(k_2(x-x_1)+k_1x_1-\omega\, t) \\ \eta_{r1} &= \frac{1}{2}\frac{c_1-c_2}{c_1+c_2}H_i\cos(k_1x-2k_1x_1+\omega\, t) \end{aligned} \tag{6.11}$$

Now consider a second step $x = x_2$ where $x_2 > x_1$. This is shown in Figure 6.2. The transmitted wave from Step 1 becomes the incident wave at Step 2. The abrupt depth change at Step 2 will result in reflected and transmitted waves η_{r2} and η_{t2}. These can be written as follows,

$$\begin{aligned} \eta_{t1} &= \frac{H_{t1}}{2}\cos(k_2x - \omega\, t + \varepsilon_{t1}) \\ \eta_{t2} &= \frac{H_{t2}}{2}\cos(k_3x - \omega\, t + \varepsilon_{t2}) \\ \eta_{r2} &= \frac{H_{r2}}{2}\cos(k_2x + \omega\, t + \varepsilon_{r2}) \end{aligned} \tag{6.12}$$

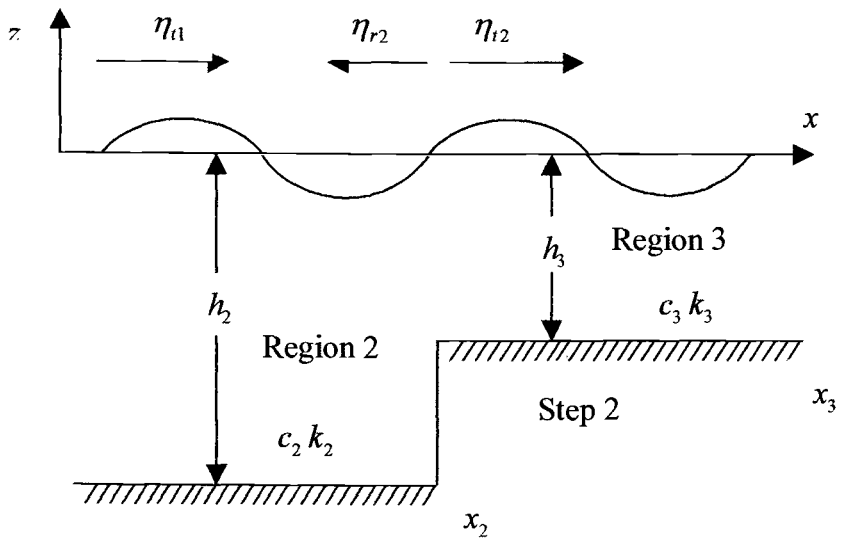

Figure 6.2 Sketch of Step 2

The procedure followed at Step 1 is repeated to solve the system of equations at Step 2. This technique can be repeated for an arbitrary number of steps to obtain the general result.

$$H_{t(n)} = 2\frac{c_n}{c_n + c_{n+1}} H_{t(n-1)}$$
$$H_{r(n)} = \frac{c_n - c_{n+1}}{c_n + c_{n+1}} H_{t(n-1)} \qquad (6.13)$$

$$\varepsilon_{t(n)} = (k_n - k_{n+1})x_n + \varepsilon_{t(n-1)}$$
$$\varepsilon_{r(n)} = -2\ k_n x_n - \varepsilon_{t(n-1)} \qquad (6.14)$$

If $(n-1) = 0$, then $H_{t(n-1)} = H_i$ and $\varepsilon_{t(n-1)} = \varepsilon_i = 0$. Using (6.13) and (6.14), we write the general free surface equation as

$$\eta_{t(n)} = \frac{H_{t(n)}}{2}\cos\left(k_{n+1}x - \omega\, t + \varepsilon_{t(n)}\right)$$
$$\eta_{r(n)} = \frac{H_{r(n)}}{2}\cos\left(k_{n}x + \omega\, t + \varepsilon_{r(n)}\right) \qquad (6.15)$$

6.2 THE RE-REFLECTED WAVE MODEL

Up to this point, the determination of reflected and transmitted waves from each step has been rather straightforward. Unfortunately, re-reflection occurs between steps, and these effects are not negligible. An example of re-reflection is as follows: the incident wave propagates across the first step to give a transmitted wave η_{t1}. This wave then partially reflects from Step 2. This reflected wave then propagates back to Step 1, where it is partially reflected again back to Step 2. It is clear that this process develops many reflected waves. Fortunately, at each reflection, the importance of this mechanism decreases. This is because at each step there is only partial reflection, so multiple reflections tend to get smaller at each re-reflection. To conserve energy, the re-reflected and re-transmitted waves must be considered. In Figure 6.3, η_{r3} is called the first order reflected wave. The re-transmitted and re-reflected waves are designated η_{r32} and η_{t32}, respectively. Waves resulting from re-transmission and re-reflection of previously reflected waves are termed second order waves. For second order waves, the subscripts *r* and *t* are used for transmitted and reflected waves, respectively. Thus, propagating waves in the positive x direction are designated by "*t*" and those propagating in the negative x direction are designated "*r*", regardless of the order of the wave. The indices (j,n) describe a wave re-transmitted and re-reflected off step n (at x_n), which previously originated in a reflection off step j (at x_j).

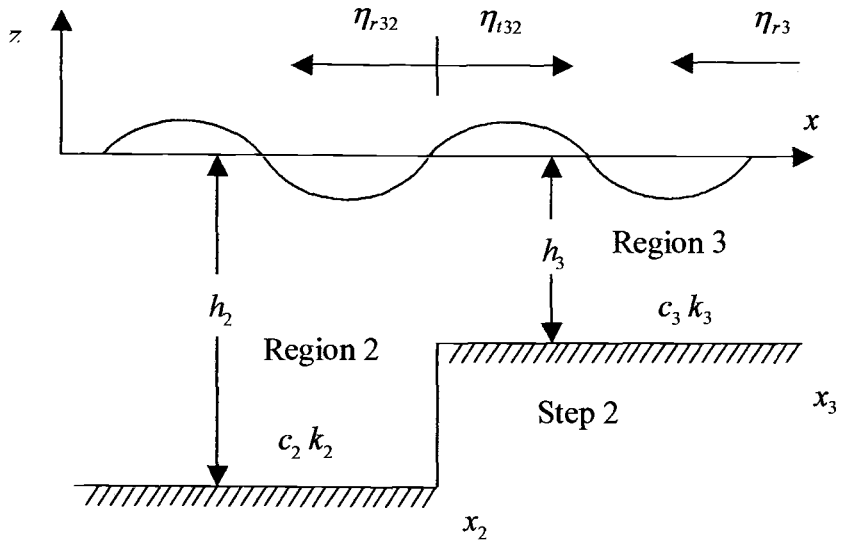

Figure 6.3 An example of re-transmission and re-reflection of the waves

The waves in Figure 6.4 can be defined as

$$\begin{aligned}
\eta_{r3} &= \frac{H_{r3}}{2}\cos\left(k_3 x + \omega\, t + \varepsilon_{r3}\right) \\
\eta_{r32} &= \frac{H_{r32}}{2}\cos\left(k_2 x + \omega\, t + \varepsilon_{r32}\right) \\
\eta_{t32} &= \frac{H_{t32}}{2}\cos\left(k_3 x - \omega\, t + \varepsilon_{t32}\right)
\end{aligned} \tag{6.16}$$

where η_{r3} is known . To solve these equations, we apply boundary conditions (6.3) and (6.7). We can write the second order wave heights and phases as

$$\begin{aligned}
H_{r32} &= 2\frac{c_3}{c_2 + c_3} H_{r3} \\
H_{t32} &= \frac{c_3 - c_2}{c_2 + c_3} H_{r3}
\end{aligned} \tag{6.17}$$

$$\varepsilon_{r32} = (k_3 - k_2)x_2 + \varepsilon_{r3}$$
$$\varepsilon_{t32} = -2\,k_3 x_2 - \varepsilon_{r3} \tag{6.18}$$

η_{r31} and η_{t31} are written as

$$\eta_{r31} = \frac{H_{r31}}{2}\cos(k_1 x + \omega\, t + \varepsilon_{r31})$$
$$\eta_{t31} = \frac{H_{t31}}{2}\cos(k_2 x - \omega\, t + \varepsilon_{t31}) \tag{6.19}$$

Applying the boundary conditions, we write the unknowns as

$$H_{r31} = 2\frac{c_2}{c_1 + c_2}H_{r32}$$
$$H_{t31} = \frac{c_2 - c_1}{c_1 + c_2}H_{r32} \tag{6.20}$$

and

$$\varepsilon_{r31} = (k_2 - k_1)x_1 + \varepsilon_{r32}$$
$$\varepsilon_{t31} = -2\,k_2 x_1 - \varepsilon_{r32} \tag{6.21}$$

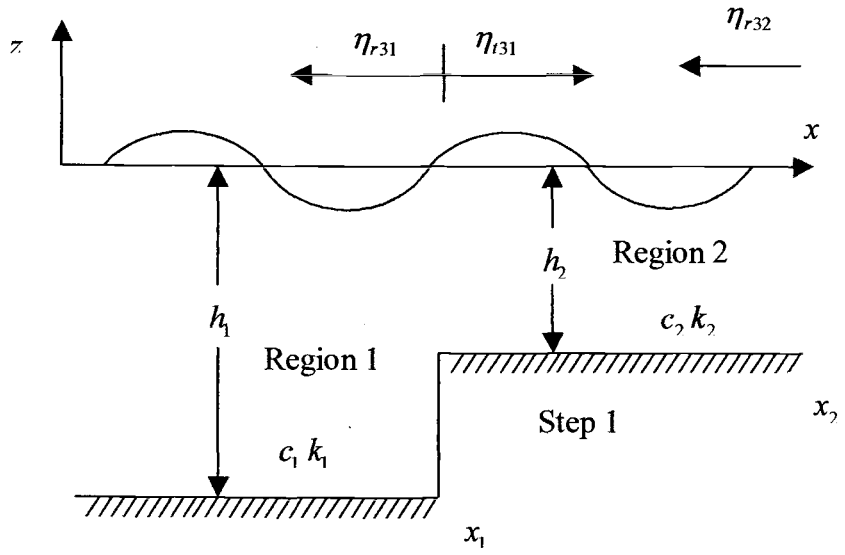

Figure 6.4. η_{r32} **is transmitted and reflected over** $x = x_1$**. It becomes** η_{r31} **and** η_{t31}**.**

We repeat the procedure described above to obtain a general expression for second order wave heights and phases

$$H_{r(j,n)} = 2\frac{c_{n+1}}{c_n + c_{n+1}} H_{r(j,n+1)}$$

$$H_{t(j,n)} = \frac{c_{n+1} - c_n}{c_n + c_{n+1}} H_{r(j,n+1)} \qquad (6.22)$$

$$\varepsilon_{r(j,n)} = \left(k_{n+1} - k_n\right) x_n + \varepsilon_{r(j,n+1)}$$

$$\varepsilon_{t(j,n)} = -2\, k_{n+1} x_n - \varepsilon_{r(j,n+1)} \qquad \text{for } n < j$$

The case $n = j$ is described by (6.13), (6.14) and (6.15). The complete secondary wave equations are

$$\eta_{r(j,n)} = \frac{H_{r(j,n)}}{2}\cos\left(k_n x + \omega\, t + \varepsilon_{r(j,n)}\right)$$
$$\eta_{t(j,n)} = \frac{H_{t(j,n)}}{2}\cos\left(k_{n+1} x - \omega\, t + \varepsilon_{t(j,n)}\right) \tag{6.23}$$

The superposition of all waves originating from step n is

$$\eta = \eta_{t(n)} + \eta_{r(n+1)} + \sum_{m=n+1}^{j} \eta_{t(m,n)} + \sum_{m=n+2}^{j} \eta_{r(m,n+1)} \tag{6.24}$$

where j denotes the final step. Figure 6.5 shows the waves over step n,

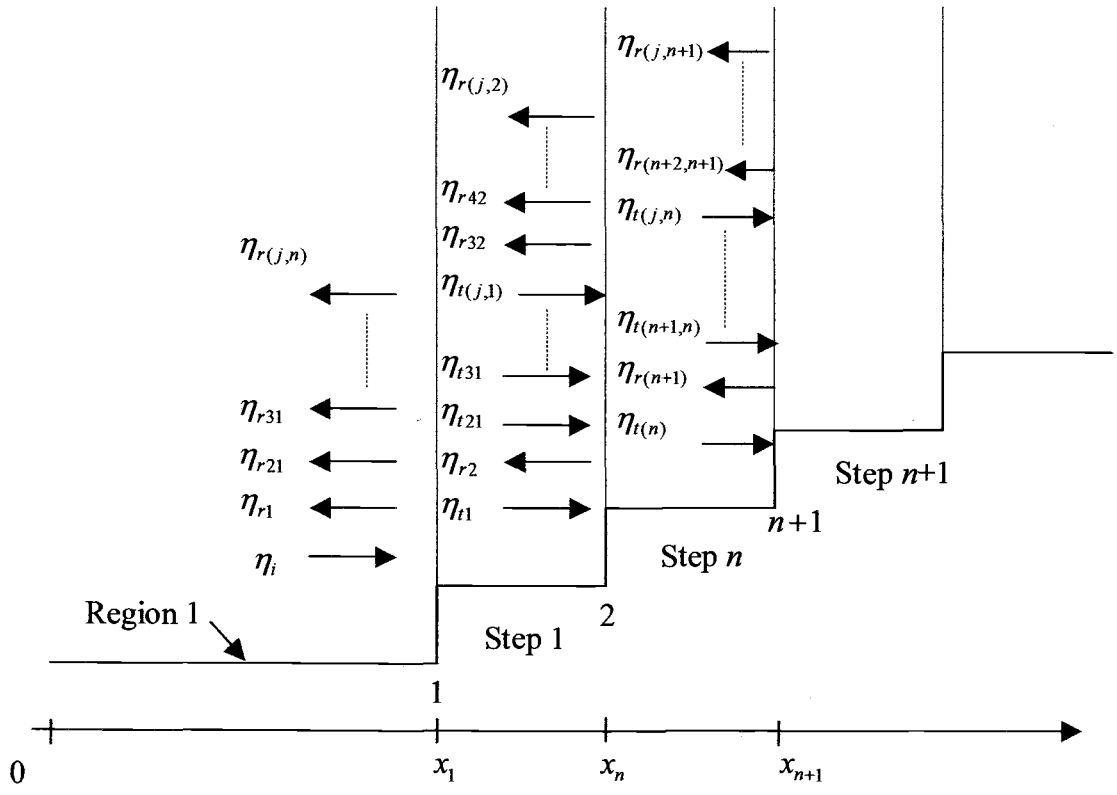

Figure 6.5. Summary of waves over step *n*

The reflection coefficient for the total system is calculated using the wave envelope of the total waveform in Region 1. For this purpose, the width of Region 1 is extended for several wavelengths. We obtain the wave envelope by taking the maximum and minimum of the total waves at each location in Region 1 with respect to time. The reflection coefficient is

$$K_r = \frac{\eta_{\max} - \eta_{\min}}{\eta_{\max} + \eta_{\min}} \qquad \text{in Region 1} \qquad (6.25)$$

where $\eta_{\max}$ and $\eta_{\min}$ are the maximum and minimum of the wave envelope in Region 1.

Figure 6.6a shows the reflection coefficient calculated for a bottom containing two steps using the wave envelope method over bottom slopes m between 0.001 and 1.0. From the figure, the waves have to be reflected and transmitted a minimum of 9 times to obtain a reflection coefficient near 1.0.

A calculation including the effects of depth-limited breaking waves was also done. The transmitted wave height $H_{t(n)}$ is subjected to wave breaking conditions

$$H_{t(n)} = 0.8\, h_n \qquad (6.26)$$

The results are summarized in Figure 6.6b. Breaking waves reduce the reflection coefficient by about 30%. The average K_r is around 0.7. More steps would yield a more realistic reflection coefficient.

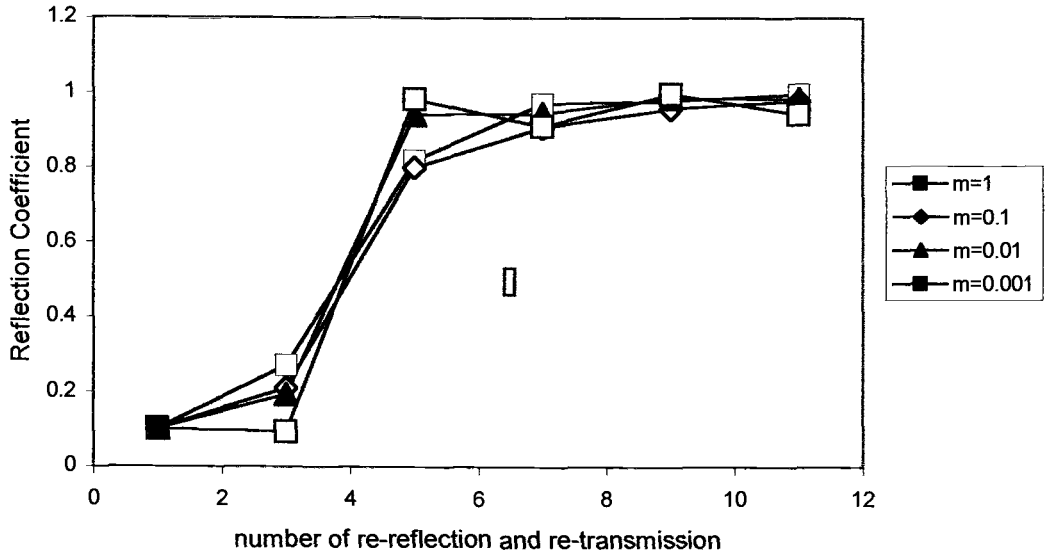

Figure 6.6a Reflected coefficient K_r over a 2-step bottom with different slopes without breaking waves.

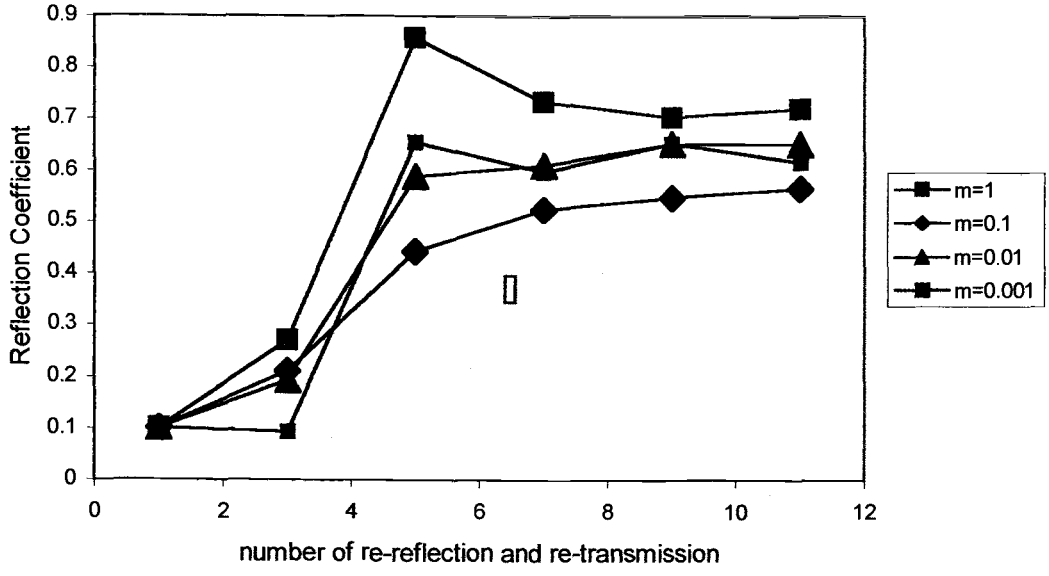

Figure 6.6b Reflected coefficient K_r over a 2-step bottom with different slopes with breaking waves

The concave-up Dean beach profile is given by

$$h = a\, x^{2/3} \tag{6.27}$$

where a is a constant depending on the beach grain size (Moore,1982). We fit the profile with a two-step bottom and considered four profiles corresponding to grains sizes of 0.1 mm, 1.0 mm, 10 mm, and 100 mm. Figure 6.7 shows an example of the best fit of 2 steps to the beach profile. The reflection coefficient is determined in Region 1 for each profile. Figures 6.8 and 6.9 show the resulting reflection coefficients without and with depth-limited breaking waves, respectively.

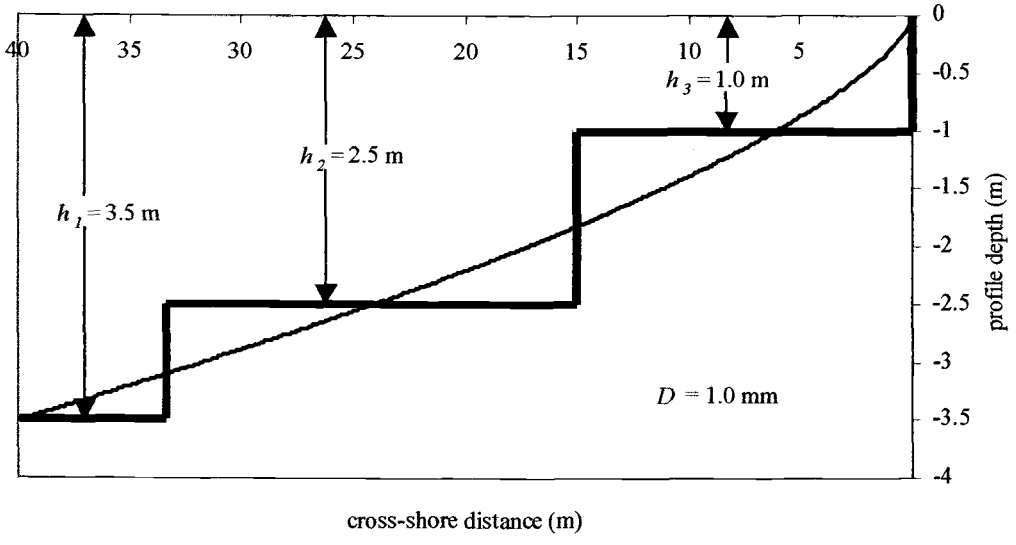

Figure 6.7 Best fit of 2 steps to the Dean beach profile with D = 1.0 mm

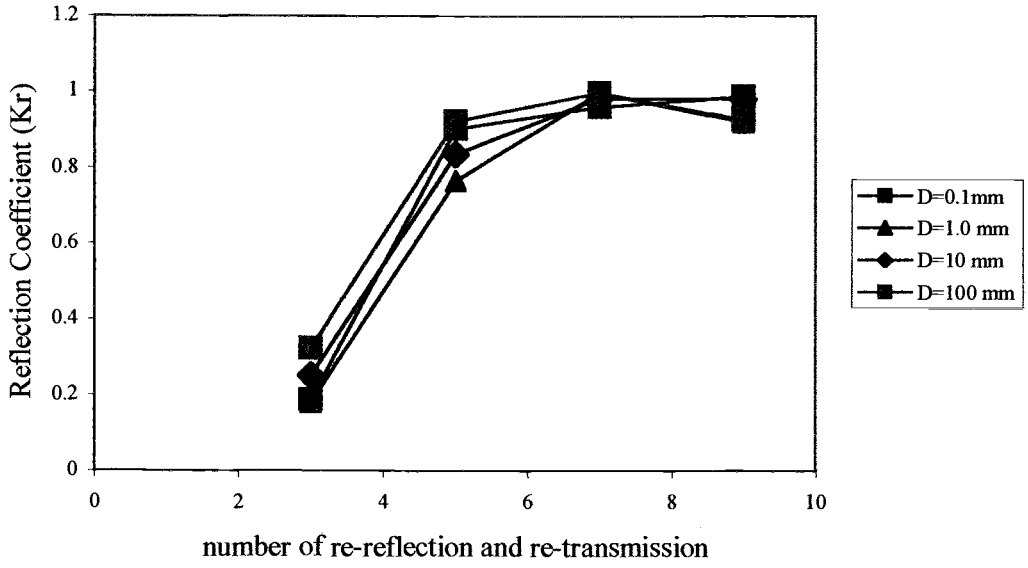

Figure 6.8 Reflection coefficient for Dean beach profile without breaking waves

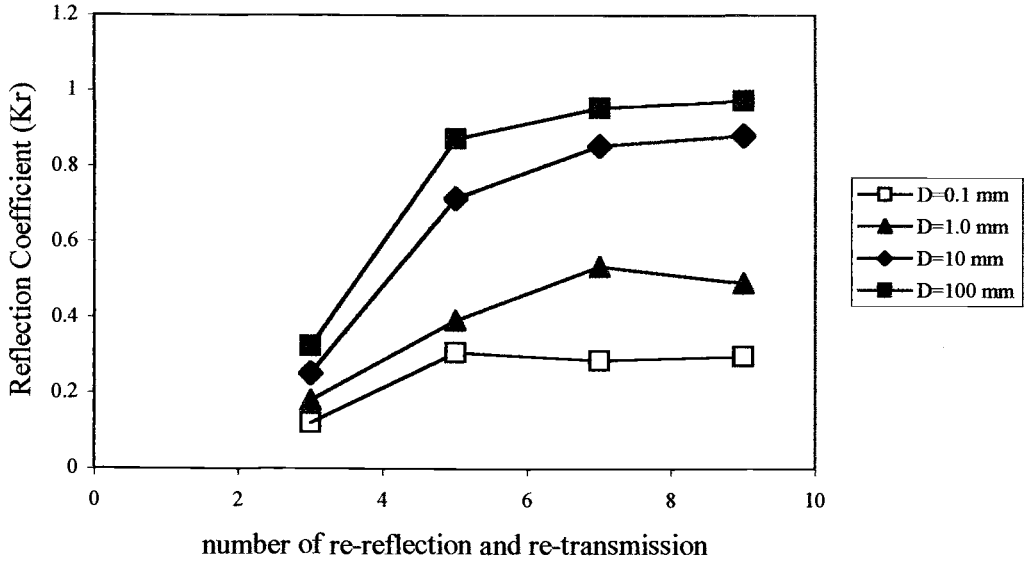

Figure 6.9 Reflection coefficient for Dean beach profile with breaking waves.

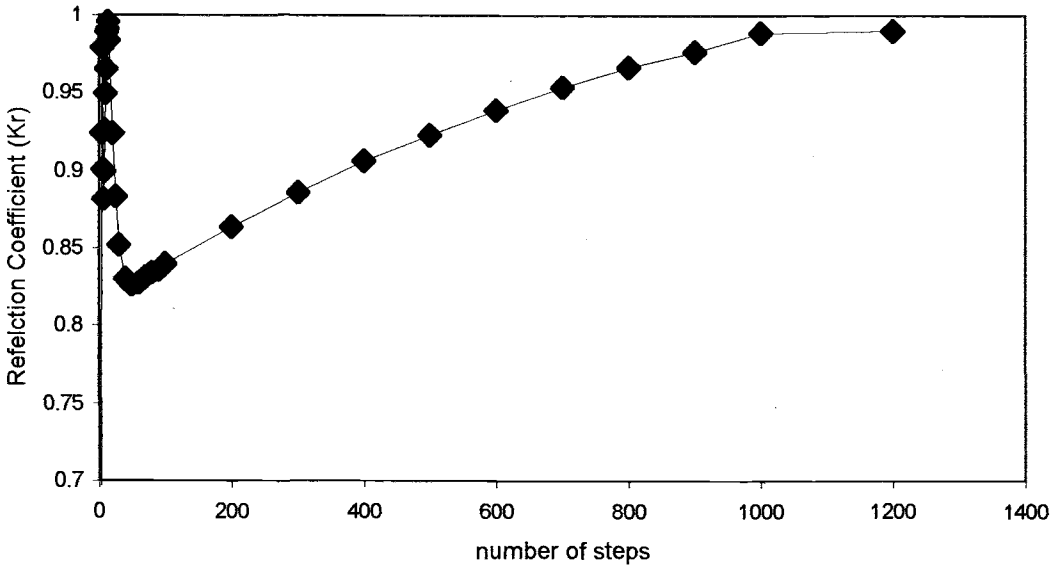

Figure 6.10 Reflection coefficient verse number of steps. In this model, the waves are reflected and transmitted once over a step.

Figure 6.8 shows that the total energy of the system is conserved when the waves are re-reflected and re-transmitted more than four times, with the reflection coefficient approaching one. Figure 6.9 shows that the reflection coefficient decreases for beaches with smaller grain size. Waves dissipate more energy on beaches with smaller grain size. The slope is milder and the waves break farther offshore. Thus, wave energy dissipates over a larger area. A beach with small grain size and mild slope is called a dissipative beach. For larger grain sizes, the beach is steeper, and the waves break at a location closer to shore. Energy is dissipated over a limited area on the steep beach. A beach with larger grain size is a reflective beach.

Initially, this model is intended to solve the problem of sloping bottom as an alternative method for the model described in Chapter 4. In Chapter 4, the sloping bottom model described by constant coefficient PDE does not conserve energy

flux. We intended to apply linear solutions of flat bottom without bottom friction derived in Chapter 4 over a series of steps. From results in Figures 6.6a and 6.8, we can see that it is impractical for us to apply linear solutions to a series of steps if we have to re-reflect and re-transmit the waves up to 9 times for the model to conserve energy. We also study the model if we only reflect and transmit the waves once over a step. The result is presented in Figure 6.10. The figure shows the reflection coefficient verse the number of steps. From the figure we can see that the energy is conserved if we use over one thousand of steps. It is impractical for us to apply linear solution on flat bottom over thousands of steps.

CHAPTER 7. CONCLUSION

In this work we have represented the irregular nature of free surface of ocean waves using fractals. We have calculated the fractal dimension of measured ocean wave profiles to be in the range of 1.5 – 1.8. This non-integer dimension confirms the fractal nature of the waves.

Field measurements indicate a positive correlation between fractal dimension and the degree of nonlinearity, estimated by the skewness of the wave distribution. Fractal dimension is also positively correlated with wave steepness. Fractal dimension is also observed to be higher in the breaking zone, where waves are highly nonlinear and dissipate energy in chaotic manner.

We first attempt to reproduce the observed changes in fractal dimension with a linear analysis. Solutions of the linear system based on the work of Fulks and Guenther (1972) are developed for several cases. In all cases, the linear solutions do not yield the change in fractal dimension observed in the measured data. Thus, we conclude that solving the nonlinear system of equations is essential.

As a first approach to solving the nonlinear system, we develop an implicit finite difference method solution with a smooth initial condition. The resulting solution contains waves propagating to the left and right. As the waves propagate, the wave form becomes asymmetric, with the crest shifting toward the front of the wave. The leading edge of the wave never extends beyond the wave base. However, the wave height decreases and the wave base width increases with time.

Next, we solve the system using the Runge-Kutta method to integrate the characteristics of the nonlinear system. The eigenvalues of the system are determined and used to decouple the equations. The characteristics of the resulting decoupled partial differential equations form a system of ordinary differential equations. Runge-Kutta numerical integration is used to obtain a solution for this system in the characteristic plane. Finally, the solution is transformed back to the $x-t$ plane.

For small time t, the finite difference and Runge-Kutta solutions are similar. At longer t, however, the Runge-Kutta solution shows the leading edge of the wave extending beyond the base of the wave. Physically, this behavior corresponds to a breaking wave. The finite difference solution does not have this result due to a mathematical property inherent in the finite difference method: multi-valued functions are not allowed. Thus, the finite difference solution is unable to describe a breaking wave, and should not be used for conditions near breaking.

In Chapter 6, we model a long wave propagating over a stepped bottom. Multiple reflections and transmissions are allowed at each step, and the resulting reflection coefficient is calculated. Our calculations indicate that energy is conserved if a sufficient number of re-reflected and re-transmitted waves are considered. In order to make the calculation feasible, we calculate the solution for two-step bottom, in which 9 re-reflections and re-transmissions are allowed at each step. The effect of depth-limited breaking waves is also considered. If we only reflect and transmit the waves once over small steps, we found that the energy is conserved if over one thousand of steps are used.

REFERENCES

1. Abramowitz, M. and Stegun, I.A. (1972) *Handbook of Mathematical Functions,* Dover Publications, Inc., New York, NY, 1046 pp.

2. Ajiwibowo, H. (1994) *Scour under Retaining Wall Toe*, Master Thesis, Department of Civil Engineering , Oregon State University, Corvallis, OR.

3. *Benoit Fractal Analysis System*, Trusoft International Inc., St. Petersburg, FL, 2000

4. Bruun, P. (1954) *Coast Erosion and the Development of Beach Profiles,* Technical Memorandum No. 44, Beach Erosion Board, U.S. Army Engineer Waterways Experiment Station, Vicksburg, MS.

5. Crow, J.A.(1991) *A Nonlinear Shallow Water Wave Equation and its Classical Solutions of the Cauchy Problem*, PhD Thesis, Oregon State University, Corvallis, OR.

6. Dally, W.R., Dean, R.G., and Dalrymple, R.A. (1984) *Modelling Wave Transformation in the Surf Zone,* Misc. Paper CERC-84-8, Coastal Engineering Research Center, U.S. Army Engineers Waterways Experiment Station, Vicksburg, MS, 51 pp.

7. Dally, W.R., Dean, R.G., Dalrymple, R.A (1985) *Wave Height Variation Across Beaches of Arbitrary Profile,* Journal of Geophysical Research, 90:11917-11927.

8. Dean, R.G. (1977) *Equilibrium Beach Profiles: U.S. Atlantic and Gulf Coasts,* Department of Civil Engineering, Ocean Engineering Report No.12, University of Delaware, Newark, DE.

9. Dean, R.G., Dalrymple, R.A. (1984) *Water Wave Mechanics for Engineers and Scientists,* Prentice Hall, Englewood Cliffs, NJ.

10. Gelfenbaum, et.al. (1999) *Grays Harbor Wave Refraction Experiment: Data Report,* U.S. Geological Survey and U.S. Department of Interior, WA.

11. Falconer, K. (1990) *Fractal Geometry: Mathematical Foundations and Applications*, Wiley and Sons, New York, NY.

12. Fulks, W., Guenther, R.B. (1972) *Hyperbolic Potential Theory in Two Dimensions*, Rendiconti Del Circolo Matematico Di Palermo, Via Archirafi, Palermo Italia.

13. Fulks, W., Guenther, R.B. (1972), *Hyperbolic Potential Theory*, Archives for Rat. Mech. Anal., Vol.49, 79-88.

14. Goda, Y. (1985) *Random Seas and Design of Maritime Structures*, University of Tokyo Press, Tokyo, Japan.

15. Gouyet, J.F. (1996) *Physics and Fractal Structures*, Springer, New York.

16. Guenther, R.B., Lee, J.W. (1996) *Partial Differential Equations of Mathematical Physics and Integral Equations*, Dover Publications, Inc., New York, NY.

17. Hildebrand, F.B.(1976), *Advanced Calculus for Applications*, Prentice Hall, Englewood Cliffs, NJ.

18. Kuznetzov (1988), Department of Ocean Research, Moscow, Russia.

19. Larson, M. and N.C. Kraus (1989) *SBEACH: Numerical Model for Simulating Storm-Induced Beach Change, Report 1: Theory and Model Foundation,* Technical Report CERC-89-9, US Army Engineer Waterways Experiment Station, Coastal Engineering Research Center, Vicksburg, MS.

20. Munzenmayer, Katja (1993) *The Fractal Structure of Surface Water Waves Near Breaking*, Master Thesis, Department of Mathematics, Oregon State University, Corvallis, OR.

21. McDougal, W.G. (1993) *State of The Art Practice in Coastal Engineering*, National Science Council, ROC and Tainan Hydraulic Laboratory, Taiwan.

22. Murphy, G.M. (1960) *Ordinary Differential Equation and Their Solutions,* Van Nostroud Company, Inc., Princeton, NJ, 451 pp.

23. Moore, B.D. (1982) *Beach Profile Evolution in Response to Changes in Water Level and Wave Height,* Master Thesis, Department of Civil Engineering, University of Delaware, Newark, DE.

24. Vanouplines, P. (1995) *Rescaled Range Analysis and The Fractal Dimension of Pi*, University Library, Free University Brussels, Belgium.